COMBINATORIAL DEVELOPMENT OF LSC-113/LSC-214 CATHODE MATERIALS FOR INTERMEDIATE TEMPERATURE SOLID OXIDE FUEL CELLS

A THESIS SUBMITTED TO
THE GRADUATE SCHOOL OF NATURAL AND APPLIED SCIENCES
OF
MIDDLE EAST TECHNICAL UNIVERSITY

BY

DOĞANCAN SARI

IN PARTIAL FULFILLMENT OF THE REQUIREMENTS
FOR
THE DEGREE OF MASTER OF SCIENCE
IN
METALLURGICAL AND MATERIALS ENGINEERING

AUGUST 2017

Approval of the thesis:

COMBINATORIAL DEVELOPMENT OF LSC-113/LSC-214 CATHODE MATERIALS FOR INTERMEDIATE TEMPERATURE SOLID OXIDE FUEL CELLS

submitted by **DOĞANCAN SARI** in partial fulfillment of the requirements for the degree of **Master of Science in Metallurgical and Materials Engineering Department, Middle East Technical University** by,

Prof. Dr. Gülbin Dural Ünver _____
Dean, Graduate School of **Natural and Applied Science**

Prof. Dr. C. Hakan Gür _____
Head of Department, **Metallurgical and Materials Engineering**

Prof. Dr. Tayfur Öztürk _____
Supervisor, **Metallurgical and Materials Eng. Dept., METU**

Assoc. Prof. Dr. Y. Eren Kalay _____
Co-supervisor, **Metallurgical and Materials Eng. Dept., METU**

Examining Committee Members:

Prof. Dr. C. Hakan Gür _____
Metallurgical and Materials Engineering Dept., METU

Prof. Dr. Tayfur Öztürk _____
Metallurgical and Materials Engineering Dept., METU

Prof. Dr. M. Kadri Aydınol _____
Metallurgical and Materials Engineering Dept., METU

Assoc. Prof. Dr. Y. Eren Kalay _____
Metallurgical and Materials Engineering Dept., METU

Assoc. Prof. Dr. Hasan Akyıldız _____
Metallurgical and Materials Engineering Dept., Selçuk Uni.

Date: *24.08.2017*

I hereby declare that all information in this document has been obtained and presented in accordance with academic rules and ethical conduct. I also declare that, as required by these rules and conduct, I have fully cited and referenced all material and results that are not original to this work.

Name, Last Name : DOĞANCAN SARI

Signature :

ABSTRACT

COMBINATORIAL DEVELOPMENT OF LSC-113/LSC-214 CATHODE MATERIALS FOR INTERMEDIATE TEMPERATURE SOLID OXIDE FUEL CELLS

Sarı, Doğancan

M.Sc., Department of Metallurgical and Materials Engineering

Supervisor: Prof. Dr. Tayfur Öztürk

Co-Supervisor: Assoc. Prof. Yunus Eren Kalay

August 2017, 119 pages

Solid oxide fuel cells are environmentally friendly, efficient and fuel versatile energy conversion devices which suffer from high operating temperatures. For lowering the operating temperatures of solid oxide fuel cells (SOFC), LSC-113/LSC-214 composite cathodes have recently attracted much attention due to their enhanced kinetics. However, the full potential of this novel system is still unknown. In this study, a combinatorial approach was used to develop cathode materials which would reduce operating temperatures of SOFCs to the range 500 - 600 °C. The kinetics of cathodic processes were investigated for LSC-113/LSC-214 composite cathode films deposited with magnetron sputtering and screened with measurement of EIS responses on symmetric cells. The study is made up of three parts. Part I is related to the fabrication of sputtering targets. Part II comprises the main study which was on combinatorial

screening of LSC-113/LSC-214 co-sputtered cathodes, and Part III is related to the stability of composite LSC cathodes for prolonged use;

In the first part of this study, a novel approach is illustrated to fabricate sputtering targets for thin film production. In this approach, deformable dies made up of poly-tetrafluoroethylene (Teflon) were used instead of conventional rigid dies. It was shown that this method is suitable for products of low volume productions. With the use of teflon rings LSC-113 and LSC-214 sputtering targets were succefully fabricated and used for the deposition of thin film cathodes.

In the second part, a combinatorial approach was used to obtain the optimum composition in LSC-113/LSC-214 composite system. A thin film composite cathode library was obtained by co-sputtering of LSC-113 and LSC-214 onto suitably positioned substrates each with controlled compositions. The cathode library was screened with an electrochemical impedance spectroscopy and showed that co-sputtered LSC-113/LSC-214 composite cathodes have low area specific resistance values (ASR) as compared to those reported in the literature. Practically useful ASR value of 0.15 $\Omega.cm^2$ was obtainable at many of the compositions in LSC-113/LSC-214 below 700 $^{\circ}C$. The best compositional range is 0.40<LSC-214<0.60 where the operating temperature can be as low as 615 $^{\circ}C$.

Refocusing the combinatorial screening to 0.40<LSC214<0.60, a new set of co-sputtered cathodes were prepared and were analysed with the same technique. As a result of combinatorial refocusing, the lowest operating temperature of 575 $^{\circ}C$ was possible in LSC-113/LSC-214 composite cathodes at mid-compositions, the best being LSC-113:LSC-214 =0.45:0.55. It was further shown that composite cathodes have an amouphous like structures in co-sputtered conditions, the structure crystallizes during its use. The nanocrystals formed at 700 $^{\circ}C$ are extremely small, their sizes are in the range of 4-10 nm. The composite structure is thought to restrict the grain growth, contributing to the stability of the as-deposited structure.

In the third part, the study aimed to estimate the stability of co-deposited cathodes and their resistances against Sr segregation which was commonly observed in LSC based

cathode materials at temperatures above 400 ^{0}C. In this part of the study, bi-layered cathodes, LSC-113/LSC-214, were fabricated via sputter deposition to investigate Sr segregation. This has shown that at 700 $^{\circ}$C, a surface layer rich in Sr content was formed, verifying that Sr segragation do occur in the bilayer. Also, it was revealed that in co-sputtered composite cathodes, no Sr segregation was observed with STEM analysis. The study of stability of co-sputtered cathodes at temperatures where ASR=0.15 $\Omega.cm^2$ showed that the LSC-113/LSC-214 co-sputtered composite cathodes are highly stable with extremely low degradation rate. The composite with the best operating temperature (575 $^{\circ}$C) is expected to have an ASR of approximately 3 $\Omega.cm^2$ after 10.000 hours of operation.

Keywords: IT-SOFC cathode, LSC-113/LSC-214 hetero-structure, combinatorial deposition, cation segregation, EIS.

ÖZ

ORTA SICAKLIKLI KATI OKSİT YAKIT PİLLERİ İÇİN LSC-113/LSC-214 KATOT MALZEMELERİNİN GELİŞTİRİLMESİ

Sarı, Doğancan

Yüksek Lisans, Metalurji ve Malzeme Mühendisliği Bölümü

Tez Yöneticisi: Prof. Dr. Tayfur Öztürk

Ortak Tez Yöneticisi: Doç. Dr. Yunus Eren Kalay

Ağustos 2017, 119 sayfa

Katı oksit yakıt pilleri, yüksek enerji verimliliklerine ve yakıt çeşitliliklerine sahip temiz enerji dönüşüm araçlarıdır. Bu avantajlarının yanı sıra, kullanımlarındaki temel problem yüksek çalışma sıcaklıklarına ihtiyaç duymalarıdır. Çalışma sıcaklıklarının düşürülebilmesi için katot kısmında gerçekleşen reaksiyonların hızlandırılması gerekmektedir. Bu amaç doğrultusunda geliştirilen yeni katot malzemelerinden LSC-113/LSC-214 kompozit katotları hızlı kinetiklerinden ötürü en çok ilgi çeken malzemelerdendir. LSC-113/LSC-214 kompozit yapısının katot kinetiği açısından son derece olumlu sonuçlar sergilediği bilinse dahi bu gelişmenin ne kadar daha arttırılabileceği henüz bilinmemektedir. Kombinasyonel bir yaklaşıma sahip olan bu çalışmada KOYP çalışma sıcaklıklarının 500 - 600 $^{\circ}$C aralığına düşürülmesi amaçlanmıştır. Bu amaç doğrultusunda kompozit yapıdaki LSC-113/LSC-214 katot malzemeleri simetrik ince filmler halinde üretilmiş ve söz konusu katotların reaksiyon kinetikleri elektrokimyasal empedans spektroskopisi yardımıyla irdelenmiştir. Söz

konusu çalışma toplamda 3 kısımdan oluşmaktadır. İlk kısımda sıçratma çöktürme tekniğinde kullanılan hedef malzemelerinin üretimi yer almaktadır. Söz konusu çalışmanın temelini oluşturan ikinci kısımda ise kombinasyonel yaklaşım ile en uygun LSC-113/LSC-214 kompozisyonunun elde edilmesine yer verilmektedir. Üçüncü ve son kısımda ise elde edilen katot malzemelerinin çalışma ömürleri anlatılmaktadır.

Hedef malzemelerinin üretimini ele alan ilk kısımda temel amaç kaplama tekniğine uygun yapıca sağlam ve uzun ömürlü hedef disklerinin üretilmesidir. Bu amaç doğrultusunda, düşük ölçekli üretimler için son derece maliyetli ve yavaş ilerleyen geleneksel yöntemlere alternatif olarak deforme edilebilir polimer esaslı kalıpların kullanıldığı yeni bir teknik geliştirilmiştir.

Çalışmanın ikinci kısmında, farklı içeriklere sahip LSC-113/LSC-214 katotları üretilmiştir. Söz konusu katotlar farklı pozisyonlara koyulmuş elektrolit altlıkların üzerine eş zamanlı olarak kaplanmıştır. Bu sayede üretilen katot malzemelerinin farklı sıcaklıklardaki reaksiyon kinetikleri, elektrokimyasal empedans spektroskopisi kullanılarak taranmıştır. Bu tarama sonucunda son derece düşük alan spesifik direnç değerleri gözlemlenmiştir. Çalışma sıcaklıklarının belirlenmesi için literatürde kabul görmüş ve verimli bir şekilde çalışmayı mümkün kılacak olan 0.15 $\Omega.cm^2$ değeri esas alınmıştır. Bu değer farklı içeriklere sahip katot malzemelerinin birçoğunda 700 $^{\circ}C$ altındaki sıcaklıklarda gözlemlenmiştir. En yüksek performansa sahip kompozisyon aralığı 0.40<LSC-214<0.60 olarak belirlenmiş olup bu aralıktaki en düşük çalışma sıcaklığı ise 615 $^{\circ}C$ olarak ölçülmüştür.

Daha düşük sıcaklıklarda çalışabilen kompozisyonların bulunması amacıyla ikinci bir tarama daha yapılmış ve bu taramada 0.40<LSC-214<0.60 kompozisyon aralığı genişletilerek bu aralıktaki içeriklere sahip numuneler üretilmiştir. Benzer şekilde üretilip test edilen bu ikinci numune havuzunda çalışma sıcaklıklarının 575 $^{\circ}C$ değerine kadar düşürülebilineceği sonucu çıkarılmış ve bunun için gerekli kompozsiyonun LSC-113:LSC-214 =0.45:0.55 olduğu bulunmuştur. Bunun yanısıra yürütülen yapısal incelemerler eş zamanlı kaplama ile üretilen katot malzemelerinin amorf yapıya sahip olduğunu ve yüksek sıcaklıklarda bu yapının kristalleştiğini gözler önüne sermiştir.

700 °C de uzun süre bekletme sonucunda oluşan kristal yapının 4-10 nm aralığında değişen büyüklüklere sahip nano-kristallerden oluştuğu gözlenmiş ve bunun sebebi olarak kompozit yapıdaki fazların birbirlerinin tane boyutlarındaki artışa izin vermediği öngörülmüştür. Bu durum katotların uzun vadeli kullanımına imkan kılmaktadır.

Çalışmanın son kısmı, eş zamanlı kaplanan katotların dayanıklılıklarını esas almaktadır. LSC-113 katot malzemelerinde 400 °C üzeri sıcaklıklarda sıkça rastlanan Sr çökelmesini incelemek amacıyla iki katmanlı katot malzemesi tasarlanmış ve sıçratma çöktürme yöntemiyle üretilmiştir. Katot kinetiğini son derece yavaşlatan yüzeyde Sr çökelmesi sorunu 700 °C de bekletilen iki katmanlı yapıda da gözlenmiş ve bunun üzerine Sr çökelmesinin eş zamanlı kaplanan katotların performansına yönelik etkileri araştırılmıştır. Dayanıklılık çalışmaları, söz konusu katotların 0.15 $\Omega.cm^2$ alan spesifik direncine ulaştıkları sıcaklıklarda yapılmış ve literatürle kıyaslandığında son derece uzun ömürlü oldukları sonucunu gözler önüne sermiştir. Bu çalışma doğrultusunda elde edilen çalışma sıcaklığına (575 °C) sahip olan LSC-113:LSC-214 =0.45:0.55 kompozisyonunun en düşük bozunma hızına sahip olduğu bulunmuştur. Bu katodun aynı hızla bozunduğu varsayıldığında, alan spesifik direnç değerinin, 10 000 saatlik çalışmanın ardından 0.15 $\Omega.cm^2$ den yaklaşık olarak 3 $\Omega.cm^2$ değerine çıkması beklenmektedir.

Anahtar Kelimeler: Orta sıcaklıklı KOYP katodu, LSC-113/LSC-214 çoklu yapı, eş zamanlı üretim, katyon çökelmesi, EIS.

Dedicated to my family

ACKNOWLEDGEMENTS

I would like to express my greatest thanks to my supervisor Prof. Dr. Tayfur Öztürk for his valuable guidance and support throughout this thesis work. His precious advices inspired me and enlightened my academic vision. I would also like to thank to my co-supervisor Assoc. Prof. Dr. Y. Eren Kalay for his continuous encouragement and motivation starting from my undergraduate education. During this work, the co-investigator Assoc. Prof. Dr. Yener Kuru was deceased on 03.04.2016. Although I could not get the chance of working with him, I know that he was a perfect advisor and a great scientist. Work reported in this study is fulfilled thanks to his deep academic vision.

I am also very thankful to Prof. Arcan F. Dericioğlu for his support in sample preparation, and to Dr. Meltem Sezen for her contributions in the preparation of TEM samples. Also, I am grateful to Prof. İshak Karakaya, Prof. Kadri Aydınol, Prof. Caner Durucan, Prof. Abdullah Öztürk and Assoc. Prof. H. Emrah Ünalan for their precious advices.

I owe great debt to Serkan Yılmaz, Fatih Pişkin and Berke Pişkin for their endless patience and guidance. And it was my privilege to share the same laboratory with Ezgi Onur Şahin, Cavit Eyövge, Sertaç Altınok, H. Gözde Yıldırım, H. Eda Aysal, Burak Aktekin, Pelin Livan and Necmi Avcı.

I am thankful to all the staff of the Metallurgical and Materials Engineering Dpt. and I would like to express my deepest gratitude to my dear friends and collegues Alper Şahin, Mertcan Başkan, Okan Pehlivan, Mehmet Kocabey, Selvi Kılıç, Burak Kaya, Ayşe Merve Genç Ünalan, Baran Tunç, Başar Süer, Kıvanç Alkan, Simge Bakır, Mustafacan Kutsal for their cheerful friendship and constant support in daily struggles and I would like to express special thanks to Fatih Sıkan and Sıla Ece Atabay for their extra support and being there whenever I need. I did my best with the help of my treasured friends, I will always remember their support and their heartfelt attitude.

Above all I am deeply indebted to my love Bengisu Yaşar. Her love, patience and endless support are the most precious treasures in my life and these treasures enlightened my way throughout this thesis study. She was always there to give me the power and confidence whenever I need.

This work is financially supported by the Scientific and Technological Research Council of Turkey (TUBITAK) with a project number 114M128. Due to his great contribution during this project, I acknowledge my project collegue Ziya Ç. Torunoğlu for his support and contributions enabling the achivements obtained in this project.

Last but not the least, I would like to thank to my parents, Sevda Sarı and Erdoğan Sarı for their endless support, patience, appreciation and encouragement throughout my entire life. I also thank to my great family for their understanding and support. I would like to express my hearthiest thanks to my brother Yiğitcan Sarı who has always been my best friend and the biggest supporter.

TABLE OF CONTENTS

LIST OF TABLES

TABLES

LIST OF FIGURES

FIGURES

CHAPTER 1

INTRODUCTION

Generation of clean, environmentally friendly and highly efficient electrical power by using renewable energy sources is one of the most fundamental requirements for future technology. There are number of different energy conversion devices in order to achieve this goal, but it is not easily achieved due to stringent material requirements. Fuel cells are efficient and environmentally friendly electrochemical energy conversion devices that convert the chemical energy of the fuel directly into electricity and heat. Similar to batteries, fuel cells generate electricity and heat via electrochemical combination of gaseous fuel and the oxidant gas. An advantage of this system is that it is not restricted by Carnot principles. Thus, higher energy efficiencies can be obtained compared to conventional thermo-mechanical methods. Furthermore, unlike batteries, fuel cells do not require charging and they are able to work as long as fuel is supplied. They can be operated with various hydrocarbons or with pure hydrogen depending on the type of the fuel cell.

Fuel cells are named depending on their operating principles and the electrolyte material used in the structure. They are categorized in six main groups; polymer electrolyte membrane (or proton exchange membrane) fuel cell (PEMFC), direct methanol fuel cell (DMFC), solid oxide fuel cell (SOFC), alkaline fuel cell (AFC), molten carbonate fuel cell (MCFC), and phosphoric acid fuel cell (PAFC). Of these PEMFC and SOFC are widely investigated systems.

PEMFCs use acidic polymer membranes as the electrolyte together with platinum based electrodes. Their operating temperatures are generally in the range of 80-100 $^{\circ}$C (except for high temperature PEMFC where it increases up to 200 $^{\circ}$C). These fuel cells

are appropriate for dynamic power requirements where fast start-up and shut-down processes are desired. Pure hydrogen is the only possible fuel type for PEMFCs due to low operating temperatures and their main problem is the high cost of platinum based electrodes. However, for sufficient hydrogen dissociation and protonic conduction platinum based electrodes are required at these temperatures. Therefore, in order to decrease the material cost it is important to develop new electrode materials.

Unlike PEMFC, oxygen ions instead of hydrogen are transported in the cathode and the electrolyte of SOFC which requires high operating temperatures. Therefore, SOFCs are high temperature fuel cells that have higher energy efficiencies than other versions. Moreover, SOFCs do not require precious metals as catalysis and they are not prone to floating and poisoning problems as in the case of low temperature fuel cells. Also, in SOFCs, all of the main components (anode, cathode and electrolyte) are rigid which makes the structure stronger and allows the fabrication of different geometries. During operation SOFCs produce a high quality heat as by-product and it is possible to use this heat via heat engines. For this type of SOFCs, the values of energy efficiencies can reach up to 70 % (Fu & Bazant, 2014). Although Rolls Royce, Siemens, and Westinghouse have developed operational SOFCs in the temperature range of 850–1000 $^{\circ}$C, they have not penetrated into the market because of the high operating temperatures (Brett et al. 2008). Although there are suitable materials that can function at these temperatures, it is very problematic to sustain required durability and to afford high material cost. Thus, in order to decrease the material cost and to increase the life time of the cell, it is necessary to reduce the operating temperature of SOFC. Therefore, efforts are concentrated towards the so-called intermediate temperature solid oxide fuel cells (IT-SOFC), i.e. cell that have acceptable performance between 500 - 700 ^{0}C.

While there are substantial improvements in anode and electrolyte materials for reduced operating temperature, this is not so for the cathode materials due to slow kinetics of cathodic processes. Exploration of novel materials have shown that it is possible to increase the cathode kinetics at intermediate temperatures. Especially, an

interface controlled hetero-structures of perovskite based composites have increased the kinetics of oxygen reduction and transportation. One such material was the composite formed by $La_{0.8}Sr_{0.2}CoO_{3\pm\delta}$ (LSC-113) and $(La_{0.5}Sr_{0.5})_2CoO_{4\pm\delta}$ (LSC-214) which has led to a considerable enhancement in the kinetics of cathodic processes (Sase et al. 2008). In many studies it was shown that the usage of perovskite based hetero-structures have made an enhancement on the order of magnitude which enables manufacturing novel SOFC that can operate at lower temperatures. However, these kind of hetero-structures especially LSC based ones still suffer from cation segregation at their operating regime which results in detrimental performance loss. Thus, there is a requirement for further increase in the cathode kinetics to increase the stability and performance of the whole structure.

Cathode materials are responsible for oxygen reduction reaction (ORR) which can be divided into several steps; oxygen surface exchange in which oxygen molecules are dissociated into oxygen ions, transportation of these ions to the cathode-electrolyte interface and electrochemical charge transfer between the cathode and the electrolyte. Therefore, the resistance of diffusion process in the cathode strongly depends on the thickness of the components. Thus, it is expected that for thin cathode layers the surface exchange kinetics become the rate determining step and it is possible to investigate the effect of hetero-structures which have high interface density at the surface. As a result, the surface exchange kinetics can be increased for thinner cathode layers which make it possible to reduce the operating temperature of SOFCs.

In this study, it is aimed to fabricate thin LSC-113/LSC-214 hetero-structure and to obtain the best composition via combinatorial approach. The maximum amount of interface is proposed to reach top levels of enhancement in LSC-113/LSC-214 system. For this purpose, thin films of LSC-113/LSC-214 cathodes have been co-deposited via magnetron sputtering technique. After a combinatorial fabrication of the thin film cathodes, the electrochemical performance of the symmetrical cells were analyzed with the help of electrochemical impedance spectroscopy (EIS) and electrical performance of full cells were measured to obtain the highest performance. Also,

chemical stability of new cathodes have been examined to determine the life time of the structure.

CHAPTER 2

LITERATURE REVIEW

2.1 Intermediate Temperature Solid Oxide Fuel Cells

Solid oxide fuel cells (SOFC) are one of the most promising energy conversion devices with the direct conversion of fuel energy into electricity and the production of high quality heat as by-product. The material demands increase with increasing operating temperature. This results in increased cost of material. Moreover, the durability of the structure is less due to large thermal stresses induced during heating and cooling processes. Therefore, the main trend in fuel cell research is to decrease the operating temperature of SOFCs to lower temperatures. The target was set to 500-700 °C, i.e. the so-called Intermediate Temperature SOFC (IT-SOFC) or even lower 300-500 °C, Low Temperature SOFC (LT-SOFC). To achieve such low operating temperatures all the components need to be modified.

Conceptually, SOFCs have simple operating principles. They include porous electrodes and a dense electrolyte, Figure 2.1. The electrodes are responsible for the ionization and transport of the fuel and the oxygen. The electrolyte has the role of isolating the electrodes but forming an ionic bridge between them.

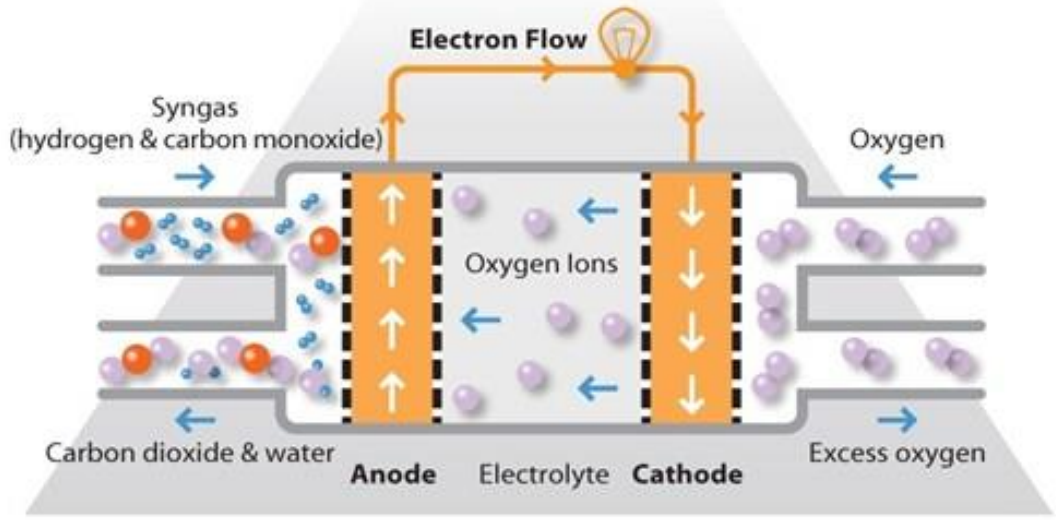

Figure 2. 1. Schematic representation of SOFC operation

Each component should possess special properties to fulfill requirements in the overall operation. In addition, all of the components should be able to perform in harmony in order to satisfy chemical and mechanical stability. Therefore, material selection is the key to the development of intermediate temperature SOFCs.

As it can be seen from Fig. 2.1, the oxygen molecules generally from air are supplied to the cathode surface and are reduced to oxygen ions given below.

$$\tfrac{1}{2}\, O_2\,(g) + 2e^- \rightarrow O^{2-} \qquad \text{(Eqn. 2.1)}$$

The oxygen reduction reaction is often abbreviated as ORR. The oxygen ions produced via ORR are transported to the electrolyte and crosses to the anode side. Since the easiest path for oxygen reduction and diffusion to the electrolyte is the triple phase boundaries (TPB), i.e. boundary formed by electrolyte, cathode and air, it is necessary/preferable to use porous cathode so that air can penetrate into the structure establishing contact with both the electrolyte and the cathode. The cathode material should be electronically conductive and preferably ionically conductive as well.

The main function of electrolyte is the transport of oxygen ions that are formed by ORR to the anode side where they will react with fuel. Therefore, electrolytes are pure oxygen ion conductors. They are insulators in terms of electronic conductivity. Since otherwise there would be short circuiting in the cell. The electrolyte is also responsible for the separation of fuel and air compartments in the cell. Thus, they are fully dense allowing neither gas passage nor anode-to-cathode contact. Since they are in contact with both oxidizing (cathode side) and reducing (anode side) atmospheres, they should be chemically stable enough to withstand these conditions at the operating temperatures.

Anode is defined as fuel electrode since it has a direct contact with the fuel and responsible for the reduction and transportation of hydrogen or reformed hydrocarbons. Therefore, a proper anode should have high protonic conductivity to carry reduced protons to the electrolyte where they meet with oxygen ions and oxidized.

$$H_2 + CO + 2O^{2-} = H_2O + CO_2 + 4e^- \quad \text{(Eqn. 2.2)}$$

As a result, electrons are produced and these electrons should be transferred to the external circuit via current collectors as shown in Fig. 2.1. Thus, besides having good protonic conductivity, electronic conductivity of the anode material should be as high as possible. Similar to the cathode, an anode should be porous to distribute the gaseous fuel and to remove produced gases such as water vapor and CO_2-CO mixture (in the case of hydrocarbon fuels other than hydrogen). The amount of porosity is proportional to the amount of triple phase boundary which facilitates the oxidation of the fuel and increases the overall performance of SOFCs.

In addition to these requirements stated above, the components must be chemically and mechanically stable during operation. In general, the formation of any kind of insulating phase between anode and electrolyte or electrolyte and cathode has a detrimental effect on the overall performance and life time of SOFC. Moreover, the components should have small mismatch in the thermal expansion coefficient to decrease the thermal stresses during start-up and shut-down.

2.1.1 Anode

Because of stringent necessities stated in Section 2.1, cermets are commonly used anode materials taking the advantage of both of the components. It should be mentioned that single phase metallic anodes often undergo sintering at operating temperature which decreases the three phase boundary junctions, negatively affecting the performance. Thus, anodes are often made as cermets, i.e. by mixing an oxide with a metallic component. The oxide is often the same oxide as electrolyte while metallic component is either Ni or Cu.

Yttria stabilized zirconia (YSZ) based cermets are one of the most common anode materials since they enhance the chemical and mechanical compatibility with YSZ electrolytes. Required electronic conductivity is generally provided by metallic components like nickel, cobalt or iron. Nickel is generally selected to form YSZ based cermet anodes because of the high cost of cobalt based cermets and corrosion problems in iron based cermets under reducing atmospheres (Shaikh et al. 2015). Ni-YSZ cermets which were first introduced by Spacil in 1970, have the advantages of matched thermal expansion coefficients and low amount of nickel aggregation that can be seen in single Ni phase anodes. Spacil has stated that the nickel is responsible for the overall electron flow in the anode since YSZ is electronically insulative. Therefore, the minimum amount of nickel in the cermet is determined by the continuity of nickel skeleton through the anode. On the other hand, the presence of YSZ islands which may be discontinuous, prevents the excess grain growth of nickel particles and thus, contribute to the stability of the anode.

Chen et al. (2011) applied a phase field approach to simulate the TPB reduction with respect to Ni coarsening in Ni-YSZ anodes. The authors have shown that the major portion of TPB reduction occurs at the beginning of the coarsening and this effect is minimized when YSZ skeleton, the supporting structure, has a larger proportion. As a result, the relative amount of YSZ in the cermet should be as high as possible to increase the life time of the anode. C. Lee et al. (1997) studied the effect of

microstructure to the anodic properties in Ni-YSZ system. Their results indicate that the best Ni loading in this system is obtained with 45 vol % Ni. They further found that when Ni loading is around 55-60 vol % cermets show high electrode activities, but the sintering of Ni particles decreases the performance with a continued cell operation. On the other hand, when Ni loading is lower than 35 vol %, this results in the reduction in TPB due to low Ni population. Additionally, they showed that similar size particles of NiO and YSZ yields the best cermet with a well-developed network structure along with rich TPB sites for the electrode reaction.

As stated by Zhu and Deevi (2003) the electronic conductivity of the anode increases with increasing Ni loading up to a certain point which is around 40 vol %. Then, further increase of Ni content does not contribute to the electronic conductivity of the anode and increases the rate of degradation. Thus, it is important to keep Ni content below 40 vol %.

Ni-YSZ anodes are well established anode materials, especially when the fuel is hydrogen. For the use of hydrocarbons, on the other hand, Ni-YSZ anodes fail since nickel catalyzes the carbon formation resulting in the so-called carbon poisoning with performance loss in the anode. Furthermore, sulfur poisoning may also occur in Ni-YSZ anodes resulting in loss of catalytic activity and of conductivity. Thus, development of alternative cermets have gained importance in recent years.

In order to prevent carbon formation, nickel is replaced with metals that are poor catalysts for carbon formation. In terms of cost and stability under anodic conditions, copper is one of the best alternatives for this purpose. Although copper based anodes show lower electro-catalytic activity towards fuel oxidation, they are intolerant to the carbon formation in the case of methane or other hydrocarbons.

There are number of studies that focuses on the comparison of Cu bearing and Ni bearing cermets as anode materials. Kim et al. (2002) have investigated the effect of alloying Ni with Cu in the performance and stability of YSZ anodes for direct oxidation of methane in SOFCs. In this study, the alloy composition was varied from 0, 50, 80, 90 up to 100% Cu and found that Ni-80% Cu composition was the best in

terms of power density. They also reported that the carbon formation is greatly suppressed on the Cu-Ni alloys compared to that of pure Ni. Horn et al. (2007), in a similar study on ceria based anodes, found that the use of Cu and Cu-Ni was beneficial in reducing the amount of carbon deposit. Sin et al. (2007), have tested the life time of NiCu-GDC anodes for direct oxidation of dry methane at 800 ^{0}C. They observed that NiCu alloy was stable for 1300 hours of operation. As a result, they concluded that alloying Ni with Cu creates a bridge between proper catalytic activity and the resistance to carbon poisoning.

A fraction of studies have focused on comparison between alternative ceramic constituent in the anode. Ceria is an alternative to zirconia which is particularly suitable for hydrocarbon fuels. It should be mentioned that the ceria have the same oxygen deficient fluorite structure as Yttria stabilized Zirconia (YSZ). Ceria is normally doped with rare earth elements for this purpose. Rare earth doped ceria is also resistant to sulfur poisoning. In addition to that, Ce^{4+}/Ce^{3+} redox couple has a low enough energy to be catalytically active for CO and hydrocarbon oxidation (Goodenough & Huang, 2007).

Iwanschitz et al. (2010) have compared the degradation of Ni-YSZ and Ni-GDC cermets upon redox cycling and showed that the degradation mechanisms were different in these two systems. At higher operating temperatures (around 950 ºC) both systems show an increase in the polarization and ohmic resistances. However, when the temperature is decreased to 850 ºC Ni-GDC system represents a stable performance whereas Ni-YSZ system degrades with continued use. Therefore, at low temperatures, i.e. 850 ºC, Ni-GDC system can be selected as an alternative of the common Ni-YSZ system. Lee et al. (2017) have compared Ni-YSZ system with Ni-GDC system for direct oxidation of methane under conditions of catalytic partial oxidation. According to their findings, Ni-GDC anode exhibits very high power densities (1.35 W/cm^2) compared to that of Ni-YSZ system (0.27 W/cm^2) at 650 ºC. Additionally they have also noted that there was a gradual degradation in the performance of Ni-YSZ system, whereas the power density values were stable for Ni-GDC system over 500 h of

operation. They have suggested that the use of GDC prevented the carbon poisoning of Ni, resulting in a more stable operation, Fig 2.2.

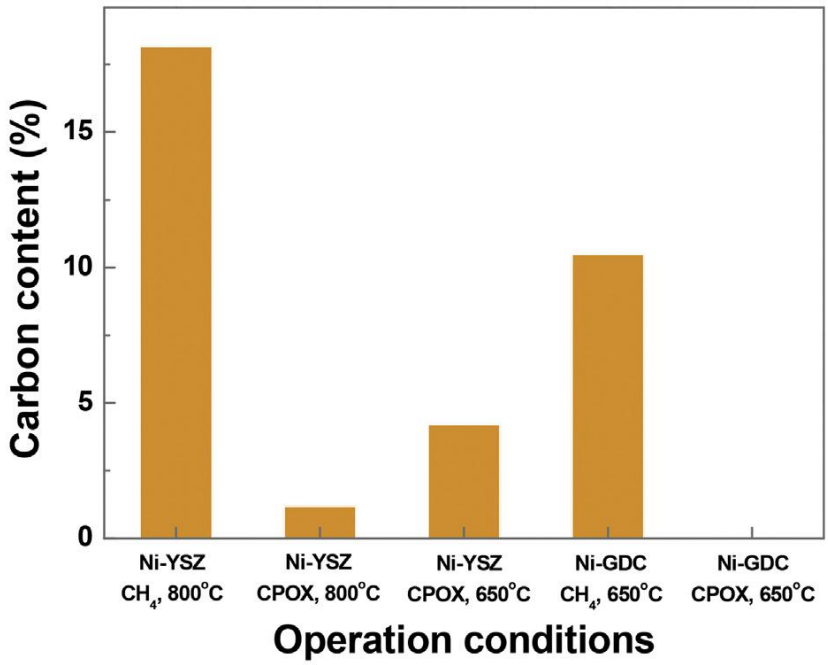

Figure 2. 2. Carbon contents of cells after electrochemical measurements for 5 hours (Lee D. et al. Journal of Power Sources 345 (2017) 30-40)

Zhang et al., (2010) in a similar study compared GDC with YSZ in terms of sulfur poisoning at 800 ^{0}C. They examined the activity and performance of these anodes in H_2 fuels with various H_2S contents. The anode potential in both cermets have decreased at higher H_2S contents. However, the decrease in Ni-GDC cermets was less than that in Ni-YSZ. They reported a decrease of 0.78 V to 0.72 V in Ni-GDC compared to a decrease of 0.61 V to 0.34 V in Ni-YSZ. They concluded that the Ni-GDC anodes was more tolerant to sulfur poisoning than Ni-YSZ anodes.

Matsui et al. (2012) have studied the anode stability in the presence of water vapor. They noted that Ni-YSZ cermets show an abrupt performance deterioration due to increased partial pressure of water vapor. They have compared the performances of

Ni-YSZ, Ni-ScSZ and Ni-SDC anodes in constant current operation. They found that there was no change in the performance of the cell with Ni–SDC anode, whereas the ohmic resistances of the cells with Ni-YSZ and Ni-ScSZ anodes increased implying sudden anode degradation.

Similar studies focusing on alternative ceramic constituents were also carried out when the metallic constituent was Cu. Gorte et al. (2000) have compared YSZ with GDC and found a better performance in the case of Cu-GDC, i.e. Cu-GDC had a maximum power density of 0.15 W/cm^2. This value should be compared with 0.03 W/cm^2 obtained with Cu-YSZ. Zhan & Ik (2010) have investigated the performance of Cu-YSZ and Cu-samarium doped ceria (SDC) systems with two types of fuels; hydrogen and propane at 800 ^{o}C. According to their findings, the maximum power densities of Cu-SDC system were higher than Cu-YSZ system with both fuels. Additionally, electrochemical impedance spectroscopies of the systems revealed that the anodic polarization resistance was much lower in the case of Cu-SDC anode.

In addition to these cermets, where the anode is a metal-ceramic composite, it is possible to use single phase material as anode material also. In this respect mixed ionic and electronic conductive materials fulfill the requirements without the use of any second phase. Therefore, perovskite based mixed ionic conductive materials have attracted considerable attention in recent years.

Scribe et al. (2006) have studied several double perovskites as possible anode materials for SOFCs that can be used with natural gas in the temperature range of 650-1000 ^{0}C. Among the compositions they studied, Sr_2MgMoO_{6-y} was the most promising candidate yielding 642 mW/cm^2 at 750 ^{0}C with hydrogen as a fuel. The performance of Sr_2MgMoO_{6-y} was stable for 2 days of operation without formation of any sulfur or carbon species. Zhang et al. (2010) have studied different double perovskite systems A_2FeMoO_{6-d} where A = Ca, Sr, Ba and they have concluded that the performances of cells with the same electrolyte and cathode follow the sequence of Sr> Ba> Ca. They have obtained a maximum power density of 831 mW/cm^2 in dry H_2 and 735 mW/cm^2 in commercial city gas for a cell with Sr_2FeMoO_{6-d} anode at 850 ^{0}C.

The field of exploring new anode materials and the performance enhancement of available anodes still constitutes one of the major research fields for solid oxide fuel cells. Currently, although Ni-YSZ cermet is an established material for anode, Cu-GDC seems to offer advantages, especially in 500-600 ^{0}C. They seem to offer better resistance to formation of carbonecous species and sulfur resistance.

2.1.2 Electrolyte

Electrolytes are mainly responsible for the transport of oxygen ions from cathode side to the anode side. Conventional electrolytes have a fluorite type (AO_2) crystal structures which provides high oxide-ion conductivities. Zirconia (ZrO_2) and ceria (CeO_2) based fluorites are the most commonly used electrolytes in SOFCs. In addition to these, there is a considerable research in perovskite based electrolytes. The ionic conductivities of these electrolytes are strongly depended on temperature which determines their working range as given in Fig. 2.3.

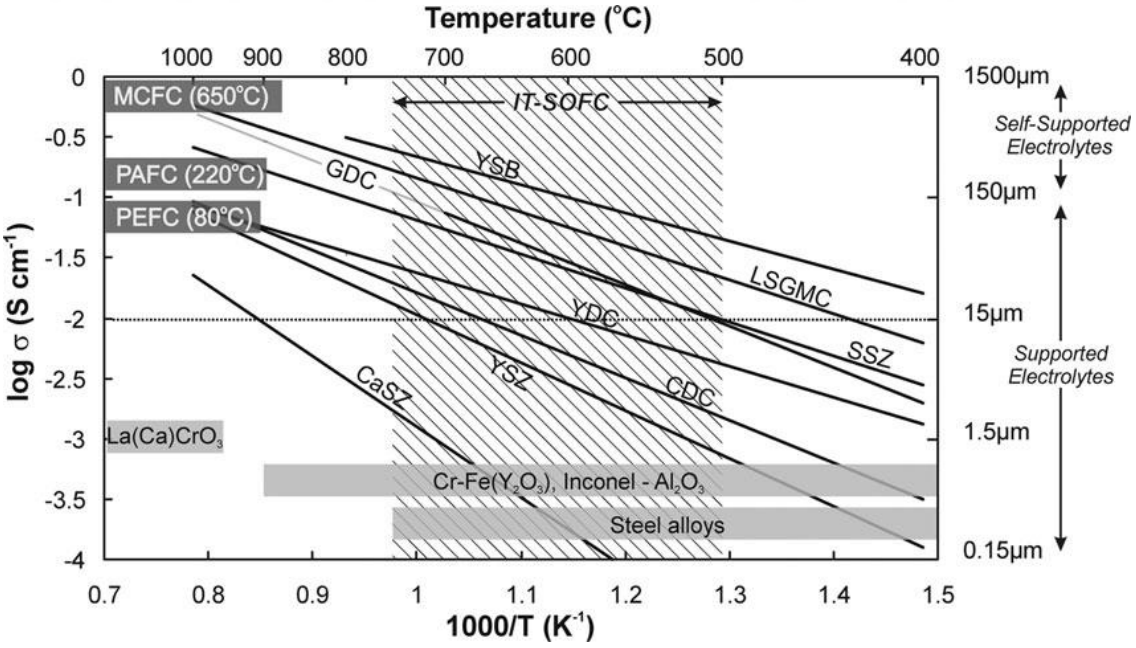

Figure 2. 3. Specific ionic conductivities of common electrolytes as a function of reciprocal temperature. (Brett et al. 2008)

Pure zirconia has the desired cubic fluorite structure only above 2300 ^{0}C, therefore it is necessary to dope it by divalent cations so as to stabilize it at lower temperature (Malavasi et al. 2010). As dopant, yttria is the most common, though alternatives are calcia and scandia, i.e. calcia - stabilized zirconia (CSZ) and scandia-stabilized zirconia (ScSZ).

YSZ is widely used electrolyte material in SOFC application due to its high ionic conductivity. Although, the stability of cubic fluorite structure increases with the dopant level, the highest ionic conductivity is obtained with 8 mol % of yttria. In addition to high ionic conductivities, YSZ is almost perfect insulator in terms of electronic conduction. Another advantage of YSZ electrolytes is their ability to work in harmony with well known anode, Ni-YSZ. Therefore, YSZ with 8 mol % yttria seems to be one of the best electrolyte materials at high operating temperatures (> 900 ^{0}C). However, for IT-SOFCs where the operating temperature lies between 500 ^{0}C and 700 ^{0}C, the ionic conductivity of YSZ is less than satisfactory.

Han et al. (2010) have used sol-gel synthesis to fabricate nano-structured YSZ and they produced very fine YSZ nanomaterials with an average particle size of 7 nm in a narrow distribution. The gas tightness were satisfied with 3 μm thick YSZ layers. They have measured acceptably high power densities (around 600 mW/cm^2) at 800 ^{0}C. This enhanced electrochemical performance was attributed to the nano-structured YSZ electrolyte. As a way of reducing the cost of YSZ, Thokchom et al., (2008) used YSZ-Al_2O_3 (20 wt %) composite electrolyte and found enhanced conductivity at temperatures lower than 900 ^{0}C. suitable for IT-SOFCs. According to their results, the peak power density of the cell working with propane and with a Cu–CeO_2 anode and LSM cathode was around 16 mW/cm^2 at 700 ^{0}C.

Chen et al. designed YSZ/SCSZ/YSZ layered electrolytes for IT-SOFCs. This layered electrolyte has the advantage that SCSZ gives high ionic conductivity while thin YSZ layers provides chemical stability and electronic insulation. They also obtained an enhanced mechanical strength due to residual thermal stresses coming from the thermal mismatches of different layers.

As it can be seen from Figure 2.3 ScSZ has the highest ionic conductivity at all temperatures among zirconia based systems. Therefore, it seems to be the best alternative for lowering the operating temperature. The use of scandium increases the material cost.

Young et al. (2015) produced a single layer thin film ScSZ electrolyte with a thickness of 280 nm via RF sputtering. They obtained a peak power densities of 227 mW/cm^2 at 500 $^{\circ}C$. Although the results indicate that ScSZ is suitable in the intermediate temperature regime due to its superior ionic conductivities than YSZ, electronically it is less resistive than YSZ as indicated by Chen et al. (2012). Badwal (2001) has investigated the conductivity of several doping level in ScSZ system. They showed that for low doping levels (7-9 mol%) the presence of metastable t' phase leads to degradation in the ionic conductivity while for doping levels higher than 9 mol % the system becomes more stable. Furthermore, for compositions of above 9 %, e.g. 10 and 11 mol % Scandia, a rhombohedral beta phase occurs during heating and cooling adversely affecting the ionic conductivity. Therefore, they have concluded that the best composition for ScSZ was 9.3 mol % Scandia. For further stabilization of the zirconia system, Politova and Irvine (2004) have co-doped zirconia with yttria and scandia and investigated the conductivity of ternary system, $(Y_2O_3)_x(Sc_2O_3)_{(11-x)}(ZrO_2)_{89}$ where x=0-11. They found that the ionic conductivity was adversely affected by yttria content, though this contributed positively to the stability of the electrolyte e.g. the electrolyte was quite stable when annealed at 800 ^0C for 1500 hours.

One of the main problems of zirconia based electrolytes are their reactions with some of the electrodes materials. For instance they form insulating secondary phases by reacting with barium and/or lanthanum bearing electrodes. The most common technique to prevent this, is the application of buffer layers between the main electrolyte and the electrodes. Shi et al. (2011) compared ScSZ electrolytes with and without Samarium doped Ceria (SDC) ($Sm_{0.2}Ce_{0.8}O_{1.9}$) interlayers. They obtained a better performance with the addition of SDC interlayer. Other kinds of interlayers are

also very common in literature to increase the chemical stability between zirconia based electrolytes and lanthanum or barium bearing electrodes.

As it can be seen from the literature, zirconia based electrolytes face with several problems; unsatisfactory ionic conductivities at temperatures lower than 900 ^{0}C and low chemical stability with some of the common electrode materials. However, their superior electronic insulating characteristics and well known fluorite structures keep them as the most common electrolyte materials for solid oxide fuel cells.

Another common fluorite type electrolyte materials is based on ceria with the dopants of samarium (SDC) and gadolinium (GDC). These oxides show much higher ionic conductivities especially at intermediate temperatures (700-500 ^{0}C).

Leng et al. (2004) produced GDC based SOFC cell where they obtained very large power densities of, 625 mW/cm^2 at 600 ^{0}C. Here, Ni-GDC cermet was the anode and $La_{0.8}Sr_{0.2}Co_{0.2}Fe_{0.8}O_3$ (LSCF)-GDC composite was the cathode and the electrolyte was 4 μm thick dense GDC. Omar et al. (2008) applied a co-doping strategy to improve the ionic conductivity of the ceria and obtained 30 % higher conductivity at 550 ^{0}C in $Sm_{0.075}Nd_{0.075}Ce_{0.85}O_{2-\delta}$ composition as compared to classically doped GDC electrolyte.

The main drawback in ceria based electrolyte is their electronic insulation is less than acceptable. In order to improve the insulation characteristics Soo et al., (2009) used $Er_{0.8}Bi_{1.2}O_3$ (ESB) / GDC bi-layered electrolyte. While ESB blocked the electronic conduction in electrolyte, GDC layer prevented possible decomposition of ESB layer and as a result they obtained quite high power densities, 1.95 W/cm^2 at 650 ^{0}C.

Perovskite electrolytes are also a common group in SOFC application. The most common member of this group is doped lanthanum gallate, with the formula of $La_{1-x}A_xGa_{1-y}B_yO_{3-d}$ (LSGM). In general, dopant A is selected as strontium and dopant B is magnesium. LSGM is a promising purely ionic electrolyte material with conductivities higher than YSZ especially at low temperatures.

Doping levels of Sr and Mg in LSGM electrolyte determines the amount of oxygen vacancies in the structure which is directly related to the conductivity of the electrolyte. Lu and Zhu (2008) carried out a study focusing on the effect of Sr and Mg doping on the property and performance of LSGM electrolyte. It was shown that, strontium and magnesium doping has a positive effect in terms of conductivity as was expected. The composition of $La_{0.8}Sr_{0.2}Ga_{0.83}Mg_{0.17}O_{3-d}$ exhibited the highest power density 1.23 W/cm^2 and 0.66 W/cm^2 at 800 and 700 ˚C respectively where $La_{0.4}Ce_{0.6}O_{1.8}$ (LDC) + Ni was the anode $SrCo_{0.8}Fe_{0.2}O_{-d}$ (SCF) was the cathode. Also, the doping level have almost no effect on the thermal expansion coefficient of the material. They obtained a stable cell performance (only 10% loss in power density) at 800 ˚C for operation of 500 hours.

Enoki et al. (2006) applied co-doping for the B-site cation in lanthanum gallate system. They used strontium as an A-site dopant while iron and magnesium is used together for B-site. By partial substitution of Mg with Fe, their purpose was to increase the ionic conductivity at lower temperatures. They obtained quite a high power densities at temperatures lower than 600 ˚C. Their report showed that $La_{0.7}Sr_{0.3}Ga_{0.7}Fe_{0.2}Mg_{0.1}O_3$ as the best composition and quoted a value of 78 mW/cm^2 as power density at 500 ˚C with the electrolyte that was 0.5 mm thick.

Ishihara et al. (2006) have partially substituted magnesium with cobalt instead of iron in synthesizing $La_{0.8}Sr_{0.2}Ga_{0.8}Mg_{0.15}Co_{0.05}O_3$ (LSGMC) electrolyte. They report a fairly large maximum power densities for this system, namely 200 mW/cm^2 and 120 mW/cm^2 at 600 and 500 ˚C, respectively. They concluded that LSGMC system can decrease the operating temperature of SOFCs to 500 ˚C with the optimization of cobalt content. In this study, Ni–$Sm_{0.2}Ce_{0.8}O_2$ was anode and $Sm_{0.5}Sr_{0.5}CoO_3$ was cathode. They have applied lanthanum doped ceria buffer layer between anode and electrolyte.

Although perovskite-structured lanthanum gallate have quite high potential as an electrolyte material, they are subject to interfacial reaction with anode. At the interface they form an insulating lanthanum nickellates ($LaNiO_3$) (Malavasi et al. 2010). In response of this, it is often necessary to apply a buffer layer, normally in the form of a

thin layer of lanthanum or gadolinium doped ceria applied to anode facing side of the electrolyte. Gong et al. (2006) have compared GDC with LDC and arrived to the conclusion, LDC was much more effective as a buffer layer. Lee et al. (2008) have investigated LSGM electrolyte using $La_{0.8}Sr_{0.2}Ga_{0.8}Mg_{0.2}O_{3-d}$ composition with LDC buffer layer at different temperatures. They reported 664 and 459 mW/cm^2 power densities at 800 and 750 ^{0}C, respectively. It was also shown that the open circuit voltage was lower than the theoretical value when the electrolyte was thin (20 μm). This was attributed to the fact that, electronic flow was not prevented in the case of thinner layers. The open circuit voltage was very close to theoretical value when the electrolyte is thickened to 60 μm.

Another way to increase the conductivity of ceria based electrolytes at intermediate temperatures are forming oxide-inorganic salt composites such as chlorides or carbonates (Figure 2.4).

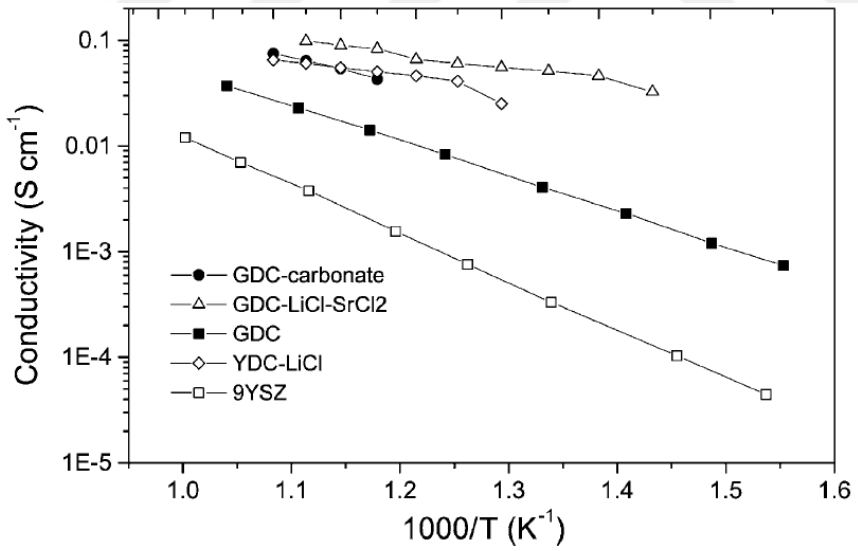

Figure 2. 4. Temperature dependence of ionic conductivity of ceria based electrolytes.

Meng et al. (2002) used of GDC–LiCl–$SrCl_2$, YDC–LiCl, GDC–LiCl and GDC–Li_2CO_3–K_2CO_3 composite electrolytes and showed that the ionic conductivity could be increased by one order of magnitude. This was mainly attributed to the dissimilar interface regions formed between doped ceria phase and the salt phase. They measured promising power densities of around 350 mW/cm^2 at 600 ^{0}C although the electrolyte layer of the samples were very thick (400 μm). In another study of the same group, Fu et al. (2002) obtained a power density of 240 mW/cm^2 at 500 ^{0}C with GDC–LiCl–$SrCl_2$ electrolyte.

Raza et al. (2010) also studied nanocomposite of SDC with Na_2CO_3. They measured the peak power density of the cell as 1150 mW/cm^2 at 500 ^{0}C. They concluded that the carbonate phase was amorphous at these temperatures (Figure 2.5) which facilitates ionic conductivity while decreasing the electronic conductivity of the electrolyte.

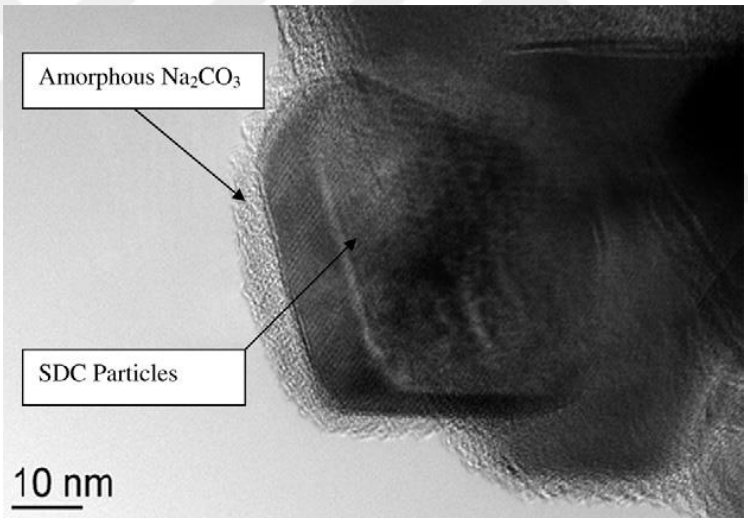

Figure 2. 5. High-resolution TEM images of SDC–Na_2CO_3 composite, (Li et al. 2009).

Li, et al. (2009) have reviewed different ceramic-carbonate composite electrolytes (CCCE) and reported SDC-Li/Na_2CO_3 (30 wt %) composite material as the most promising composition which yielded a power density value of 1.7 W/cm^2 at 650 ^{0}C (Table 2.1).

Table 2. 1. Power densities of ceria based CCCE systems at different temperature ranges. (Li, et al. 2009)

Ceria	Carbonates	Power density ($W\,cm^{-2}$)	T (°C)
GDC	22 wt.% of Li/Na_2CO_3 (2/1, mol.%)	0.20–0.78	400–660
GDC	40 wt.% of Li/K_2CO_3 (62/38, mol.%)	0.07–0.30	480–530
YDC	22 wt.% of Li/Na_2CO_3 (2/1, mol.%)	0.20–0.70	400–660
SDC	22 wt.% of Li/Na_2CO_3 (2/1, mol.%)	0.20–0.80	400–600
SDC	25 wt.% of Li/Na_2CO_3 (53:47, mol%)	0.10–1.10	400–600
SDC	30 wt.% of Li/K_2CO_3(62/38, mol.%)	0.27–0.57	400–600
SDC	30 wt.% of Li/Na/K_2CO_3(43.5/31.5/25, mol.%)	0.10–0.72	500–650
SDC	30 wt.% of Li/Na_2CO_3 (1/1, mol.%)	0.30–1.70	500–650

Although ceria-carbonate based electrolytes are quite promising, it is necessary to improve the durability of the electrolyte. According to Zhang et al. (2010) sort of interaction exists between doped ceria and carbonates. As a consequence of this interaction, the power density of the system is not stable and decreases with time. Thus, ceramic-carbonate composite electrolytes should be further improved in terms of chemical stability under working conditions.

In addition to the materials given above, there are also other alternatives such as $La_2Mo_2O_9$ (LAMOX), $Bi_4V_2O_{11}$ (BIMEVOX), fluorite-type Bi_2O_3, silicon and/or germanium apatites, and tetrahedrally-coordinated gallium oxides ($La_{1-x}Ba_{1+x}GaO_{4-x/2}$) (Malavasi et al. 2010). Moreover, different hetero-structures, i.e. phase mixtures, are under investigation with the aim of lowering the operating temperature of SOFCs. Although, these alternative electrolytes show promising ionic conductivities, YSZ and GDC based systems are currently the most popular electrolytes.

2.1.3 Cathode

Cathodes are responsible for the reduction of gaseous oxygen and then transport and incorporation of oxygen ions into the electrolyte. Similar to anode, they should be electrically conductive and preferably porous. Though not essential, it is preferable to have high ionic conductivity to facilitate the ionic diffusion through the cathode. Detailed review of operating mechanism and factors affecting the kinetics of cathodic processes will be given in Section 2.2. Because of this, here only a brief review will be presented on the cathode materials.

Noble metals due to their high ORR activity and conductivity can be used as cathode materials. However, the field of material research for cathodes is dominated by perovskites. There are plenty of options as perovskite cathodes (ABO_3). Here, the A-site cation is a combination of alkaline and rare earths (La, Sr, Ca, or Ba). The B-site is made up of reducible transition metals such as manganese, cobalt, iron, and nickel. They are generally classified as manganites, ferrites, nickelates, cobaltites, and their combination.

Manganites are commonly used at high operating temperatures namely 800-1000 °C. Among variety of manganite systems, $La_{1-x}Sr_xMnO_{3\pm d}$ (LSM) is the most common. Normally, doping in most perovskite oxides changes the stoichiometry and creates oxygen vacancies which help to improve ORR kinetics, but in the case of LSM the purpose of doping with Sr is different and its primary effect is to help improving the electronic conductivity (Sun et al. 2010). The electronic conductivity depends on doping level and it increases up to x = 0.50:50.

The main problem with LSM is that it reacts with YSZ, which is a common electrolyte material. Lanthanum zirconate (LZ) and/or strontium zirconate (SZ) which are formed as a result of this reaction act as a barrier for ion transport and decreases the cell performance. In addition, since LSM has a low ionic conductivity the diffusion of oxygen ions is restricted to TPBs, since the bulk LSM makes very little contribution in the ionic transport. To improve ionic transport it is a common practice to mix LSM

with the electrolyte material. A very popular example is LSM/YSZ mixtures. Suzuki et al. (2006) studying LSM-YSZ composite have obtained an area specific resistance value (ASR) of 0.14 $\Omega.cm^2$ at 800 °C. They reported a power density of 0.26 W/cm^2 at 850 °C in a cell where Ni-YSZ was anode and YSZ was electrolyte. Although this system yields high power densities at high temperatures, the system is not stable enough since it suffers from LZ and/or SZ formation in long term use (Aijie et al. 2008).

In recent years, substitution of manganese by cobalt and/or nickel as an alternative method of increasing the ionic conductivity in LSM is widely investigated. By this way it was also possible to decrease the operating temperature of the cathode. Gupta et al. (2009) have studied such a system in $La_{0.75}Sr_{0.25}Mn_{0.95-x}Co_xNi_{0.05}O_{3+d}$ ($0.1 \leq x \leq 0.3$) where the manganese was partially substituted by cobalt and nickel at around 600°C, (Fig. 2.6).

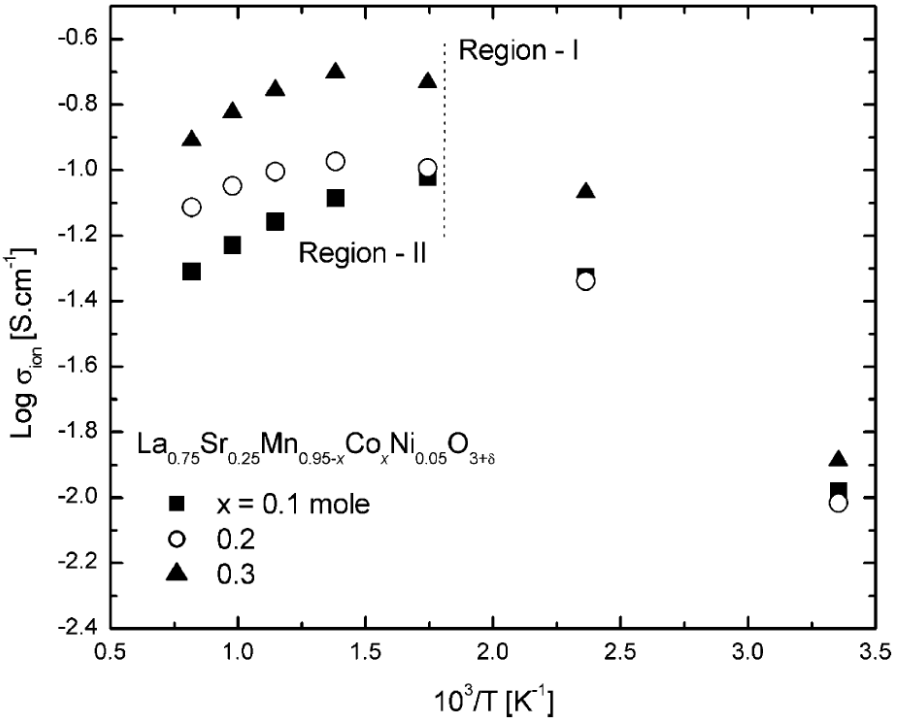

Figure 2. 6. Logarithm of ionic conductivity (σ_{ion}) versus 1/T plots for $La_{0.75}Sr_{0.25}Mn_{0.95-x}Co_xNi_{0.05}O_{3+d}$ ($0.1 \leq x \leq 0.3$)

They showed that the ionic conductivity of the system was increased by an order of magnitude with increasing cobalt content, this was at the expense of a decrease in the electronic conductivity. Additionally, no secondary phase was obtained between the cathode and YSZ electrolyte. Therefore, it is concluded that the cathode can be operated at around 600°C. In a similar study, Bai et al. (2012) tested the stability of $La_{0.8}Sr_{0.2}Co_{0.17}Mn_{0.83}O_{3-d}$ cathode with YSZ and found that the system was highly stable even at temperatures as high as 1150 °C.

There are other alternative manganites that also operate at reduced temperatures. It was shown that the use of Nd, Pr, Gd, Bi, and Sm instead of La, prevented the formation of Zirconate phases and increased the life time of the system by an order of magnitude. Thus, Li et al. (2015) studied $Sm_xSr_{1-x}MnO_3$ cathodes with x = 0.3, 0.5 and 0.8 and have measured the oxygen reduction reaction activity and compared them with the conventional LSM cathode. They found that SSM cathodes were better than LSM in terms of electrochemical activity and the highest activity of oxygen reduction reaction was obtained with $Sm_{0.5}Sr_{0.5}MnO_3$ at all temperatures in the range of 800-650 °C. Similarly, Liu et al. (2011) studied $Bi_{0.5}Sr_{0.5}MnO_3$ (BSM) and BSM-SDC composites as novel cathodes for IT-SOFCs and reported power density values of 277 mW/cm^2 (BSM) and 349 mW/cm^2 (BSM-SDC) at 600 °C, much higher than the power densities of LSM. In this study, the electronic conductivity of the cathode was around 82–200 S/cm in the temperature range of 800-600 °C which makes it highly suitable for cathode application. Although the oxygen ion diffusivity of BSM was already much higher than that of LSM, Liu et al. further improved this by mixing BSM with SDC. Authors further pointed out that the use of BSM together with YSZ electrolyte was unsuitable as they react with each other forming undesirable SZ phases. Instead, the system was chemically compatible with ceria based electrolytes e.g. SDC.

As it is summarized above, various approaches could be used to decrease the operating temperature of manganite based cathode materials. Although the results are quite promising, the levels of ionic conductivities and electrochemical activities required for

IT-SOFCs normally are much higher which makes it necessary to switch to a more favorable oxide system.

Ferrite based cathodes are another group of cathodes for IT-SOFCs. They are more stable than cobaltites in terms of their reactivity with YSZ electrolyte. Unfortunately their ionic conductivities are not as good as cobaltites. One such ferrite $LaFeO_3$ was investigated by Bidrawn et al. (2008) where the A site was doped with Ca, Sr, and Ba. They found that strontium doping was quite effective in improving the ionic conductivity and performance, in the temperature range 800-650 °C. Yu et al. (2014) studying $SrFe_{1-x}Ti_xO_{3-d}$ (SFT) system measured the cathode performance at different titanium doping level. The maximum power density of 475 mW/cm^2 was obtained with the doping level of Ti=0.05 at 800 °C. They increased the power density up to 605 mW/cm^2 with the composite of SFT and samarium doped ceria (SDC). In a similar study of $SrFe_{0.75}Mo_{0.25}O_3$ (SFMO), Zhou et al. (2014) revealed that the operating temperatures could be decreased to 700 °C with a power density of 221 mW/cm^2. They have combined SFMO cathode with YSZ electrolyte to increase the ionic conductivity and to sustain chemical compatibility with the electrolyte. Niu et al. (2011) compared the cathode kinetics of bismuth and lanthanum doped $SrFeO_{3-d}$ and represented that LSF has higher oxygen diffusion coefficient than BSF. Similar other studies indicate that strontium doped lanthanum systems exhibit higher cathodic kinetics and more suitable for IT-SOFCs but it is still required to enhance the ORR activity and ionic conductivity of ferrite based cathodes.

Another system that has attracted considerable interest was cobalt-based cathodes. Cobaltites are the so-called MIEC oxide, i.e. mixed ionic and electronic conductor. MEIC oxides in particular LSC based cobaltites are the subject of this thesis and the topic will be reviewed in greater detail in a separate section below. The main drawbacks of cobaltites are high thermal expansion coefficients. Also they are quite reactive with YSZ electrolytes even at intermediate temperatures. As a result, insulating phases occur at the cathode/electrolyte interface and lead to fast degradation of the structure.

It was shown in many studies that, strontium doped lanthanum cobaltite ($La_{1-x}Sr_xCoO_{3-d}$) are the most promising candidates for IT-SOFCs, due to their enormous mixed ionic and electronic conductivities and high ORR activities. A major problem with cobaltites is that they have high CTE which constitutes a thermal mismatch with electrolyte. Therefore rather than pure cobaltites many of the studies made use of ferrocobaltites which have acceptable CTE values. Kim et al. (2010) have compared the electrochemical performance of a ferrocobaltite, namely $La_{0.6}Sr_{0.4}Co_{0.8}Fe_{0.2}O_{3-d}$ with the conventional $La_{0.8}Sr_{0.2}MnO_{3-d}$ cathode at 800 °C. The power density of 0.77 W/cm^2 was obtained with LSCF (LSM cathode yielded a power density of 0.60 W/cm^2 under the same conditions). Torres-Garibay et al. (2009) investigated the effect of lanthanum substitution with neodymium and replacement of cobalt with iron in ($La_{0.6}Sr_{0.4}CoO_{3-d}$). They found that in the temperature range of 800-600 °C cobalt substitution effectively reduces thermal expansion coefficient of the cathode with a slight decrease in the power density (from 232 mW/cm^2 (LSC) to 159 mW/cm^2). In the case of substitution of La by Nd on the other hand, the power densities were decreased significantly at all temperatures which was attributed to the reduced electronic conductivity. At 700 °C the power densities were 192 mW/cm^2 with Nd substitution and 66 mW/cm^2 with both Nd and Fe substitution. They have suggested to use Ag infiltration to increase the power density by improving the electronic conductivity and obtained a power density of 83 mW/cm^2 with Ag infiltration cathode.

Alternatives for La replacement in ferrocobaltites are barium and praseodymium (BSCF and PSCF). Kim et al. (2010) studying $Ba_{0.5}Sr_{0.5}Co_{0.8}Fe_{0.2}O_{3-d}$ cathode and obtained a power density of 910 mW/cm^2 at 800 °C. They compared the performance of BSCF with other cathodes and found that the power density of BSCF cathode were higher than LSCF and LSM. The performance of $Pr_{0.6}Sr_{0.4}Co_{0.8}Fe_{0.2}O_{3-d}$ (PSCF) – GDC composite cathode was investigated by Ji et al. (2008). This yielded 303 mW/cm^2 peak power density at 700 °C. They also showed that the area specific resistance of the composite cathode was around 0.046 Ω.cm^2 at 800 °C. Thus, the material was a promising cathode for in IT-SOFCs.

Strontium-based cobaltites suffer from the same problem, i.e. high CTE. B-site doping (generally by Nb, Ta, Sb, Sn, Ti, and Sc) is applied to decrease thermal mismatch with the electrolytes, stabilize the cubic perovskite phase and increase the thermal stability. Wang, et al. (2010) studied $SrCo_{1-y}Nb_yO_{3-d}$ cathodes with different doping levels (y= 0.1, 0.15, and 0.2). The maximum power densities of the cathodes were 675, 642 and 625 mW/cm^2 at 800 °C, respectively. As the temperature was decreased $SrCo_{0.9}Nb_{0.1}O_{3-d}$ still remained as the best composition with a power density of 175 mW/cm^2 at 650 °C. In all of the samples the cathodes were chemically compatible with LSGM electrolyte. Aguadero et al. (2009), studying effect of Sb doping in $SrCo_{1-x}Sb_xO_{3-d}$ (x = 0.05 - 0.2) found that the electronic conductivity was enhanced significantly at intermediate to low temperatures (800-400 °C) by doping. x=0.05 was the best composition yielding the lowest polarization resistance values, namely 0.009 and 0.23 Ω.cm^2 from 900 to 600 °C. The cathodes were chemically compatible with ceria based electrolytes and displayed power densities higher than 300 mW/cm^2 at 700 °C. Titanium is another alternative as B-site dopant for $SrCoO_3$ cathodes and Shen, Wang et al. (2011) have obtained very promising power densities for $SrCo_{1-y}Ti_yO_{3-d}$ cathode system at temperatures as low as 650 °C. They have tested different compositions, y=0.05, 0.10, 0.15, and 0.20 in which the highest power densities was obtained at y=0.05 for all temperatures. $SrCo_{0.95}Ti_{0.05}O_{3-d}$ cathode displayed a power density of 240 mW/cm^2 at 650 °C.

Qu et al. (2014) have investigated $SrCo_{0.7}Fe_{0.2}Ta_{0.1}O_{3-d}$ (SCFT) system for IT-SOFCs. They obtained considerably high power densities in the intermediate temperature range (800-600 °C), the power density of 120 mW/cm^2 could be obtained even at 600 °C. In this study, the Ni-SDC anode and SDC electrolyte were used. In order to increase the chemical stability of the system LSGM buffer layer were applied between SDC and SCFT. As a result, chemically compatible structure was obtained which was tested at elevated temperature (950 °C) for 10 hours.

Recently, layered cobaltites have gained importance as cathodes for IT-SOFCs. In this structure, the oxygen vacancies are aligned along specific direction which greatly

accelerates the diffusion of oxygen ions. In addition, it is proved that in surface defects in the layered structure act as highly active sites for oxygen reduction and significantly increases the surface exchange coefficient of oxygen. These layered/composite systems will be dealt with separately in Section 2.3.2.

Nickel-based systems are another common cathode materials used for IT-SOFCs. The most promising ABO_3 type member of this group is $LaNi_{0.6}Fe_{0.4}O_3$ (LNF). Iron doping increases the chemical stability of the material at high temperatures. LNF has many important advantages such as high electronic conductivity, strong catalytic activity and less TEC mismatch compared to cobaltites. However, they have a strong tendency to form insulating phases when they are used together with YSZ electrolyte. Ding et al. (2017) formed a composite cathode by adding small amounts of $Ba_{0.5}Sr_{0.5}CoO_{3-d}$ with LNF. Their single cell measurements showed that it was possible to obtain a power density of 110 mW/cm^2 at 700 ˚C.

Other nickelate systems has K_2NiF_4 type structure. Perez-Coll and Aguadero, (2011) have studied La_2NiO_4-$Ce_{0.8}Sm_{0.2}O_{1.9}$ composite cathode at different temperatures. In this study, the system was supported by 150 μm thick $Ce_{0.8}Sm_{0.2}O_{1.9}$ electrolyte and the anode was a composite of nickel and $Ce_{0.8}Sm_{0.2}O_{1.9}$. Since the skeleton of the structure is formed by SDC, the performances of the samples were stable which was tested for 40 hours. They reported a power density of 190 mW/cm^2 at 750 ˚C. Lalanne et al. (2008) have used a similar cathode where lanthanum was replaced by neodymium, i.e. $Nd_{1.95}NiO_{4+d}$. They reported a power density of 500 mW/cm^2 at 750˚C. This high density was attributed to a high ionic and electronic conductivity achieved by excess oxygen that could be accommodated in this type of structure.

As it has been reviewed above, there are four major groups of oxides namely, manganites, ferrites, cobaltites (including ferrocobaltites), and nickelates. Manganite-based cathodes have well-established properties and commonly used especially for high temperature SOFCs. Cobalt-based cathode materials seem to be the best alternative for lowering the operating temperatures of SOFCs. However, they suffer from high thermal mismatch and from reaction with conventional electrolytes.

Although the use of ferro-cobaltites and nickelates may solve the thermal mismatch, it is still necessary to enhance the chemical stability of these materials for long term operations.

2.2 Structure and Geometry of SOFCs

In addition to the main components summarized above; cell design, stack construction, selection of interconnects and sealant materials play important roles for high performance cells. SOFCs cover a wide range of application area, from high power required stationary to low power required mobile applications. The maximum power density that can be obtained from a single cell is around 2 W/cm^2. Thus, large scale applications where power demand is as high as 10-100 MWs, it is required to operate units that comprise a large number of stacks. The connection between the cells are provided with the use of suitable interconnects (Fig. 2.7).

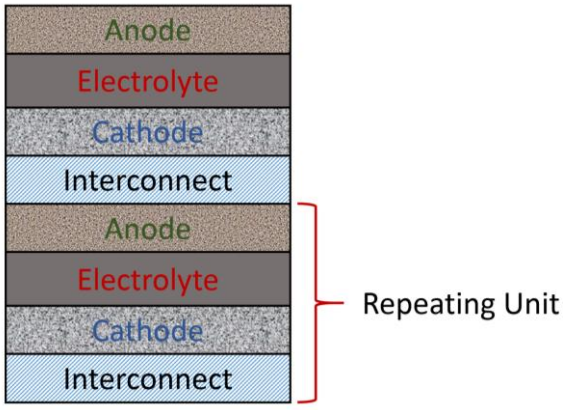

Figure 2. 7. SOFC stack components.

Interconnect materials should be electronically conductive and resistant to reducing and oxidizing atmospheres at the operating conditions. They also separate the gaseous fuel in the anode from the air in the cathode side of the adjacent cells. The use

lanthanum chromite ($LaCrO_3$)-based ceramic interconnects were very common, at high-temperatures (900- 1000 °C), due to high chemical stability under both oxidizing and reducing atmospheres. At relatively reduced temperatures (below 900 °C), ferritic stainless steels provide more advantages especially in terms of cost and the mechanical strength. Additionally, ferritic stainless steels are easily machined to obtain suitable channels for fuel and air flow inside the stacks. A special attention is given to ferritic steel with a trade name of Crofer 22 APU (with a chemical content of 22.2 wt. % Cr, 0.46 wt. % Mn, 0.07 wt. % La, 0.06 wt. % Ti, 0.1 wt. % Al, Ni and Si) to be designed as an interconnect material for IT-SOFCs. However, there are several issues that should be solved for long term use of these interconnect materials, such as chromium poisoning and increase in the electrical resistance. The studies have shown that desired oxidation resistance of Crofer comes from formation of a protective chromium oxide layer at the surface, Przybylski et al. (2014). For prolonged use the thickness of this layer increases which results in an increase in the electrical resistance of the interconnect material due to low electrical conductivity of chromium oxide layer. The other problem is chromium poisoning which occurs generally at the air exposed surface of the interconnect material. Chromium poisoning is commonly observed in chromia rich materials in which it reacts with oxygen or water and form volatile species, $Cr_2(OH)_2$ and Cr_2O_3 under SOFC operating conditions Yang, et al. (2006). These volatile species diffuse towards the cathode where they deposit as insulating secondary phases, like $SrCrO_4$ and consequently, causes a degradation in the cathode. It is possible to prevent chromium poisoning and increase in the electrical resistance by the application of different coatings or surface modifications in the interconnect materials (Shaigan et al. 2010).

As pointed out in section 2.1, all components making up the cell should be as thin as possible to decrease the ohmic losses. However, it is required to support the cell mechanically so that it is strong enough for handling and the assembly. Thus, at least one of the components should be thick enough to support the cell. Obviously there are four alternatives for the support, namely anode supported, cathode supported, electrolyte supported and interconnect supported SOFCs, Fig. 2.8.

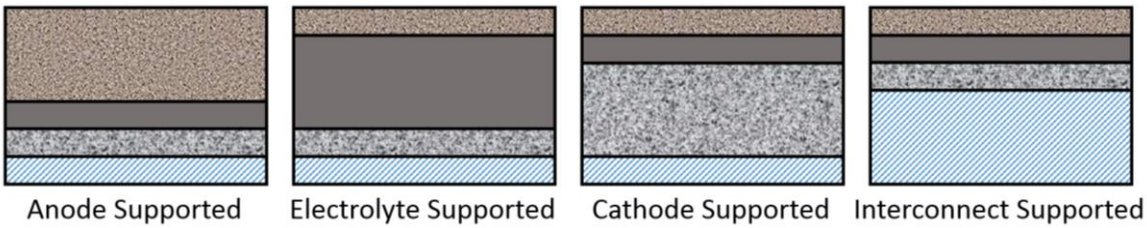

Figure 2. 8. Illustration of cell support types in solid oxide fuel cells.

In general the thickness of the supporting layers lie between 100-250 μm while the other layers have thicknesses in the range of 10-50 μm. The choice of electrode and electrolyte materials also affect the choice made for SOFC construction. However, anode supported cells are the most common configurations. This is due to the fact it is necessary to keep cathode thin due to slower kinetics of cathodic processes, and similarly it necessary to keep electrolyte and interconnects thin so as to reduce ohmic losses. In addition to cell configurations, stack designs play an important role for fuel-air flows and life time of the stack. Although there are a number of geometries, all could be classified in two groups, planar and tubular SOFCs, Figure 2.9 and 2.10 in the respective order.

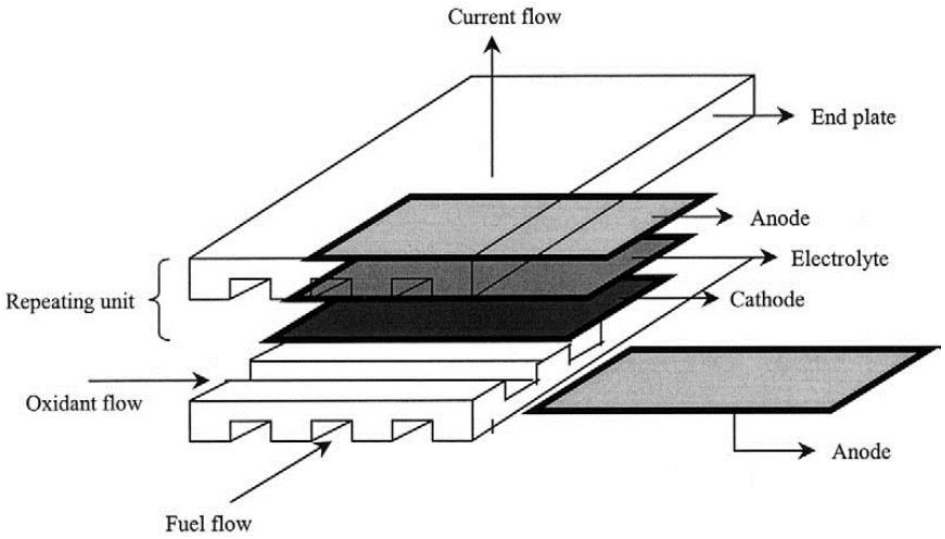

Figure 2. 9. Schematic illustration of planar SOFC.

(Stambouli & Traversa, 2002)

A schematic representation of a planar cell is given in Fig. 2.9. As seen in the figure, fuel is maintained along channels machined on the interconnect materials. On the interconnect material, consecutive layers of porous cathode, dense electrolyte and porous anode were positioned. Since the anode side is in contact with fuel while air or another oxidant flows through the cathode side, these two compartments should be isolated from each other. Therefore, it is necessary to use suitable sealant materials for the isolation of oxidant and fuel compartments in planar configuration. Planar SOFCs have higher current densities and easier production.

As in the case of other components, there are several important requirements for the selection of proper sealant material. The sealant must be able to prevent gas leakage at the operating temperatures of SOFCs. Also, the sealant should stay chemically and mechanically stable under both oxidizing and reducing atmospheres at the operating temperatures. It is also necessary to have high electrical resistivity to prevent short-circuiting between anode and cathode. Glass ceramics especially barium-aluminosilicates and diopside-based systems are commonly used sealant materials in SOFCs (Fergus, 2005). Their thermal expansion coefficients and electrical resistivities are generally tailored by changing the compositions. Although there are promising sealant materials their use is still problematic especially for long term applications.

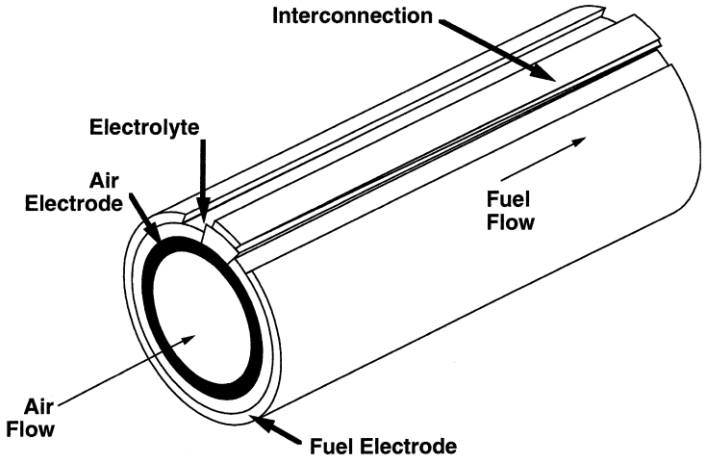

Figure 2. 10. Schematic illustration of tubular SOFC, (Singhal, 2000).

In tubular SOFCs, shown schematically in Fig. 2.10, the geometry is quite different. In general tube of porous electrodes are fabricated as the starting point and then the other cell components were assembled to the tube. Thus, these fuel cells are either anode or cathode supported structures. Fuel and air flows are already separated with dense electrolyte layer which creates an opportunity to produce seal-less SOFCs. Additionally, tubular SOFCs are quite fast both in start-up and shut-down because they have a single cell configuration. Furthermore, their resistance to thermal cycling are higher than planar stacks which increases their life time quite considerably.

The main drawbacks of these systems is the requirement of large scale production and difficulties in repair processes. In order to solve these problems there are several novel designs which combines the advantages of planar and tubular SOFCs.

One such design is given by Zha et al. (2005) shown in Fig.2.11. This is based on a honeycomb design where the skeleton is made up of electrolyte. With the use of suitable die the whole honeycomb structure is fabricated from the electrolyte material. Channels in this honeycomb structure alternate, one air, the other fuel so on. The use of this new design decreased the amount of sealant material and greatly simplified the fabrication of the assembly.

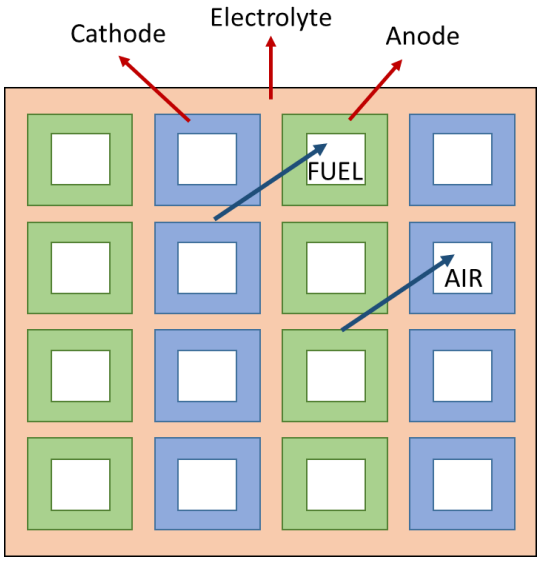

Figure 2. 11. Schematic illustration of honeycomb SOFC (Zha et al. 2005).

Another interesting novel design is cone shaped tubular SOFCs, (J. Ding & Liu, 2009). In this approach, identical segments are produced and according to the power demand the number of segments can be increased without any change in the fuel and air flow systems, see Fig. 2.12. The main purpose of segmented design is to produce portable SOFCs and for such purposes this novel approach is quite promising.

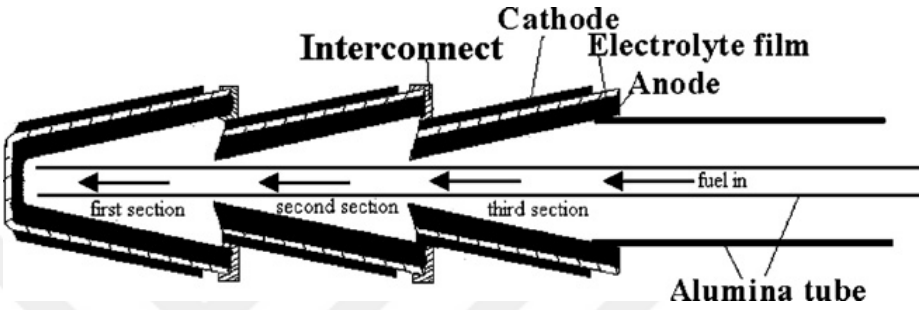

Figure 2. 12. Schematic representation of cone shaped tubular SOFCs (J. Ding & Liu, 2009)

2.3 Development of High Performance Cathode Materials for IT-SOFCs

As given in section 2.1, the performance losses in SOFC have a number of origins. Of these, causes leading to losses in the electrolytes are clearly understood and most have been solved (Stuart B. Adler, 2004). Performance losses related with anode materials are also quite considerable in the case of hydrocarbon fuels, but very promising performances were obtained with hydrogen fuel. New anode systems are currently under development for hydrocarbon fuels where a considerable reduction is achieved in the anode resistance [Gorte et al. (2000), Zhan & Ik, (2010)].

In terms of the performance losses, the cathode materials are the most problematic and appears to be the main obstacle in lowering the operating temperature of SOFCs. Thus so as to reduce the operating temperature of the SOFC down to 500-700 °C, i.e. IT-SOFC, it is necessary to focus on means of improving the cathode performance. In

order to increase the kinetics of cathodic processes it is crucial to fully understand the steps involved in these processes and investigate them one by one. In this section we will look at these processes in some detail and review cathode materials of high performance suitable for IT-SOFCs.

2.3.1 Factors Affecting the Kinetics of Cathodic Processes

The overall reaction that takes place in the cathode with reference to Fig. 2.13 is given by,

$$\tfrac{1}{2}\, O_2 \text{ (gas)} + 2e^- \text{ (cathode)} \rightarrow O^{2-} \text{ (electrolyte)},$$

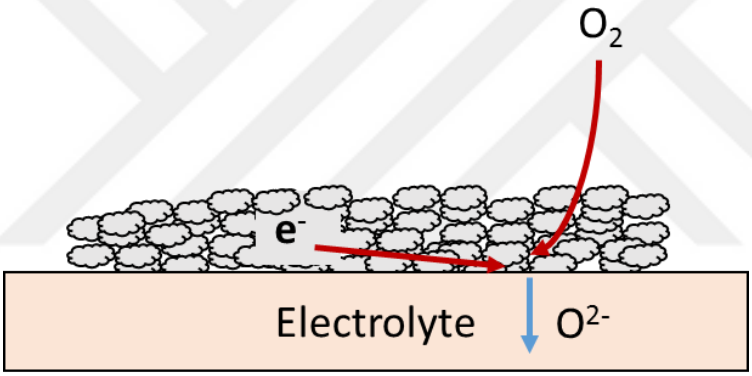

Figure 2. 13. Schematic illustration of oxygen reduction reaction.

This overall reaction, Oxygen Reduction Reaction (ORR), may have different routes depending on the choice of cathode material. In the case of cathodes, not having ionic conductivity, the reaction is limited to the triple phase boundaries in which reduced oxygen ions are incorporated directly into the oxygen vacancies in the electrolyte, Fig. 2.14 (a). This is the case in LSM cathodes where it is necessary to increase the density of TPB by controlling the porosity in the cathode material. In the case of cathodes having mixed ionic and electronic conductivity (MIEC), the available regions for ORR are more since oxygen ions can be incorporated into the electrolyte both via from TPB and from ionic diffusion across the cathode, Fig. 2.14 (b). The main examples of this

group of cathode materials are LSC, LSCF, and BSCF as reviewed above in section 2.1. For the composite cathodes in which one phase is electronically conductive while the other is ionically conductive such as LSM-YSZ mixture, the route for oxygen reduction is indicated in Fig. 2.14 (c). In this case, ORR kinetics can be increased by increasing the density of TPB region.

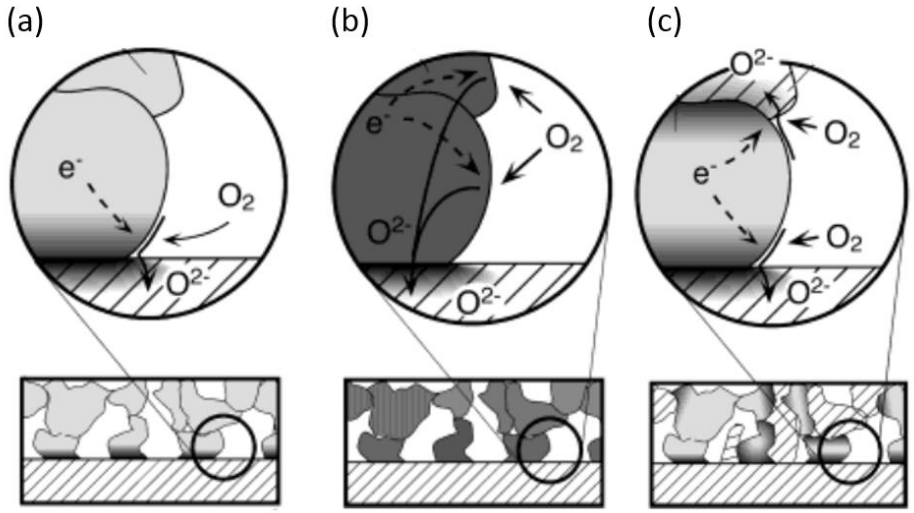

Figure 2. 14. Schematic illustration of ORR in (a) electronically conductive, (b) mixed ionically and electronically conductive, and (c) composite cathodes.

Among these routes, the use of MIEC cathodes increases the reactive sites most effectively. In MIEC cathodes the overall reaction can be divided into three steps;

i. Surface oxygen exchange: At this step the oxygen molecules in the air are reduced and incorporated into oxygen vacancies at the surface of the cathode
ii. Diffusion of oxygen ions: Here, incorportated oxygen ion diffuses through the cathode to the cathode/electrolyte interface, though at TPB the interface is reached already without the diffusion
iii. Electrochemical charge transfer: Here, oxygen ions are transfered from the cathode to the the oxygen vacancies in the electrolyte.

Surface oxygen exchange given above, which is commonly stated as the slowest process in these 3-step process in reality is made up of sub-steps involving chemisorption, dissociation, and incorporation. Chemisorption involves the diffusion of oxygen molecules in the gas phase and their attachment at the cathode surface. Then the oxygen molecule dissociates into oxygen ions and these oxygen ions incorporate into oxygen vacancies of the cathode material, Fig. 2.15.

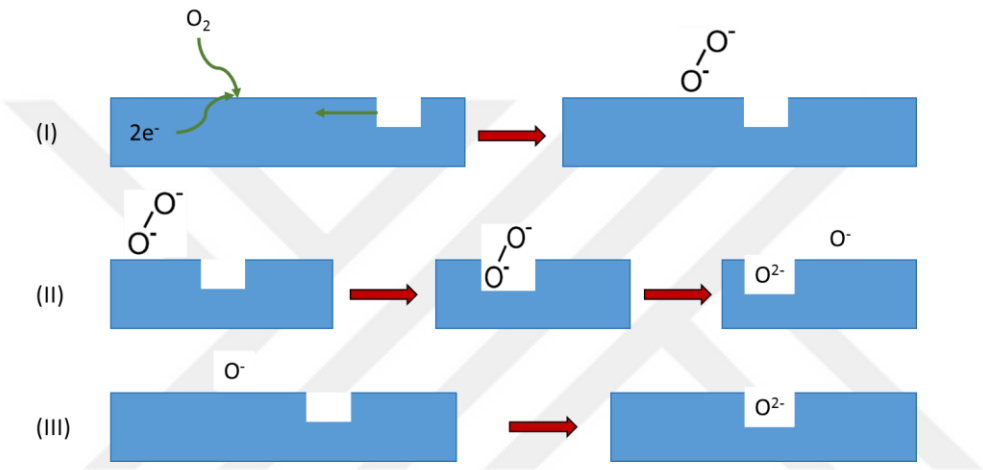

Figure 2. 15. Schematic illustration of chemisorption, dissociation and incorporation steps at the surface of MIEC cathode.

(Adapted from L. Wang et al. 2012)

Operating conditions of SOFCs create difficulties for in-situ surface analysis and thus it is hard to determine the slowest step in the overall surface exchange process Kuklja et al. (2013). In these steps, oxygen vacancies may take an active role by diffusing towards chemisorbed oxygen atoms or they may behave just as oxygen sinks in the structure. Furthermore, according to the thermodynamic model given by Adler, (2004), operating conditions especially temperature and oxygen partial pressure strongly affects the surface oxygen exchange kinetics. They stated that the driving force for the surface oxygen exhange increases with the increases in temperature, partial pressure of oxygen, and the mole fraction of oxygen vacancies.

In most of the studies, a coefficient, k, i.e. oxygen surface exchange coefficient, is used to measure the surface oxygen exchange in cathode materials. There are two common experimental techniques, as clearly explained by (Kuklja et al., 2013), to determine k; secondary ion mass spectroscopy and electrochemical impedance spectroscopy.

For conventional LSM cathodes it is generally stated that in the oxygen exchange the incorporation step is the rate determining step due to low amount of oxygen vacancies. For LSF and LSC cathodes, on the other hand, the amount of oxygen vacancies are increased and as a result LSC based cathodes show much faster surface oxygen exchange kinetics than LSM cathodes (Fig. 2.16) and thus they are one of the most promising cathode materials for IT-SOFCs.

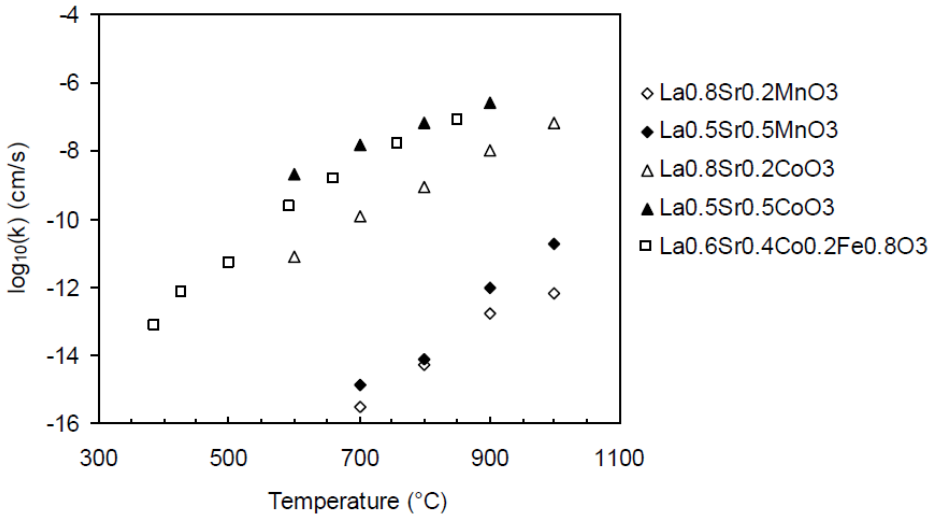

Figure 2. 16. The values of oxygen surface exchange coefficients of LSM, LSC and LSCF cathodes as a function of temperature.

(Lassman & Lassman, 2011)

LSC based cathodes have the most promising surface exchange kinetics among ABO_3 type perovskite materials. However, the surface oxygen exchange kinetics are increased further with the use of layered perovskites (Tarancón et al. 2010). For these

layered cathodes, the value of k can increase up to 10^{-5} – 10^{-6} cm/s at 500°C. Details about the performance of these cathodes will be given in section 2.3.2.

Following the incorporation of the oxygen to the surface of the cathode, oxygen ions are transported across the cathode to the elctrolyte. This process is related to the ionic conductivity of the cathode material.

The ionic conductivity is determined by the number of charge carriers in the material, and by their mobility at a given temperature. Since the charge of the carriers are fixed in the case of oxygen ion transport and its mobility is determined by operating temperature, it is necessary to increase the number of charge carriers, i.e. oxygen ions, in the material. For this purpose, perovskites are generally doped with various elements as reviewed in section 2.1.

Different cathodes are generally compared with one another in terms of the oxygen self diffusion coefficients, D^*. As indicated above cobaltite and ferro-cobaltite cathodes are able to maintain higher vacancy concentrations than magnatite (LSM) cathodes. Thus the oxygen self diffusion coefficient of LSM is around 10^{-20} cm^2/s while the values increases up to 10^{-10} cm^2/s and 10^{-7} cm^2/s in the case of LSC-LSCF and BSCF cathodes, respectively (Tarancón et al. 2010). It should be mentioned that, because of this, the cathode architecture in the case of LSM is different where oxygen ions are transferred to electrolyte at TPB making little use of ionic conductivity of the cathode.

As a final step in the cathodic processes, it is necessary to complete electrochemical charge transfer between the cathode and electrolyte. Since it includes an electrochemical process between two solid phases the reaction follows Tafel (or Butler-Volmer) kinetics. If charge transfer between cathode and electrolyte is the rate limiting step the relationship between the current and the potential is expected to be exponential. Although in some systems this Tafel behavior is obtained, it does not necessarily mean that the process is limited by the electrochemical charge transfer between the cathode and the electrolyte. According to Svensson et al. (1997,1998) and Adler (2004) the adsorption at the cathode surface and diffusion processes may also

produce a Tafel behavior in these materials. Therefore, it is difficult to find the rate determining step in cathode materials.

Electrochemical impedance spectroscopy, is the most beneficial techniques for the characterization of the kinetics of the cathodic processes. It is also possible to obtain the rate determining step by altering the operating conditions of the cathode. For example, surface oxygen exchange kinetics are sensitive to changes in oxygen partial pressure and depends linearly on the temperature. If the rate limiting step is diffusion of oxygen ion then there should be an Arrhenius type temperature dependence in EIS measurments. If the rate determing step is the electrochemical charge transfer between the cathode and the electrolyte the characteristic feature is the dopant level of the electrolyte material.

2.3.2 Layered Materials for Fast Oxygen Reduction Reaction

MIEC perovskites show high ionic conductivities, thus, their cathodic processes are not restricted to the TPBs and they have larger active regions. The values of oxygen exchange coefficient and oxygen self-diffusion coefficient determine the extent of the active cathode region. As the value of D^* increases, the structure carries the incorporated oxygen ions rapidly to the electrolyte interface. This causes an increase in the active region of the cathode material which is commonly described as the critical length, L_c. L_c generally decreases with decreasing D^*/k ratio.

For IT-SOFC, the cathode material should have high k and D^* values ($k.D^*$ should be larger than 10^{-14} cm^3/s^2) and wide active regions (D^* / k should be greater than 0.01 cm) (Tarancón et al. 2010). Some of the cobaltite based ABO_3 type perovskites such as LSC, LSCF, BSCF satisfy these values and therefore are suitable cathode materials for IT-SOFCs. ABO_3 type perovskite cathode materials were already reviewed in section 2.1.

Additionally, there are relatively new structures such as double perovskites and layered Ruddlesden-Popper structures that display enhanced cathodic kinetics at intermediate temperatures, Fig. 2.17.

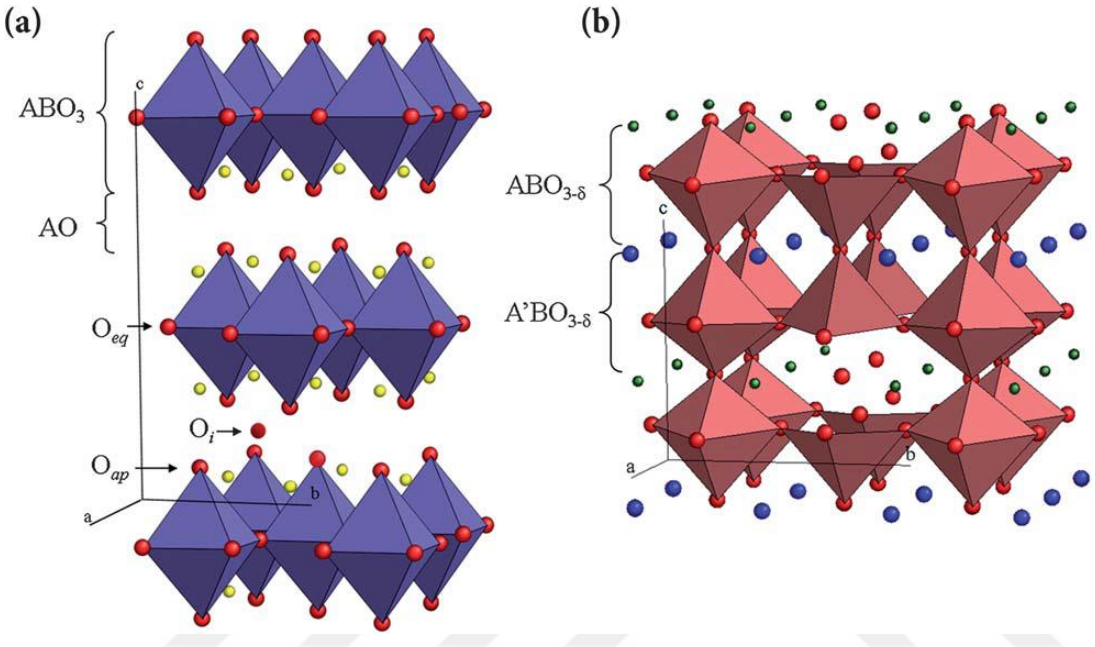

Figure 2. 17. Polyhedral view of layered (RP) structure with alternating ABO_3 and AO rock-salt layers (a) and double perovskite structure (b).

The oxygen transport properties of these structures are improved with the anisotropic oxygen diffusion which also improves also the oxygen surface exchange kinetics. Ruddlesden-Popper phases include alternating layers of ABO_3 perovskite structure and an AO rock-salt structure which results in a general formula of A_2BO_4, Fig. 2.17 (a). These materials have shown that there is an excess amount of oxygen interstitials that can be accommodated in the rock-salt layers. Thus, they have high ionic conductivities and high catalytic activity for oxygen surface exchange. There are many different compositions based on R-P that are suitable cathode materials for IT-SOFCs. La_2NiO_{4+d} based oxides are particularly popular.

Oxygen diffusion and surface exchange in $La_{2-x}Sr_xNiO_{4+d}$ cathode material was measured by Skinner and Kilner (2000) using isotope exchange depth profiling method. They have reported that La_2NiO_{4+d} has higher oxygen diffusivity than commonly used LSCF and LSC cathode. In this study, self diffusion coefficient of oxygen was found to be $D^* = 2{,}71 \times 10^{-8}$ cm^2/s for La_2NiO_{4+d}. Also they have found that the activation energies for both surface exchange and oxygen diffusion were smaller in the case of $La_{1.9}Sr_{0.1}NiO_{4+d}$.

B-site doping effect have been analyzed by Boehm et al. (2003) and Munnings et al. (2005). Boehm et al. have shown that copper doping may increase the thermal stability and electronic conductivity of the La_2NiO_{4+d} at the expense of some decrease in the surface exchange and oxygen diffusion kinetics. Munnings et al. have investigated the effect of B-site cobalt doping on oxygen diffusion and surface exchange processes. They have reported that the surface exchange coefficient and oxygen diffusion coefficients were increased with increasing cobalt content reaching the maximum value for La_2CoO_{4+d} composition, Fig. 2.18 and Fig. 2.19. It was also shown in this study that La_2CoO_{4+d} meets the $D^*k > 10^{-14}$ cm^3/s^2 requirement (Tarancón et al. 2010) even at temperatures as low as 470°C.

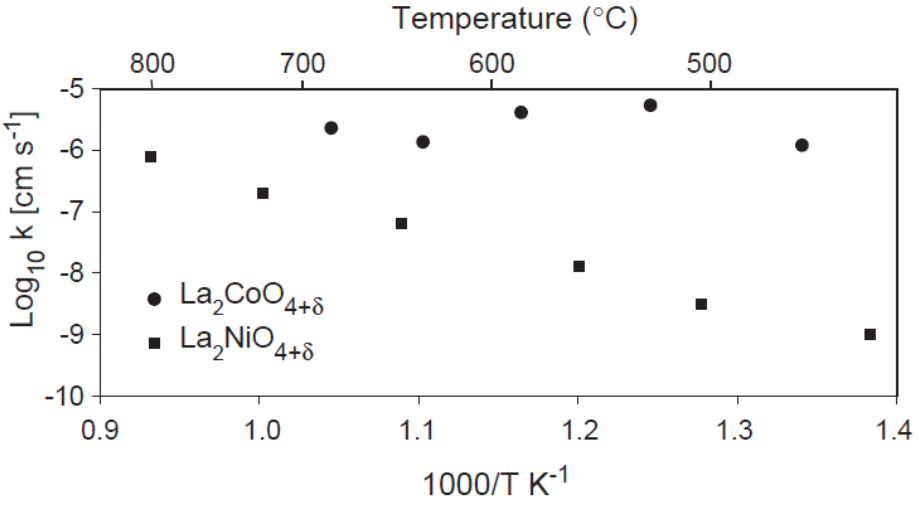

Figure 2. 18. Comparison of La_2CoO_{4+d} and La_2NiO_{4+d} cathodes in terms of surface exchange coefficients. (Tarancón et al. 2010)

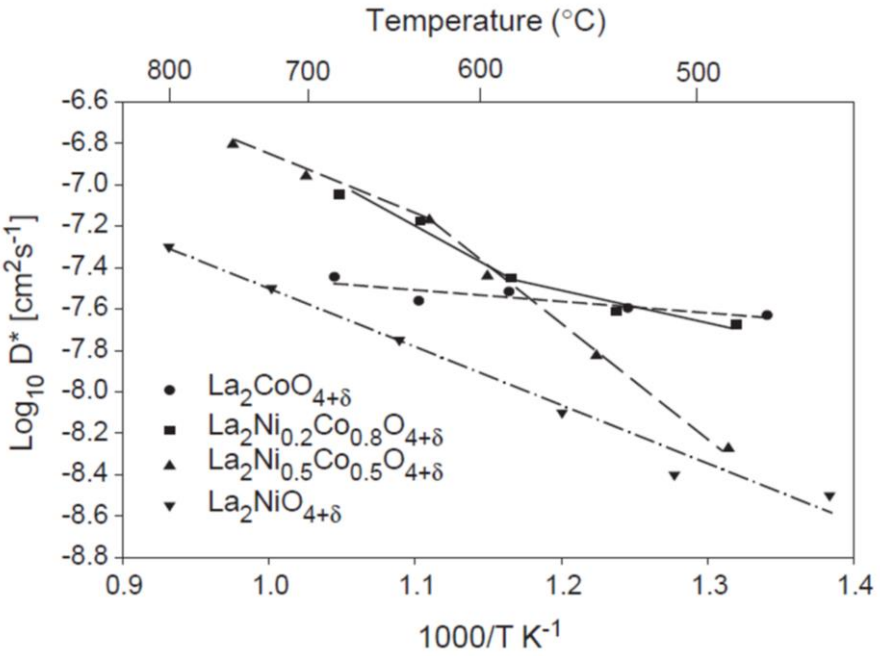

Figure 2.19. Diffusion coefficients of $La_2Ni_{1-x}Co_xO_{4+d}$ cathodes at different temperatures. (Tarancón et al. 2010)

Another group of layered materials for SOFS are the so-called double perovskites. These materials are in the form of alternating perovskite layers that results in a general formula of A-A'B_2O_{5+d}, see Fig. 2.19. In this structure there two types of A-site cations (one of them is rare earth, the other is alkaline earth) that form each layer of alternating structure. There are various examples of double perovskite systems but the most common system is $GdBaCo_2O_{5+d}$. This material was reported by Taskin et al. (2007) where they measured very promising oxygen diffusivities D* =3x10^{-6} cm^2/s at 500°C. This high diffusivity was explained by the cation ordering in the half-doped perovskite materials. The performance of this material as SOFC cathode was investigated by Chang et al. (2011) and an ASR value of 0.53 Ω.cm^2 was obtained at 645°C. In a similar study, Tarancón et al., (2007) have reported a power density of 300 mW/cm^2 at 700°C for $GdBaCo_2O_{5+d}$ cathode which is fabricated via screen printing.

$PrBaCo_2O_{5+d}$ (PBCO) based cathodes are another common double perovskite cathodes with promising results. Kim et al. (2007) showed that these cathodes can increase the

surface exchange and oxygen diffusion kinetics several orders of magnitude as compared to those of LSC cathodes. Using an electronic conductivity relaxation technique they measured $D^* = 10^{-2}$ cm^2/s and k= $4*10^{-5}$ cm/s.

C. Zhu et al. (2008) studied the electrochemical performance of PBCO cathode reported power densities of 866 mW/cm^2 and 115 mW/cm^2 at 650°C and 500°C, respectively. These results were quite promising, but PBCO suffered from the high thermal expansion coefficient as in the case of other cobalt based systems. To reduce TEC, Zhao et al. (2010) have partially substituted Co with Cu, i.e. $PrBaCuCoO_{5+d}$ (PBCCO). Although the electronic conductivity was decreased as a result of this substitution, TEC values were close to those of ceria based electrolytes. Additionally, they reported a power density of 791 mW/cm^2 at 700°C which is close to the power density of PBCO system.

Another alternative double perovskite is $NdBaCo_2O_{5+d}$. Recently, Yoo et al. (2013) have partially substituted Ba by Sr, $NdBa_{1-x}Sr_xCo_2O_{5+d,}$ and found that the performance of the cathode was increased with increasing Sr content reaching a maximum value between x=0.5 and x=0.75. The performance was then suddenly dropped at x=1. They reported a power density close to 1 W/cm^2 at 700°C. $SmBaCo_2O_{5+d}$ (SBCO) is also in the same group that have higher thermal and chemical stability with SDC electrolytes. Jun et al. (2012) have partially replaced Ba with Sr in this double perovskite, $SmBa_{1-x}Sr_xCo_2O_{5+d}$, and obtained a maximum power density of 1039 mW/cm^2 with x=0.7 at 600°C. This performance was quite impressive which makes $SmBa_{0.25}Sr_{0.75}Co_2O_{5+d}$ one of the best cathode material for IT-SOFCs.

In summary, there are promising RP phases and double perovskite structures to enhance the kinetics of the cathodic processes and to lower the operating temperature of SOFCs. Although these novel systems yielded enhanced performances, further enhancement is required for IT-SOFC applications for temperatures less than 600°C.

2.3.3 Heterostructured Perovskites for Fast Oxygen Reduction Reaction

The development of new cathode materials opened the way for high efficiency IT-SOFC, but unfortunately none of these cathodes provide all desired features. Thus, further improvements are required to satisfy fast ORR, high chemical and thermal durability under the operating conditions and enough compatibility with the electrolyte and interconnect materials. For this purpose, combination of different materials with such methods as the surface decoration or by forming composites offer novel approaches.

The use of composite materials was first started with mixing ionically conductive electrolytes (e.g. YSZ) with electronically conductive cathode materials (e.g. LSM) to improve ORR kinetics that are limited to TPBs. This traditional approach was extended to MIEC cathodes where new methods are employed to fabricate these mixtures with a controlled microstructure or even to form nanocomposites. These include the combination of catalytically active LSC and LSCF cathodes with GDC electrolytes. For example, Leng et al. (2008) have fabricated LSCF-GDC composite cathodes by ball milling and obtained a refined microstructure with large surface area. Their experiments showed a power density of 139 mW/cm^2 even at 500°C. There are other techniques such as spraying or impregnation to form composites of these oxides.

In addition to cathode-electrolyte composites, the application of two different cathode materials has shown very promising properties in terms of high catalytic activity for ORR. As reviewed by Janek, (2009), the interfaces have much faster transport properties than the bulk and moreover, they provide more open structures for surface oxygen exchange. Either by controlling the volume fraction of phases or via the formation of graded structure they sustain the chemical and thermal compatibility between the cathode and the electrolyte. One of the first examples of this was fabricated by Van herle et al. (2001) where the consecutive layers of LSC and LSM cathodes were formed to obtain a chemically stable structure. As a result, they obtained

power densities of 500 mW/cm^2 at 750°C which was one of the highest reported at that time.

In 2008 M Sase et al. accidentally found an enormous enhancement in the ORR kinetics using a composite made up of $(La_{1-x}Sr_x)CoO_3$ (LSC-113) and Ruddlesden-Popper $(La_{1-x}Sr_x)_2CoO_4$ (LSC-214) phases. They obtained LSC-214 precipitates after sintering LSC-113 cathode at elevated temperature and they obtained an extremely high surface exchange coefficient (10^{-5} cm/s) at dissimilar interfaces between the precipitate (LSC214) and the matrix (LSC113) using SIMS. This value is three orders of magnitude larger than the single phase LSC-113 cathode. This result was supported by an electrochemical impedance study of Yashiro et al. (2009). In this work, a layered cathode was prepared where LSC-113 and LSC214 were screen printed as alternate layers on GDC electrolyte. They showed that the low frequency arc which corresponds to surface oxygen exchange was much smaller in the hetero-structured cathode compared to single phase LSC-113 or LSC-214.

In order to optimize the enhancement achieved by LSC-113 and LSC-214 composite cathodes, it is important to learn the root cause of this catalytic effect. Crumlin et al. (2010) have prepared 85 nm thick LSC-113 cathodes in which the surface was decorated by LSC-214. The surface coverage varied between 0.1-15 nm. They compared a partially covered LSC-113 with that which was fully covered. They showed that the samples with low coverage showed higher catalytic activity where the surface oxygen exchange coefficient was an order of magnitude higher, Fig. 2.20.

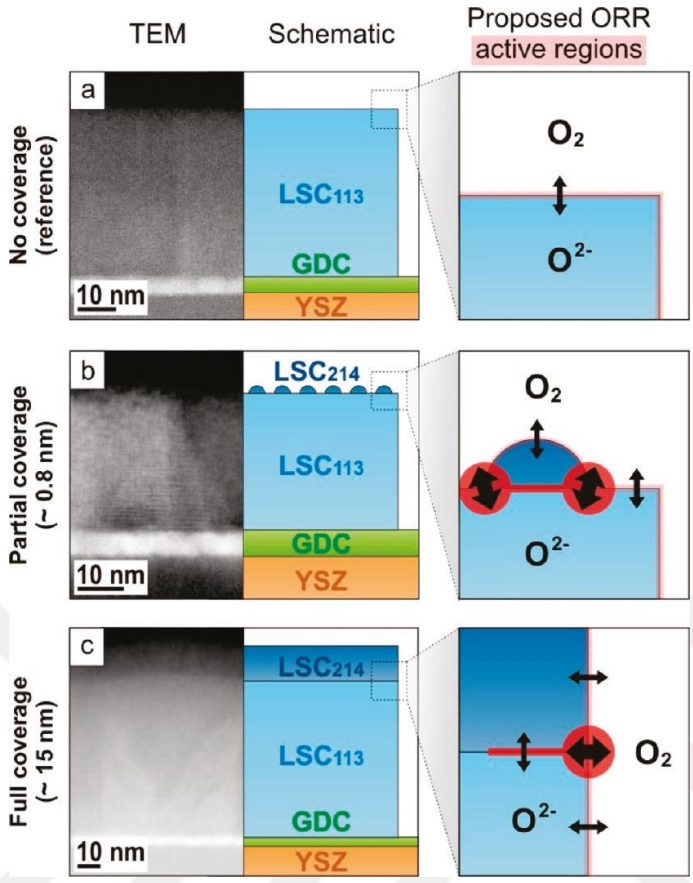

Figure 2. 20. Illustration of the interface effect in oxygen surface exchange step in LSC-113/LSC-214 composite cathodes. (Crumlin et al. 2010)

LSC-214 was subject to a further study. Han and Yildiz (2012), using density functional theory (DFT) suggested that the LSC-214 phase shows an anisotropic surface exchange kinetics. The coupling between LSC-113 and 214 is such that makes use of this anisotropy in a positive way and as a result facilitates the oxygen adsorption, dissociation and incorporation steps. Additionally, it was found that the lattice strain effects occurring at the interface increases the kinetics of oxygen incorporation in LSC-113. Han et al. proposes that it is these combinations of effects that increases the surface exchange kinetics up to three orders of magnitude at 500°C.

Tsvetkov et al. (2014) proposed an electronic activation mechanism to explain the enhanced exchange kinetics. They proposed that the transfer of oxygen vacancies and electrons across the interfacial from LSC-113 was easier, as proved by the greater reducibility cobalt in the hetero-structured LSC-214- LSC113.

From the studies reviewed above, it is apparent that LSC-113/LSC-214 hetero-structured cathode has desired properties for IT-SOFCs. In order to further investigate the performance of the cathode, Ma et al. (2015) have formed a vertically aligned nanocomposites having columns of LSC-113 and LSC-214 cathodes using pulsed laser deposition (PLD), Fig. 2.21.

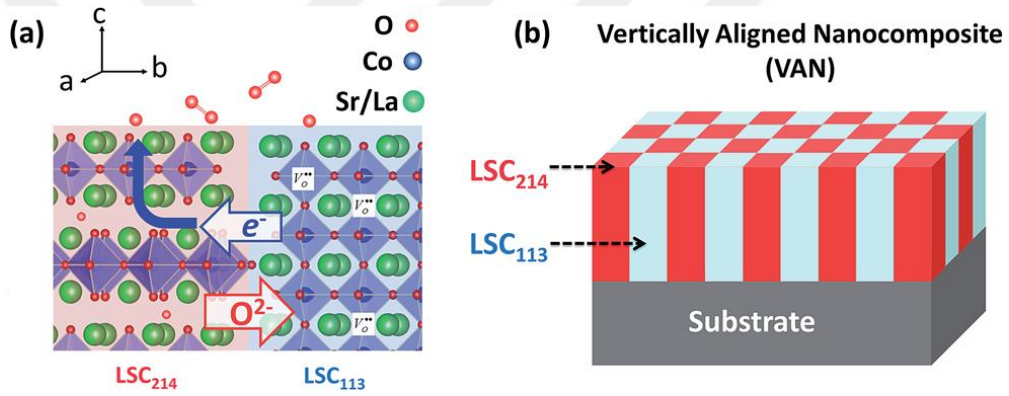

Figure 2. 21. Enhanced cathode kinetics in vertically aligned nanocomposite LSC-113/LSC-214 cathodes. (Ma et al. 2015)

In this study, the cathode was enriched in terms of the interfacial region and the interfaces started from the surface of the cathode and continued all the way down to the electrolyte. The area specific resistance values measured via EIS were quite low for this vertically aligned structure. The values were strikingly low at low temperature regime (below 500°C). Moreover these structures were highly stable, more so than the single phase versions. However, this stability was lost at temperatures higher than 400°C due to Sr segregation.

Forming composite structures is not the only way of fabricating high performance hetero-structured cathodes. Infiltration and impregnation techniques can also be used for the same purpose. These techniques were used several studies as reviewed by Ding et al. (2014) aiming to increase TPB length, chemical compatibility and electrocatalytic activity resulted in promising performance enhancements, Fig.2.23.

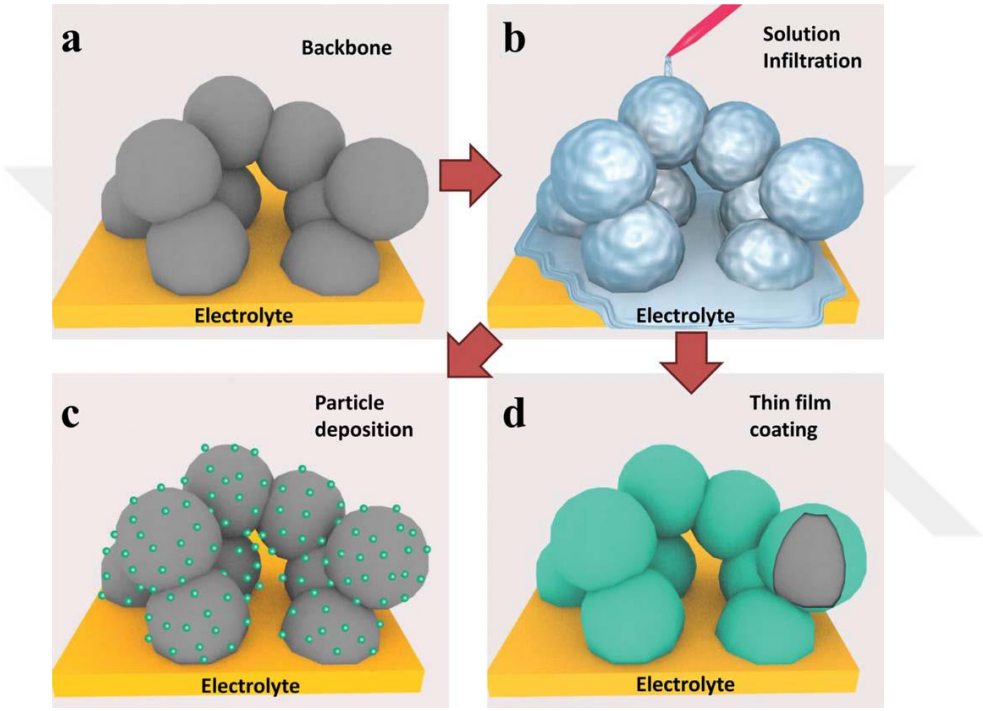

Figure 2. 22. Schematic illustration of surface modifications via solution infiltration. (Ding et al., 2014)

In an early study on infiltration was carried out by Lou, et al. (2009) where LSCF cathode was coated with 50-100 nm thick, catalytically more active $Sm_{0.5}Sr_{0.5}CoO_{3-\delta}$ phase by infiltration. They reported an ASR value of 0.688 $\Omega.cm^2$ at 550°C. As a result, the peak power density was increased considerably and reached a value of 700 mW/cm^2 at 700°C. Recently, a similar study was carried out by Yoo, et al. (2017) and they have coated LSCF cathode with $PrNi_{0.5}Mn_{0.5}O_3$ thin film which also included precipitated PrO_x nanoparticles. They obtained a power density of 1200 mW/cm^2 at

750°C. In addition, the polarization resistance measured at 750°C was 0.022 $\Omega.cm^2$ which was about 1/6 of that measured for single phase LSCF cathode.

Another interesting example of ORR kinetics enhancements was demonstrated by Navarrete et al. (2015) in which a composite cathode of LSM-GDC used as a backbone following sintering were infiltrated by a suitable precursor forming nanoparticles of Co, Ba, Pr, Ce, Sm, or Zr as catalysts. Of these, Co and Ba increased the surface exchange resistance and therefore negatively affected the performance. The other elements, Pr, Sm, Zr, and Ce have increased the performance of the cathode of Pr was the best yielding a power density values close to 600 mW/cm^2 at 700°C.

Zhou, et al. (2011) have created a concentration gradient so as to create an A site vacancy at the surface. In this study, the cathode material was BSCF. The cathode at the electrolyte interface had a composition of $Ba_{0.5}Sr_{0.5}Co_{0.8}Fe_{0.2}O_{3-d}$ and at the surface, the A-site, i.e. (Ba, Sr) was deficient, i.e. less than 1 which improved the oxygen surface exchange kinetics. They reported an ASR of 0.148 $\Omega.cm^2$ even at temperatures as low as 550°C. The stability of the cathode was tested at this temperature for 200 hours and without a sign of any significant degradation. It should be mentioned that the A-site deficient cathodes were more reactive with common electrolytes and the use of hetero-structured cathode was suggested with concentration gradient has eliminated the problem of this reactivity.

As a summary, it should be mentioned that the application of hetero-structures takes the advantage of catalytic effects of interfaces. Among the possible systems the combination of LSC-113/LSC-214 appears to be very attractive due to the associated surface exchange kinetic enhancements. The current work, therefore, deals with LSC-113/LSC-214 hetero-structures so as to establish the full potential of these cathode materials.

CHAPTER 3

PREPARATION OF $La_{0.8}Sr_{0.2}CoO_{3-\delta}$ SPUTTERING TARGETS USING A DEFORMABLE COMPACTION DIE

3.1 Introduction

For voluminous processing of ceramics, it is customary to carry out an extensive preliminary work to determine the fabrication parameters. Once these are determined, a die of suitable dimension is prepared and the powders are compacted and sintered under carefully controlled conditions. In the case of sputter targets, the use of hot-press greatly simplifies this process as it ensures controlled densification with proper dimensional control (Rezaei et al. 2016). Where the hot-press is not available, it is necessary to revert to the conventional practice of compaction and sintering which require, as pointed above, a lengthy preliminary work. This is quite demanding especially for a low volume production.

Sputter targets, especially for research purposes, of necessity, is of low volume, but with stringent requirements [(Lik et al. 2013),(Wu, 2012)]. First, they should have high relative densities (higher than 0.90) as otherwise there would be compositional deviations between the sputtered film and the target (Lo & Hsieh, 2012). Also, they are expected to have a uniform distribution of grain size so as to suppress the nodule formation which could lead to problems in the deposited films (Medvedovski et al. 2008).

The current work is a part of the effort to develop an efficient cathode material for solid oxide fuel cell via sputter deposition. The aim is to produce sputter targets of high density with uniform grain size suitable for the deposition of cathode thin films $La_{0.8}Sr_{0.2}CoO_{3-\delta}$ (LSC-113) as well as $La_{0.8}Sr_{0.2}CoO_{3-\delta}$ /$(La_{0.5}Sr_{0.5})_2CoO_4$ (LSC-113 /

LSC-214) mixture. For this purpose, we utilize a method that relies on the use of deformable die for compaction.

3.2 Experimental Procedure

LSC-113 as well as LSC-214 powders were synthesized using Pechini method. Although both powders were synthesized, the details reported below refer to LSC-113 only. In this method, the solution of respective nitrates is mixed with ethylene glycol and citric acid by stirring at 100 °C. After drying at 250 °C calcination was applied to remove remaining organics at 750 °C for 5 hours. Powders were obtained in a crystalline form without any additional phases. Particles were in the form of agglomerates approximately 5 micron in size made up of submicron oxides.

Compaction was carried out with an 800 kN hydraulic press. The dies were in the form of PTFE (trade name Teflon) rings 5 mm in height with 5 mm wall thickness, Fig. 3.1. Sintering was carried out in a muffle furnace at the selected temperature, with heating /cooling rates of 2 °C / min with a hold during heating at 750 °C for 1 hour.

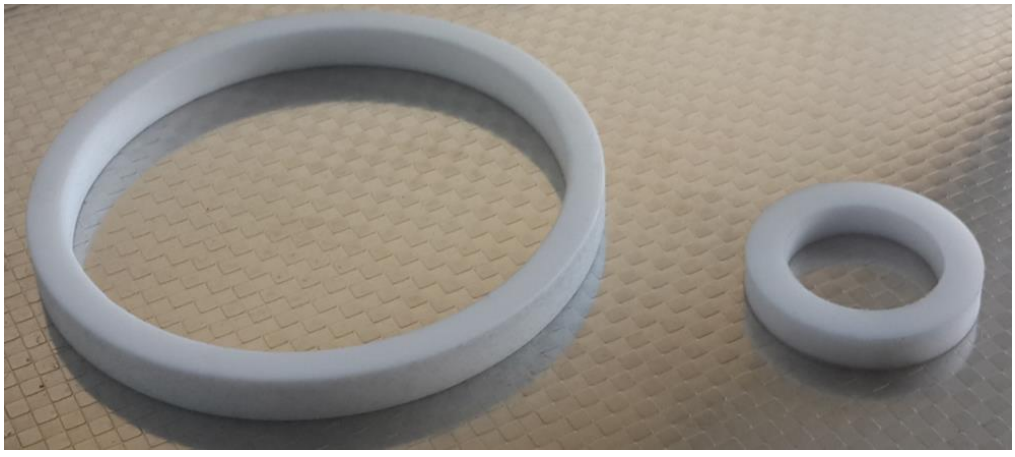

Figure 3. 1 PTFE rings used as a deformable die. Smaller diameter ring on the right was used for preliminary experiments. While the one on the left was used to fabricate 2 inch diameter La0.8Sr0.2CoO3-δ (LSC-113) sputter gun.

Density of both compacted and sintered discs were measured with Archimedes method. For this purpose, the samples were made water impermeable by application of lacquer. Results were expressed as the relative density which is the ratio of measured density over the full density of the oxides. Microstructural characterization, with regard to grain structure of the deposited films, was carried out using a scanning electron microscope (SEM-FEI) with a FEG gun.

Sputter deposition was carried out in a special system designed for combinatorial thin film work (Piskin & Öztürk, 2017), incorporating both R.F. and D.C. sputter guns. Target holders were 2 inch in diameter with a copper base. Targets were mounted onto this base with the use of a ring, 49 mm in inner diameter that could be fastened onto the base. This allows the use of targets of 50 mm in diameter ± 0.7 mm in tolerances.

3.3 Results and Discussion

Initial work was carried out with a conventional die. Thus a steel die, 50 mm in inner diameter, was used for compaction of LSC 113 powder. Compaction was carried out under a pressure ranging from 80 MPa to 120 MPa. Densities of the green compacts are reported in Table 3.1. It is seen that the density increases with increase in the compaction pressure.

Table 3. 1. Green density and the relative density of LSC113 compacted in rigid and deformable die at different compaction pressures.

Pressure	Rigid Die		Deformable Die	
	Density (g/cm^3)	Relative Density	Density (g/cm^3)	Relative Density
80 MPa	3.974	0.552	3.953	0.549
100 MPa	4.075	0.566	4.018	0.558
120 MPa	4.142	0.575	4.147	0.576

Compacts were then sintered at 1300 °C for 4 hours. Representative microstructures after sintering are given in Fig. 3.2. Here the sample compacted with 80MPa was not considered satisfactory as there was a lack of fusion in the sintered oxide, Fig. 3.2 (a). The relative density measured for this sample was 0.80. With the compaction pressure of 110 MPa, the powders were fused together with the presence of occasional small pores yielding a relative density of 0.96. The microstructure in this sample was also quite satisfactory in terms of its uniformity. As a result, a relative density of 0.95 was taken as the minimum target value.

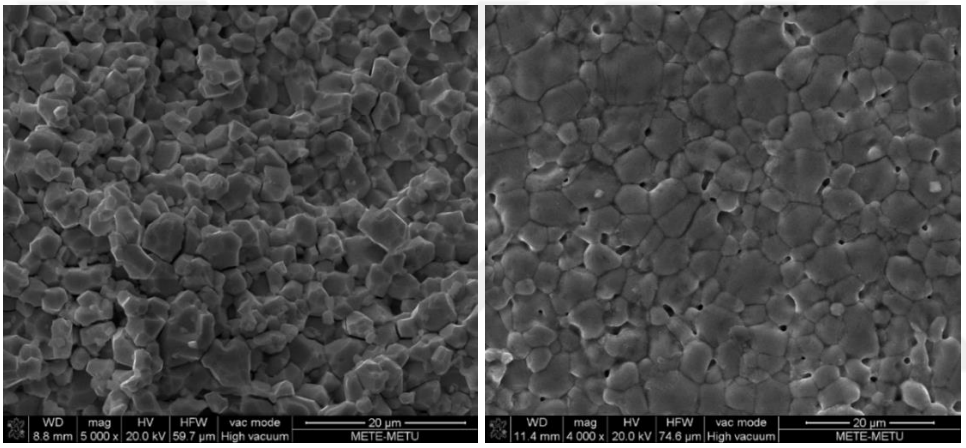

Figure 3. 2. SEM micrographs of LSC after sintering at 1300 °C compacted with a conventional die with a pressure of a) 80 MPa, b) 110 MPa.

Based on the sintered density and the associated shrinkage, a rigid compaction die could be prepared for the fabrication of 2 inch LSC-113 target. It appears that a compaction die of 65 mm inner diameter, would be required for this purpose. The compact would then shrink to 50 mm after sintering. Since the relative density and shrinkage after sintering would change depending on choice of powder, it is necessary to repeat the above work for LSC-214 as well as LSC-113/LSC-214 mixtures.

Compaction dies are normally fabricated from tool steels machined to close tolerances followed by quenching and tempering. The fabrication is, therefore, rather an involved process and a simpler alternative would be highly desirable. Here, we propose the use of deformable die as an alternative.

Deformable dies used for the fabrication of LSC-113 target are in the form of rings of low aspect ratio, i.e. height is small in comparison to the diameter, see Fig.3.1. For preliminary experiments, in order to save the powder, small diameter dies were used. Therefore, a large number of PTFE rings of 20 mm inner diameter were machined from PTFE rods of a suitable diameter.

The experiments, described for the conventional die for LSC-113 target were repeated for 20 mm PTFE die where the compaction pressure varied from 50 to 135 MPa. It should be pointed out that the geometry of compaction, here, is different from the conventional practice. The PTFE ring is pressed between two parallel platens deforming the ring and compacting the powder. Thus the ring is used once and then discarded. This is in contrast to the conventional compaction where powders are compacted within a die – punch system, a process that can be repeated many times with the same toolset, Fig. 3.3.

In the experiments, PTFE rings were filled with powder, tapped to obtain uniform density. They were then pressed uniaxially to the preselected value of compaction pressure. During pressing, PTFE rings were reduced in height, flow occurring in the radial direction. Interestingly, there was almost no change in the inner diameter of the ring. The diameters of the green pellets measured for 5 experiments were within 20.2 mm.

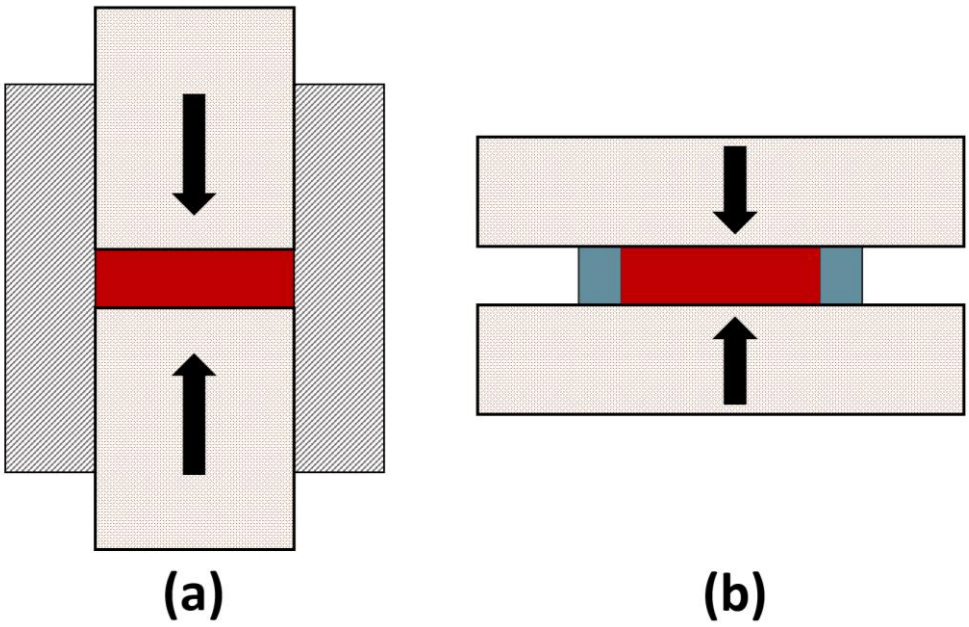

Figure 3. 3. Schematic representation of compaction, a) Conventional approach, b) Compaction with a deformable die. Note that in (b) while powders are compacted, the die is deformed.

Densities of green compacts obtained with deformable die are included in Table 3.1. The values should be compared with those obtained with the rigid die. It should be noted that the values are almost the same in both rigid and deformable die under the same pressure. This implies that the processes in both dies are quite similar to each other and that the use of deformable die does not alter the compaction in any significant way.

Compacted pellets were then sintered at 1300 °C for 4 hours. Density of the pellets was measured with Archimedes method both before and after sintering. The values are shown plotted in Fig. 3.4 as a function of the compaction pressure.

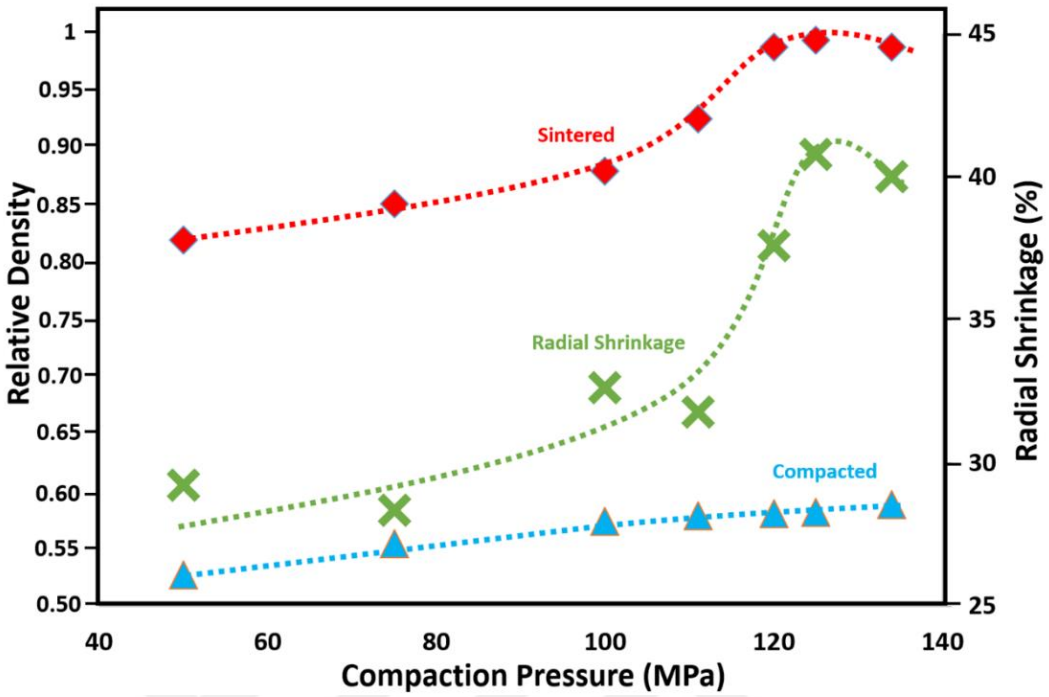

Figure 3. 4. Relative density and radial shrinkage in LSC as a function of compaction pressure. Note that sintered density increases with increasing compaction pressure, reaching a value of more than 0.95 at around 110 MPa.

As seen in Fig. 3.4, the relative density after sintering, increases with increasing compaction pressure reaching values higher than 0.95 at around 110 MPa. It may be noted that there is a sign of density decrease with the application of a too high compaction pressure. This unexpected decrease in the sintered density with excessively high compaction pressure was also reported by other workers (Ning et al. 2010) and explained on the basis of trapped pores that could not escape during sintering. Given in the same graph are the green densities of the compacts. Shrinkage after sintering was also reported. For this purpose, diameters of samples were measured before and after sintering and the shrinkage was calculated as % radial shrinkage.

Following the observation made above, a relative density of at least 0.95 would be desirable for the LSC-113 sputtering targets. Both compaction force and the actual diameter of the deformable die can be determined with an extrapolation procedure. Shrinkage in sintering with 125 MPa compaction pressure was 41%. This translates to an inner diameter of 67 mm for the deformable die.

Based on this expectation, a PTFE ring of 67 mm inner diameter 5 mm wall thickness and 5 mm in height were prepared. The die filled with the powder and compacted with a compaction pressure of 125 MPa. The compact was sintered under the same condition as above i.e. 1300 °C for 4 hours, which yielded a sputter target that was quite dense. The density of this target was 6.98 g/cm^3 which corresponds to a relative density of 0.97 (fully dense LSC has a density of 7.2 g/cm^3). The diameter of the sintered oxide was 50.5 mm ± 0.3 mm which was within the tolerances of the sputter gun holder.

The sputter target of 2.7 mm in thickness produced in this way was tested for the deposition of thin film cathodes. The target was loaded to the holder and it was sufficiently flat so no backing layer was used. The sputtering was carried out for 5 hours with argon flow maintained at 5 mTorr pressure. The substrate was a gadolinium doped ceria disc maintained at 400 °C. This yielded a thin film cathode of 500 nm in thickness which was satisfactory in all respects, i.e. the film was uniform and free from voids, Fig. 3.5. In fact, films co-sputtered using two targets LSC-113 and LSC-214 both fabricated with the deformable dies were produced and tested electrochemically yielding quite satisfactory results.

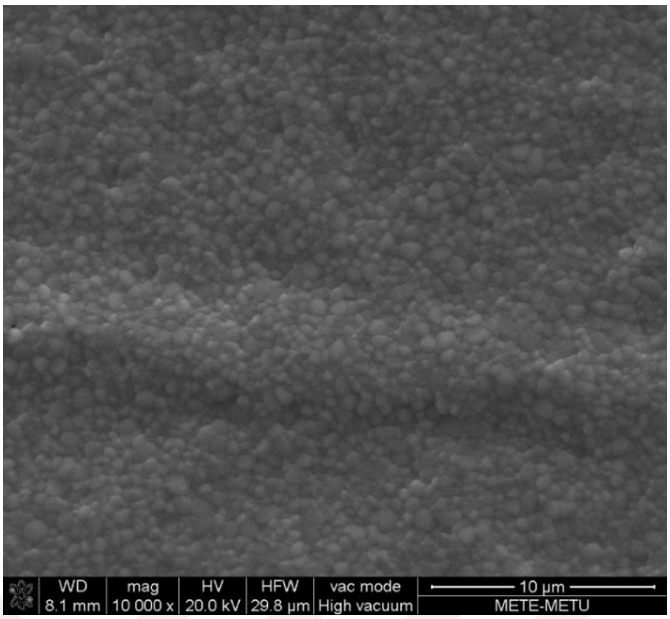

Figure 3. 5. Thin film LSC113 cathode deposited using the sputter target fabricated with the deformable die.

The approach described in this work is useful and facilitates the production of sputter targets or similar other products. It should be mentioned that the approach is applicable because there is a very little change in the inner diameter of the PTFE die during pressing. This is probably due to the restriction of the radial flow of the powders due to the friction between the powder and the platen. Therefore the approach described here is applicable to thin products as when the height increases, there would be a radial flow of powders away from the platen. The limiting value of diameter to height ratio is difficult to estimate. It should also be emphasized that with particulate material, the friction in the radial flow would also be high away from the platens. These observations imply that in particulate materials for the geometry in question, compaction occurs more in axial direction than it is with radial direction.

Considerations given above may imply that the use of PTFE die is not necessarily confined to products of circular cross-section. If arguments advanced above, about the restricted flow of the material in radial direction are applicable, then flat products of

irregular shape with a reasonable diameter to height ratio may well be manufactured with the same approach.

3.4 Conclusions

In this study, a simple method was proposed for the fabrication of flat ceramic products of reduced aspect ratio. The method makes use of deformable die that can suitably be made from thermoplastic polymers or similar deformable materials. The die is filled with powders of tapped uniform density and pressed between parallel platens compacting the powders while deforming the die. Before actual fabrication, it is useful to carry out tests using smaller diameter dies, generating data with regard to sintered density and shrinkage with respect to the applied compaction pressure. The deformable die is then dimensioned based on the extrapolation of the relevant data. This approach was illustrated with the fabrication of 2 inch $La_{0.8}Sr_{0.2}CoO_{3-\delta}$ (LSC-113) target with a sintered density greater than 0.95 and dimensions within the tolerances of the sputter gun. It is proposed that the approach is not necessarily restricted to circular products, as high friction in tapped particulate media makes the lateral flow difficult, confining the compaction mainly to axial direction. Therefore fabrication of flat products of irregular shape may also be possible with the same approach. Limiting value of the product height is difficult to estimate, but it is not necessarily small.

CHAPTER 4

COMBINATORIAL DEVELOPMENT OF LSC-113/LSC-214 COMPOSITE CATHODE WITH IMPROVED PERFORMANCE

4.1 Introduction

There is a considerable interest in the reduction of operating temperature of solid oxide fuels cell (SOFC). Thus, numerous studies have been conducted to develop the so-called intermediate temperature SOFCs [Gong et al. (2006), Brett et al. (2008)]. The bottle neck in IT-SOFCs is the cathode material as there are suitable alternatives for anode and electrolyte that could operate with acceptable kinetics at temperatures as low as 600 °C. In the case of cathode materials, the main problem is oxygen reduction reaction (ORR) which becomes unacceptably slow at reduced temperatures.

For IT-SOFC, new cathode materials are currently under development. These include perovskite based oxides that have mixed ionic and electronic conductivity; $La_{1-x}Sr_xFeO_{3-\delta}$ (LSF), $La_{1-x}Sr_xCoO_3$ (LSC), $La_{1-x}Sr_xCo_{1-y}Fe_yO_{3-\delta}$ (LSCF), $Ba_{1-x}Sr_xCo_{1-y}Fe_yO_{3-\delta}$ (BSCF). Of these, LSC has attracted considerable attention with its attractive ORR at relatively low temperature [Imanishi et al., (2004), Niedrig, et al. (2015)]. It was shown recently that the kinetics of cathodic processes can be improved dramatically when LSC-113 is combined with Ruddlesden-Popper type $(La_xSr_{1-x})CoO_4$ (LSC-214) cobaltites. Feng et al., (2013) and Leonard et al., (2013) found that with these mixed oxides ORR kinetics were enhanced quite substantially. This enhancement was attributed to the beneficial effect of hetero-interfaces in the composite cathode (Sase et al. 2008). Thus, efforts have concentrated in maximizing the interfaces in LSC based composite cathodes.

Mutoro et al. (2011) have used multilayer approach where LSC-113, the main phase, was covered completely by LSC-214, or they used a surface decoration technique where the interfacial regions were more abundant. Ma et al. (2015), so as to obtain further maximization, have deposited vertically aligned nanocomposites where the individual columns were 100-500 nm in width. In all these studies, the volume fractions of LSC-214 were quite low varying from 0.10 up to 0.35, in the respective order.

In maximizing the interfacial regions, the volume fraction is an important parameter as well as the scale of the structure. Therefore, the current study was undertaken to investigate how the cathode performance is affected by the phase fractions, while keeping the structure at nanoscale. For this purpose, we adopt a combinatorial approach based on sputter deposition where the volume fraction of LSC-214 varied from 0.10 to 0.90 in terms of mole fractions.

4.2 Experimental Procedure

LSC-113 as well as LSC-214 powders were synthesized using Pechini method. Details of powder synthesis as well as the preparation of the sputter targets from the powders are given in (Sari et al. 2017) and (Torunoglu et al. 2017).

Combinatorial deposition of Cathodes: Thin film cathodes of mixed oxides were produced via sputter deposition in a specially designed vacuum deposition system (Pişkin & Öztürk, 2017). A schematic representation of deposition geometry employed in this work is given in Fig. 4.1. As seen in the figure, the system comprises two sputter guns (2 inch diameter); LSC-113 and LSC-214 which are 130 mm apart. Above the guns, the system contains a rectangular magazine comprising circular substrate holders.

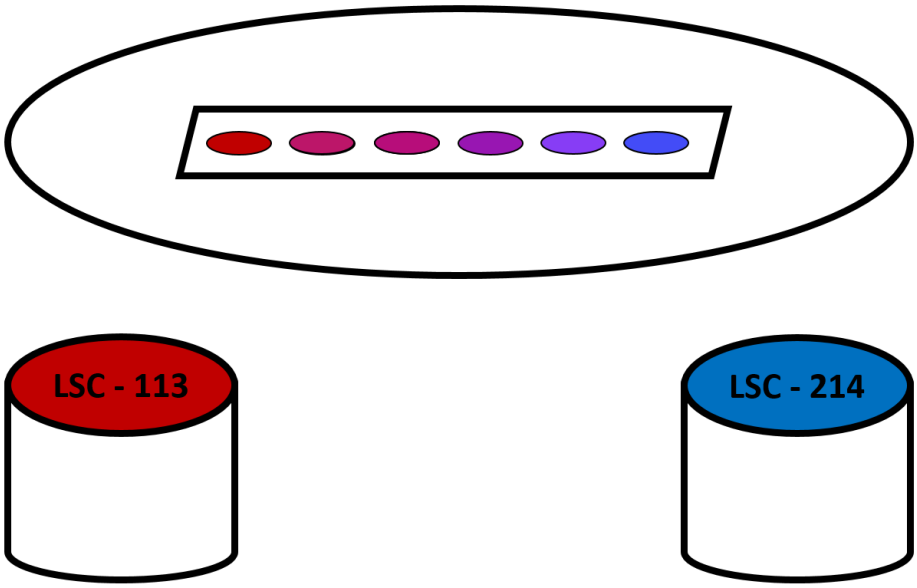

Figure 4. 1. Schematic representation of sample holder, LSC-113 and LSC-214 sputter guns

A library of 6 cathodes were deposited simultaneaously. Each cathode had a different LSC-113 and LSC-214 make-up as a result of their diffierent position with respect to the targets. The base pressure of the chamber was typically $1x10^{-7}$ Torr. Argon flow was adjusted (≈10 cm^3/min) so as to maintain 5 mTorr pressure during sputtering. The substrates were kept at 400 $^{\circ}C$ using a substrate heater inside the chamber. To obtain a library of cathodes, both guns were operated simultaneously, with power loading of 30 Watts. Sputtering was carried out for a duration of 10 hours yielding a cathode thickness of approximately 700 nm.

Measurement of EIS response: EIS response of thin film cathodes were measured on symmetric cells. The substrates were gadolinium doped ceria (GDC) typically 1 mm in thickness and 19 mm in diameter. Schematic drawing of the symmetric cell used in this study is given in Fig. 4.2. Here, it is seen that the symmetric cell is made up of three layers. Top and bottom layers were cathodes which were in contact with gold current collectors. These are sputter deposited on the midlayer, i.e. GDC. Two

sets of masks were used to control the surface area of the cathodes and the current collectors. These masks were stainless steel flat rings with 12 mm (cathode) and 10 mm (current collector) in inner diameter.

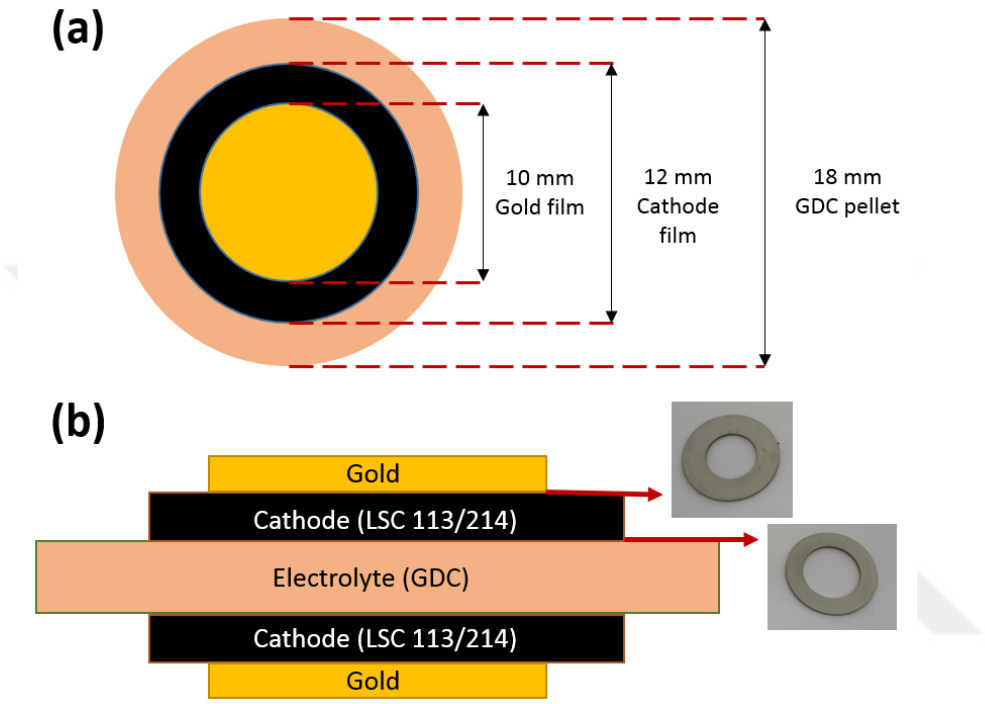

Figure 4. 2 Schematic drawing of the symmetric cells used in electrochemical impedance spectroscopy, (a) top view, (b) side view.

The current collector which was in the form gold layers, 10 mm in diameter was sputter deposited onto the cathode layers to a thickness of 150 ± 10 nm. This has left a ring of uncoated cathode materials at the periphery which had an area of 0.34 cm^2 exposed to the atmosphere. Connections were made with gold wires to the inner gold region using a gold paste (8884-G ESL Europe).

The symmetric cell as decribed above were installed to one end of an alumina tube 25 mm in inner and 36 mm in outer diameter. The cell was located at one end of the tube

and selaed with the use of ceramic sealant (AREMCO). The whole assemby was placed inside a tubular furnace as shown in Fig. 4.3.

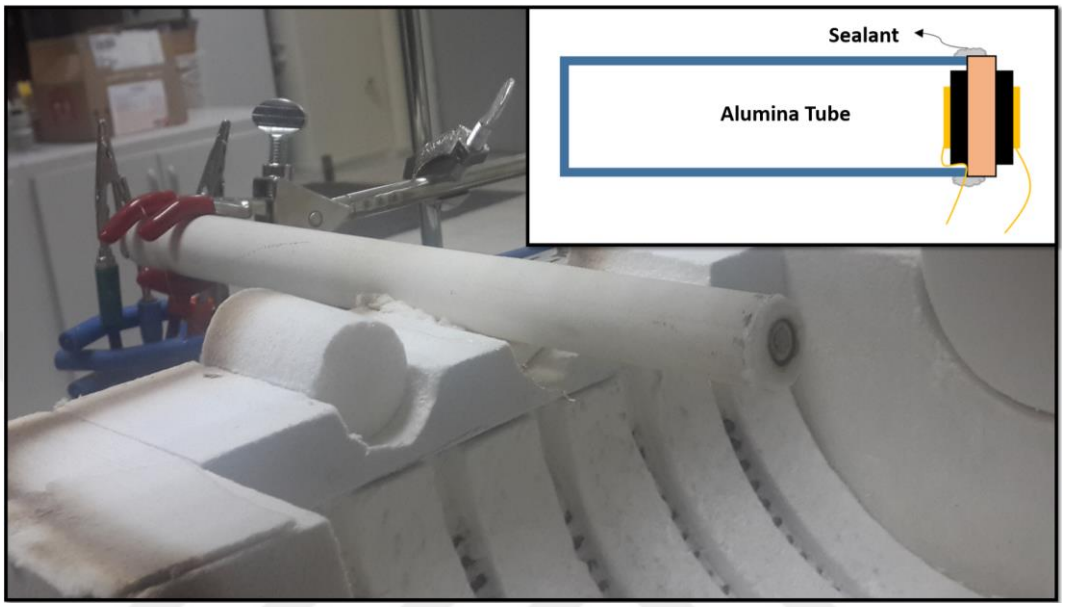

Figure 4. 3 Assemby of the symmetric cell for EIS measurements in a tubular split furnace; the inset indicates the schematic representation of the assembly.

The symmetric cell at the end of the tube located at the very center of the furnace. Measurements were carried out in the range of 700-300 $^{\circ}$C using potentiostat-galvanostat (Gamry Inst. Reference 3000). Electrochemical impedance spectrums were collected with a perturbation voltage of 10 mV from 1 MHz to 10 mHz. To gather more information about the electrochemical spectrum of the cells the frequency range could be increased with the expense of test time. Since chemical and structural stability problems could be arised for LSC based cathodes, as it was summarized in section 2.1.3, the frequency range was determined as 1 MHz-10 mHz. Measurements were carried out at constant temperatures in the range of 700-300 ^{0}C.

In order to analyze the EIS spectrums, it is necessary to adopt a model that has a good fit with the relevant data and comprises all the relevant components. In EIS analysis

of the cathode material, certain amount of perturbation voltage is applied to trigger the chemical processes involved in the operation. The frequency range of the response of a particular process depends on its kinetics, i.e. if the chemical process, such as oxygen surface exchange, is slow, then relevant EIS response can be observed at low frequencies and vice versa (Baumann et al. 2006). As it is summarized in section 2.3.1, there are three components in the cathodic processes namely, surface oxygen exchange, diffusion of oxygen ions through the cathode material, and the electrochemical charge transfer between the cathode and the electrolyte. Thus, it is required that the model accounts for all of these components and ideally there should be four separate arcs, one of which is corresponding to the electrolyte resistance at high frequency region, and three consequtive arcs corresponding to surface oxygen exchange, bulk diffusion and charge transfer between the electrode and the electrolyte (Adler, 2000). In certain conditions one or more of these components have negligible contributions to the overall cathode resistance, e.g. the diffusion process has almost no effect on the cathodic resistance when the cathode is thin enough. For the thin film studies similar to the experiments explained above, the thickness of the cathode layers are generally well below the critical thickness values and therefore, the arc related with the diffusion process shrinks considerably. As a result of this, the model can also be simplified into two consecutive arcs, i.e. omitting the diffusion related sub-circuit, for the investigation of the cathodic processes. Moreover, it is commonly observed that the arcs in the impedance spectrums merge at certain temperatures. In these cases, it is almost impossible to differentiate the resistances of different sub-steps and it is required to simplify the model in which the total resistance of the cathode can be measured with comprising single resistance corresponding to overall cathode contribution.

For LSC cathodes the value of critical thickness, L_c, lies in the range of 1-40 μm in the temperature range of 400-700 °C [(Tarancón et al., 2010) and (Souza & Kilner, 1999)]. Since the cathodes fabricated in this study have thicknesses in submicron level, the resistance of diffusion of oxygen ions have negligible effect on the cathodic process at temperatures higher than 400 °C. Therefore, it is possible to model the spectrum with

a resistor connected in series to a sub-circuit where a resistor is connected to a constant phase element (CPE) in parallel, Fig. 4.4. While the first resistor corresponds to the ohmic resistance of the electrolyte layer, the second one corresponds to overall cathode resistance (Januschewsky et al. 2009).

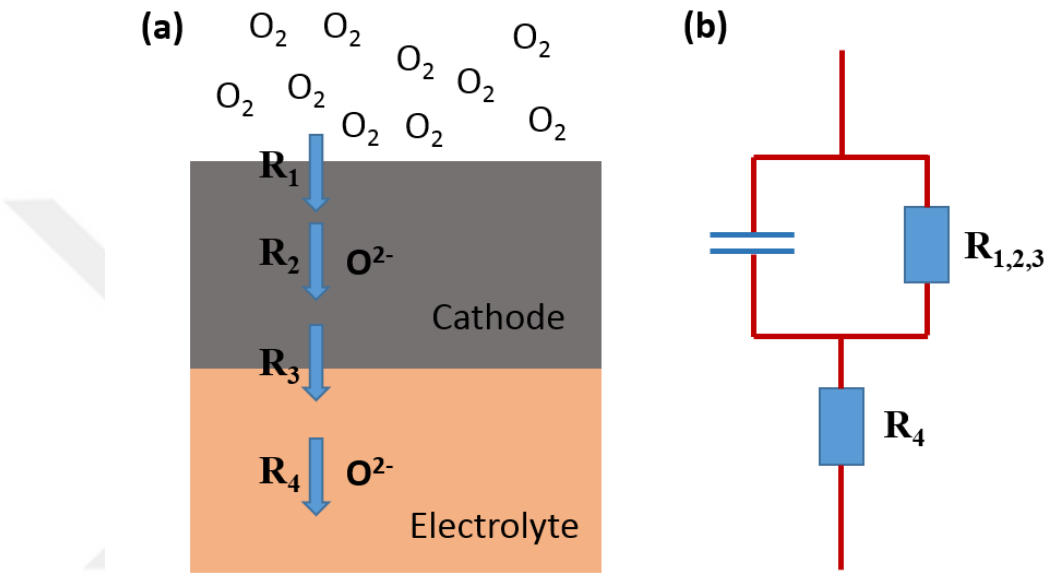

Figure 4. 4 (a) Kinetic model of electrochemical oxygen exchange comprising resistances due to surface exchange (R_1), ion transport (R_2), interfacial processes (R_3) and electrolyte resistance (R_4). (b) Equivalent circuit mostly used for fitting the impedance spectra.

In this study, the model given in Fig. 4.4 (b) is used to extract the area specific resistance values of the cathode layers in the temperature range of 400-700°C. At lower temperatures, on the other hand, the critical length diminishes to values in the range of 10-500 nm which creates an extra contribution to the overall resistance due to the bulk ionic diffusion (Adler, 2004). In these cases, alternative models or exrapolation techniques were used to estimate ASR values.

4.3 Results and Discussion

In order to control the volume fraction of the phases in the material library, a special test was carried out using quartz substrates in the sample magazine, Fig 4.2. In these tests, LSC-113 and LSC-214 targets were in their respective positions and first LSC-113 was operated for a duration of 10 hours with parameters given in section 4.2. As a result of these tests, a set of 6 samples were obtaied. Coatings produced measured using profilometry (Rtec instruments) had diffferent thicknesses in each sample. The same experiements and measurements were repeated for LSC-214 using the same parameters. For the actual deposition of the cathodes, both guns were operated simultaneously using exactly the same parameters as before. Here, the expected total thickness of the deposited layer in sample i was $t^i_{total} = t^i_{113} + t^i_{214}$ where t^i_{113} and t^i_{214} are the thicknesses of the deposited layer 113 and 214 when they were deposited on their own. The volume fractions were expressed t^i_{113}/ t^i_t and t^i_{214}/ t^i_t. The fractions for each member of the library are shown in Fig 4.5.

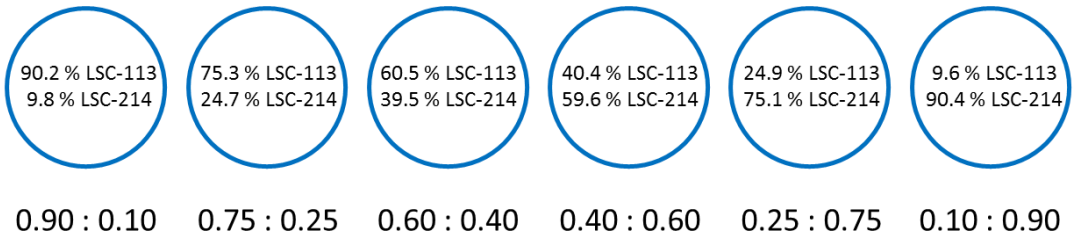

Figure 4. 5 Approximate volume fractions of co-sputterd thin films. Values refer to the volume fractions of LSC-113 and LSC-214 constituents.

Symmetric cells produced with co-sputtering of LSC-113 and LSC-214 targets were analysed with regard to their electrochemical impedance spectrums. Measurements were carried out at constant temperatures in the range of 700-300 ^{0}C.

Fig. 4.6 refers to EIS responses obtained with LSC-113:LSC-214=0.90:0.10 at 300 °C. As seen in the figure, there are two arcs; the one at the high frequency region, on the left, represents the resistance arising from the electrolyte and the other at the low frequency region, on the right, represents the resistance from cathodic processes. At higher temperatures, the high frequency arc diminishes while the one at the low frequency shrinks to smaller arcs resulting in lower resistance values as expected.

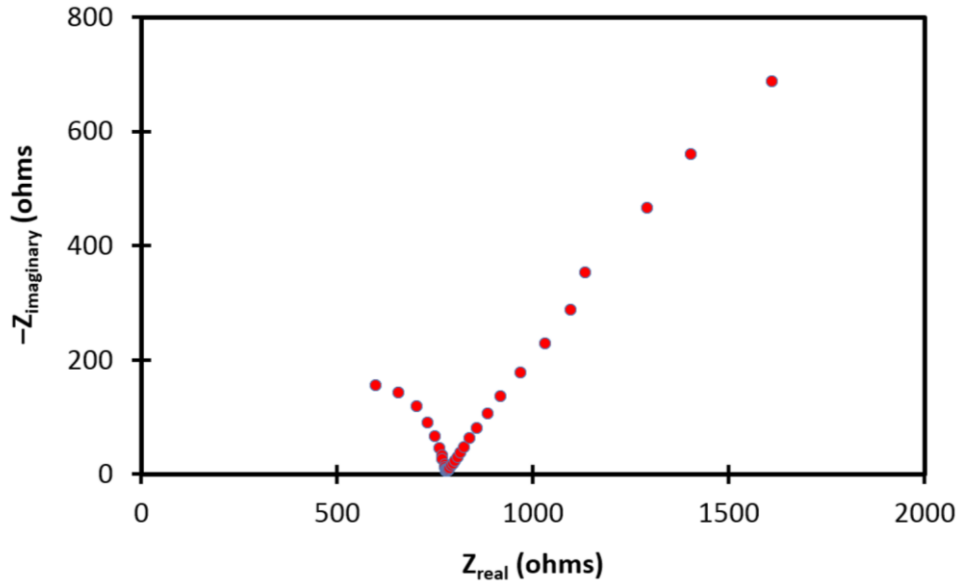

Figure 4. 6 Illustration of an EIS example observed in co-sputtered symmetric cells at 300 °C. The sample composition was LSC-113:LSC-214=0.90:0.10.

As it can be seen from Fig. 4.6, the EIS response of the cathode at 300°C showed almost a linear like behavior. Therefore, at such low temperatures it was difficult to apply a suitable model to interpret the data because it is not possible to estimate the upcoming behavior of the spectrum. The difficulty of divergent EIS spectrum was observed for all of the samples tested at temperatures less than 400 °C. In these cases, rather than measuring the ASR directly from the spectra, an exrapolation procedure was used and the values were estimated from log(ASR) vs 1000/T [K^{-1}] curves determined by the measurements at high temperatures.

At temperatures higher than 400 °C, the spectrums started to show a convergent behavior after certain temperatures depending on the composition. For instance, convergent EIS curve obtained at 450 °C for the composition LSC-113:LSC-214=0.90:0.10 while this was the case at 380 °C for LSC-113:LSC-214=0.60:0.40.

Where EIS spectrums were convergent, the model given in Figure 4.4 (b) was used to extract the ASR values of the cathodes. An example of such a spectrum is given for the sample LSC-113:LSC-214=0.90:0.10 at 550 °C, in Fig. 4.7.

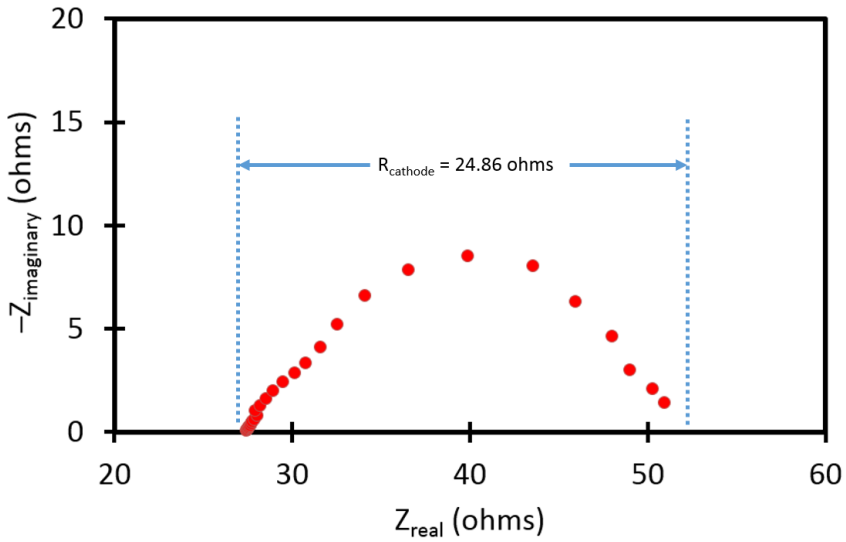

Figure 4. 7 Illustration of an EIS example observed in co-sputtered symmetric cells at 550°C. The sample composition was LSC-113:LSC-214=0.90:0.10.

As it can be seen in Figure 4.7, the low frequency arc was almost complete by intersecting the x-axis at about Z_{real} = 52 ohms. It can be observed that the arc was not in the form of a perfect semi-circle. This is due to the the fact that the arc, in reality, combines separate cathodic processes instead of a single step process. The total $R_{cathode}$ value of 24.86 ohm was extracted from the model as shown on the figure. $ASR_{cathode}$ was obtained by multiplying $R_{cathode}$ with the active cathode area (0.34 cm^2) and dividing it by 2 (due to the use of symmetric cells). The value of $ASR_{cathode}$ corresponding to this spectrum for example was 4.22 $ohm.cm^2$. EIS spectra measured for the material library at 400°C and 550°C are given in Figure 4.8.

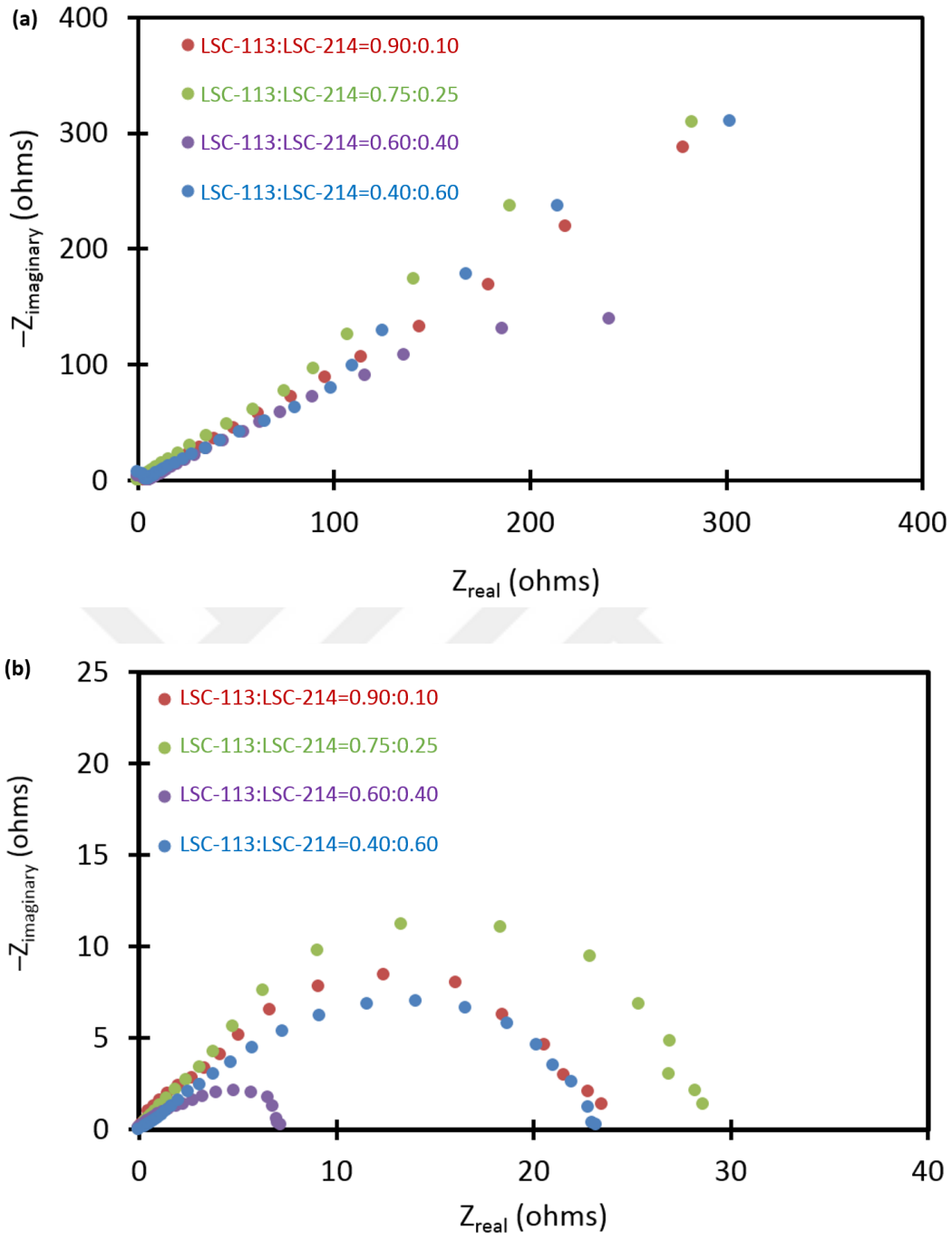

Figure 4. 8 EIS spectrums of samples with LSC-113:LSC-214 = 0.90:0.10, 0.75:0.25, 0.60:0.40, and 0.40:0.60 at (a) 400°C and (b) 550°C.

It should be mentioned that the spectra were shifted on the X-axis so that low frequency arcs start from the same position, i.e. spectra were shifted to the left by substracting the electrolyte resistance[1] in the X-axis.

As seen in the figures, arc arising from the cathodic processes shrinks to smaller radii as the composition is enriched in terms of LSC-214. Thus while the arc has a value of Z_{real}= 25 ohms in LSC-113:LSC-214 = 0.75:0.25, this value shrinks to values less than 10 ohms in LSC-113:LSC-214=0.60:0.40. It should also be noted that the trend reverses afterwards and the value returns to Z_{real}= 25 ohms with further increase of LSC-214.

Using the model given in Figure 4.4 (b) electrochemical impedance spectra were analysed to extract the area specific resistance (ASR) values of the cathodes at each temperature. These values are shown plotted in the form of log(ASR) vs 1000/T for each composite cathode. It should be noted that the relative position of the composite cathodes depends on the temperature. Excluding LSC-113:LSC-214=60:40, a crossover seems to be present at around 600 $^{\circ}$C. Above this temperature ASR decreases in the order of LSC-113:LSC-214=0.10:0.90, 0.25:0.75, 0.75:0.25, 0.40:0.60, and 0.90:0.10 while above this temperature ASR decresaes in the opposite order. This is quite reasonable as LSC-113 is known to have a higher ORR activity than LSC-214 at higher temperatures.

[1] Since GDC electrolytes of these samples were prepared by pressing and sintering GDC powders, the electrolyte thickness values varied from one sample to the other. As a result of this, electrolyte resistances were varied from sample to sample resulting in displacement of the arc in X-axis.

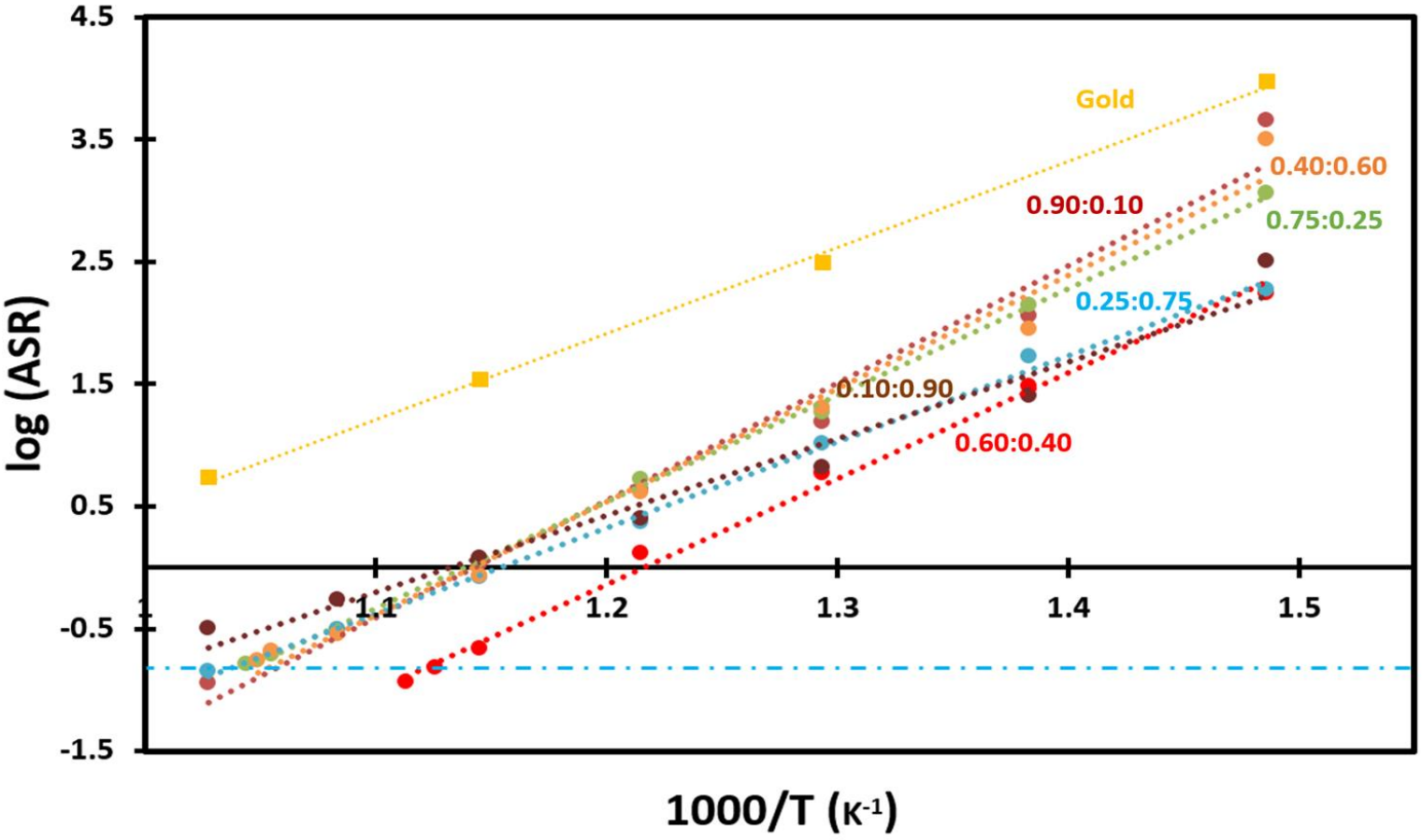

Figure 4.9 The relationship between log(ASR) vs 1000/T [K^{-1}] for the co-sputtered cathode library in the composition range of LSC-113:LSC-214=0.90:0.10 and 0.10:0.90.

In these measurements, thin gold layers sputtered on cathode layers were used as current collectors and therefore, it was required to determine possible contribution of the gold layer to overall cathode processes. For this purpose, a special sample was produced in which there was no open cathode surface. Thus, it was possible to obtain the overall contribution of the current collector gold layers in the EIS analyses of the material library. As it can be seen from Figure 4.9 there was orders of magnitude difference between the gold and the cathode materials which implies that the contribution of the current collector was quite negligible. As a result of this observation, all of the measured impedance spectra were assigned to the co-sputtered cathodes with confidence.

In order to better follow the variation with the composite composition, ASR values are shown plotted as a function of volume fraction of LSC-214 phase, Figure 4.10.

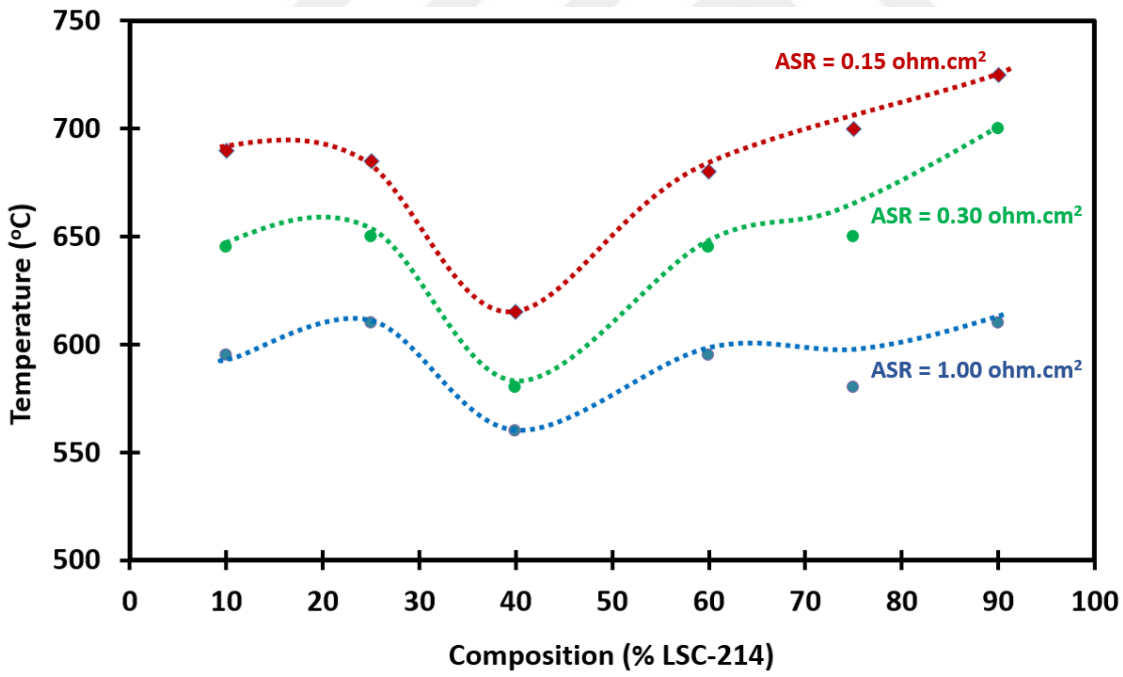

Figure 4.10 Temperature-Area specific resistance-composition diagram.

It is seen that the ASR values tend to decrease with increasing LSC-214. The lowest values were obtaied at LSC-113:LSC-214= 0.60:0.40. Beyond this, the values tend to increase again which means that the mid-compositions were useful in minimizing the ASR.

Fig. 4 10 covers three ASR values, namely 0.15, 0.30 and 1.0 ohm.cm^2. It should be mentioned that an ASR value of 0.15 ohm.cm^2 is usually taken as the target value for cathodes in practical applications. For this reason the temperatures at which ASR= 0.15 ohm.cm^2 was reached has a special significance. In this respect, the best case, i.e. the lowest operating temperature applicabe, was obtained as 615^{o}C with the cathode composition of LSC-113:LSC-214=0.60:0.40.

The trend depicted in Fig 4.10 is such that even lower ASR values may be obtained at around mid-compositions. To explore this posssibility, a second set of samples were prepared in a narrower compositional range, from LSC-113:LSC-214=0.35:0.65 to 0.65:0.35. The relative positions of the samples were arranged such that there were a total of 5 samples with diffrenet compositions. Approximate volume fractions of the samples are given in Figure 4.11.

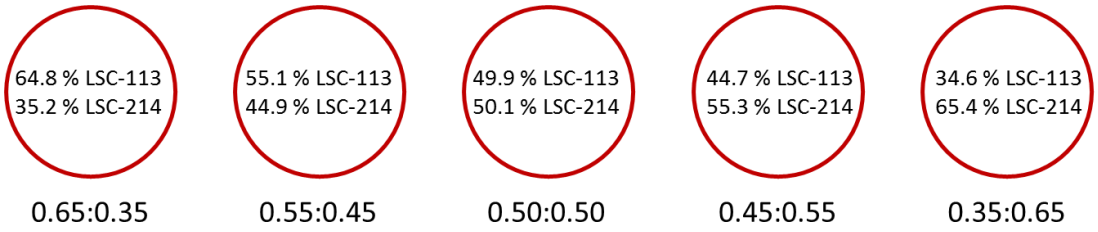

Figure 4.11 Approximate volume fractions of the second set of co-sputterd thin films. Values refer to the volume fractions of LSC-113 and LSC-214 constituents.

The same procedures were applied to the second set of samples and the corresponding log(ASR) vs 1000/T curves as well as Temperature - ASR - Composition diagrams were obtained. These are given in Fig. 4.12 and 4.13, in the respective order.

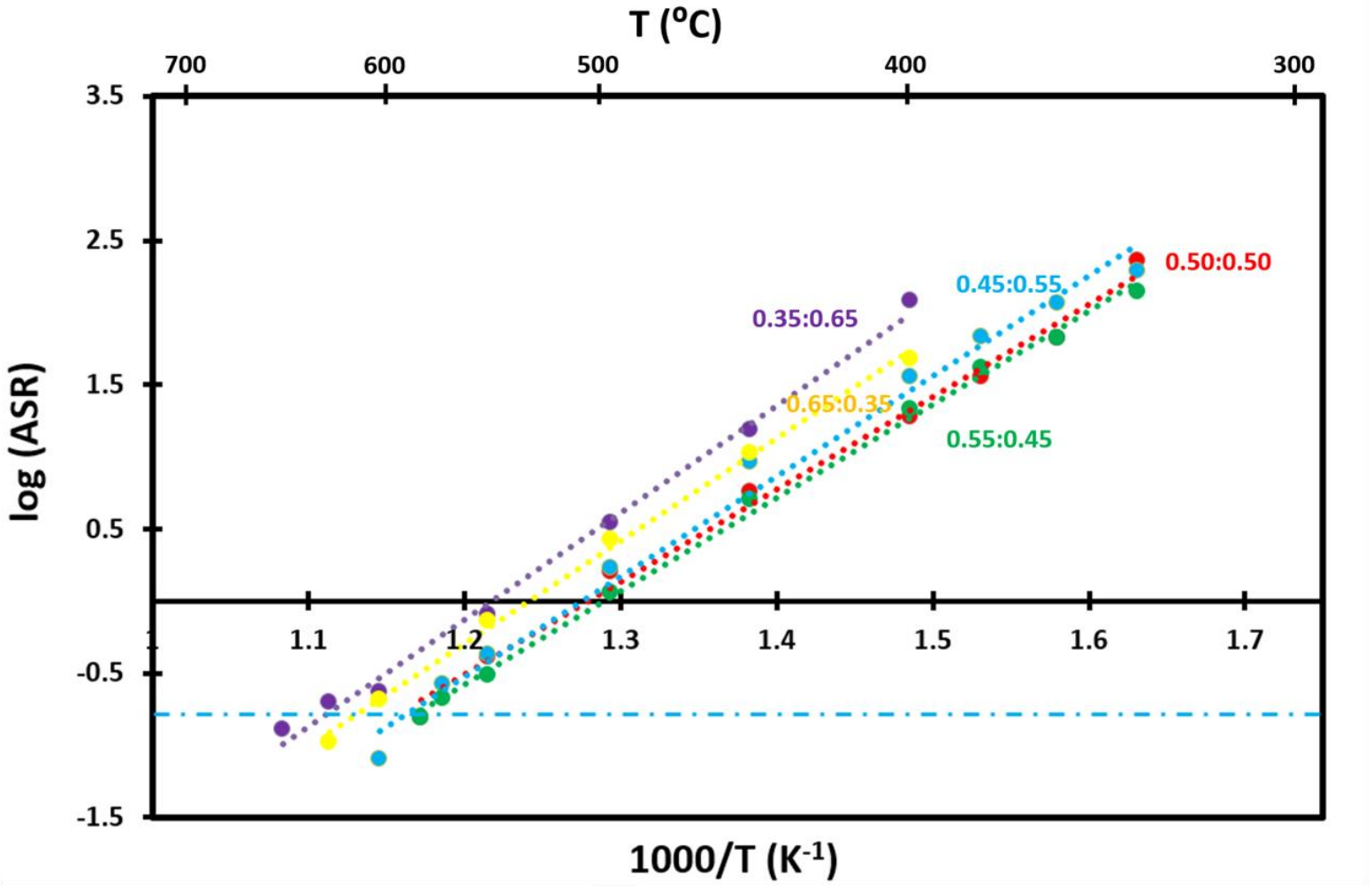

Figure 4.12 The relationship between log(ASR) vs 1000/T [K^{-1}] for the second set of co-sputtered cathode library in the composition range of LSC-113:LSC-214=0.65:0.35 and 0.35:0.65.

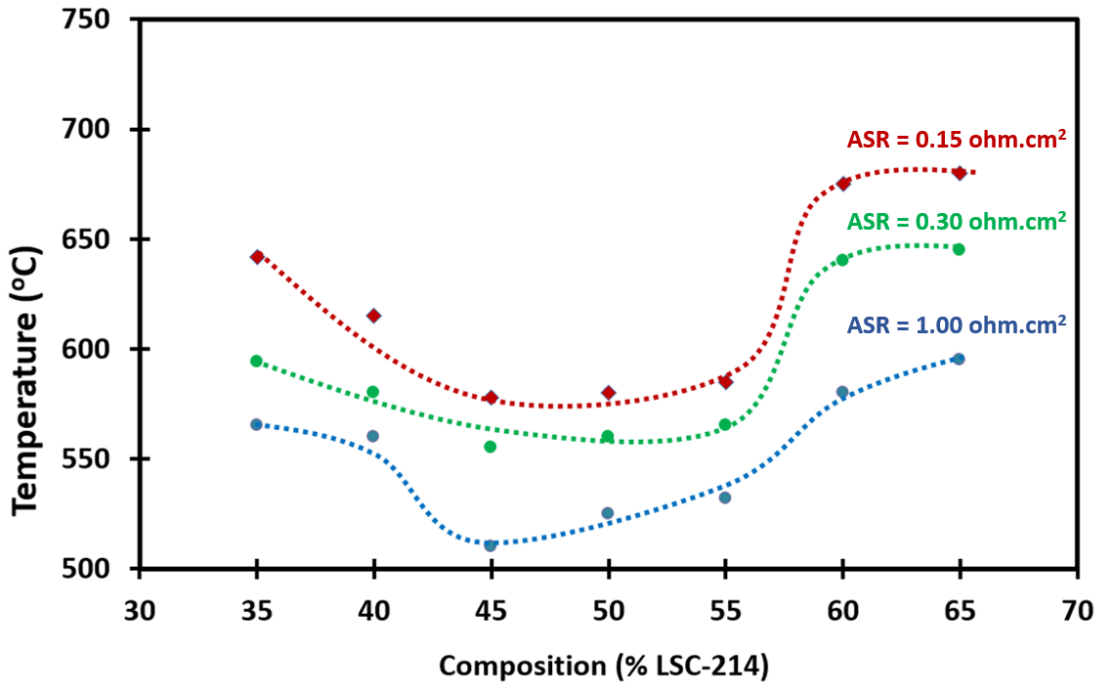

Figure 4.13 Temperature-Area specific resistance-composition diagram for the second set of samples in the composition range of LSC-113:LSC-214=0.65:0.35 and 0.35:0.65.

Variation of ASR with composition given in Fig.4.13 shows that even better values of ASR are possible around mid-compositions. In this mid-region, taking ASR value of 0.15 ohm.cm^2 as the reference, the minimum temperature which was 615 °C with LSC113:LSC214=0.60:0.40 reduces down to 575 °C in the composition range of 0.45<LSC-214<0.55 range. In this range, diffrences in the applicable operating temperatures at which ASR = 0.15 ohm.cm^2 are very small. Still LSC-113 : LSC- 214 =0.55:0.45 may be taken as the best composition, though the diffrence in temperature is less than 5 °C as compared to LSC113:LSC 214=0.45:0.55.

In fact that the observation of attaining the lowest ASR value at the mid-composition region was not surprising, since the maximization of the dissimilar interfacial regions occurs as the volume fractions of LSC-113 and LSC-214 phases become closer to each other. However, it was seen that co-sputtering created a positive effect even for the samples that were dominated by the presence of either LSC-113 or LSC-214. For

instance, LSC-113:LSC-214= 0.65:0.35 yield an ASR value of 280 ohm.cm^2 at 400^{o}C This value should be compared with ASR = of 1000 Ω.cm^2 obtained by Ma et al., (2015), in vertically aligned LSC-113 and LSC-214 columns with a similar volume fractions. It should be mentioned that the formation of the composite cathode via co-sputtering resulted in an order of enhancement compared to vertically aligned structure, Figure 4.14.

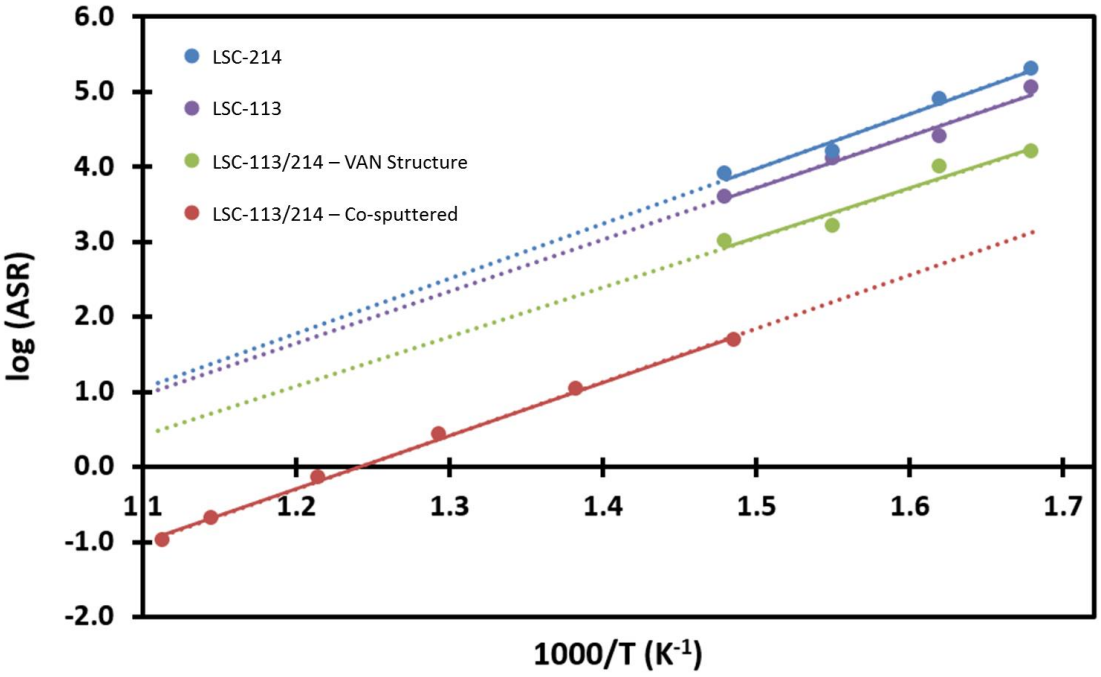

Figure 4.14 log (ASR) vs 1000/T curves of LSC-113, LSC-214 single phases and vertically aligned structure with an approximate volume fraction of LSC-113:LSC:214 = 0.65:0.35 (Ma et al., 2015) together with co-sputtered sample with LSC-113:LSC:214 = 0.65:0.35.

As it can be seen from the figure, the data were collected at different temperature ranges. Therefore, an extrapolation method was used to compare these data and in all cases a linear trend was shown. It should be mentioned that co-sputtered sample has an almost same slope with the vertically aligned nanocomposite prepared by pulsed laser deposition which is an indication of similar type of rate determining step.

Although the rate determining step might be the same, it appears that co-sputtering technique has a positive effect in cathode performance at all temperatures.

In order to find the root cause of this enhancement, co-sputtered cells were investigated structurally with the help of transmission electron micsroscope. For this purpose, LSC-113:LSC-214=0.50:0.50 composition was selected for futher characterizations. The sample from this composite cathode was prepared with the help of focused ion beam microscopy (FIB).

Figure 4.15 is the cross sectional bright field image of the sample showing both electrolyte and the cathode layers. As it can be seen from the image, the electrolyte has a granular structure with the grain size of approximately 1 micron. This is followed by a cathode layer of approxiametely 700 nm which appears featurless in the micrograph. The layer at the top is gold which was deposited on the cathode for measurement purposes.

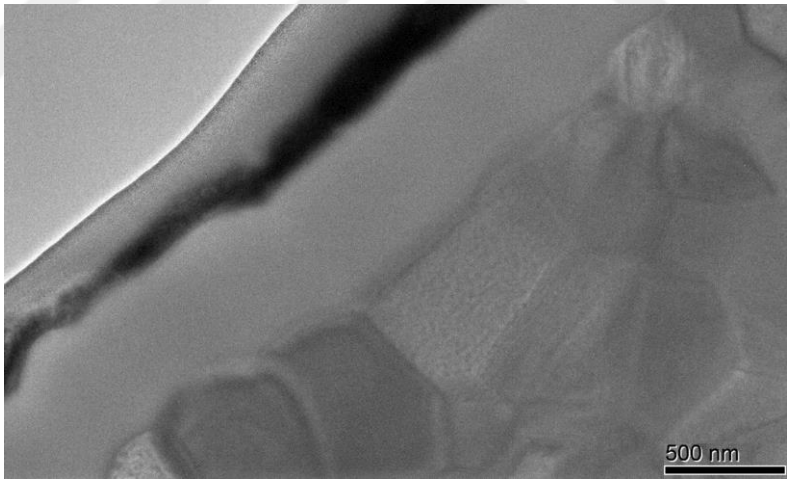

Figure 4.15 Bright field image of co-sputtered composite cathode with a composition of LSC-113:LSC-214=0.50:0.50.

Fig. 4.16 is the selected area diffraction pattern taken from the cathode area. The pattern is consistent with the pattern expected from an amorphous material. This means that, during sputter deposition in the cathode, LSC-113 and LSC-214 phases were mixed at an extremely fine scale yielding an amourphous-like structure.

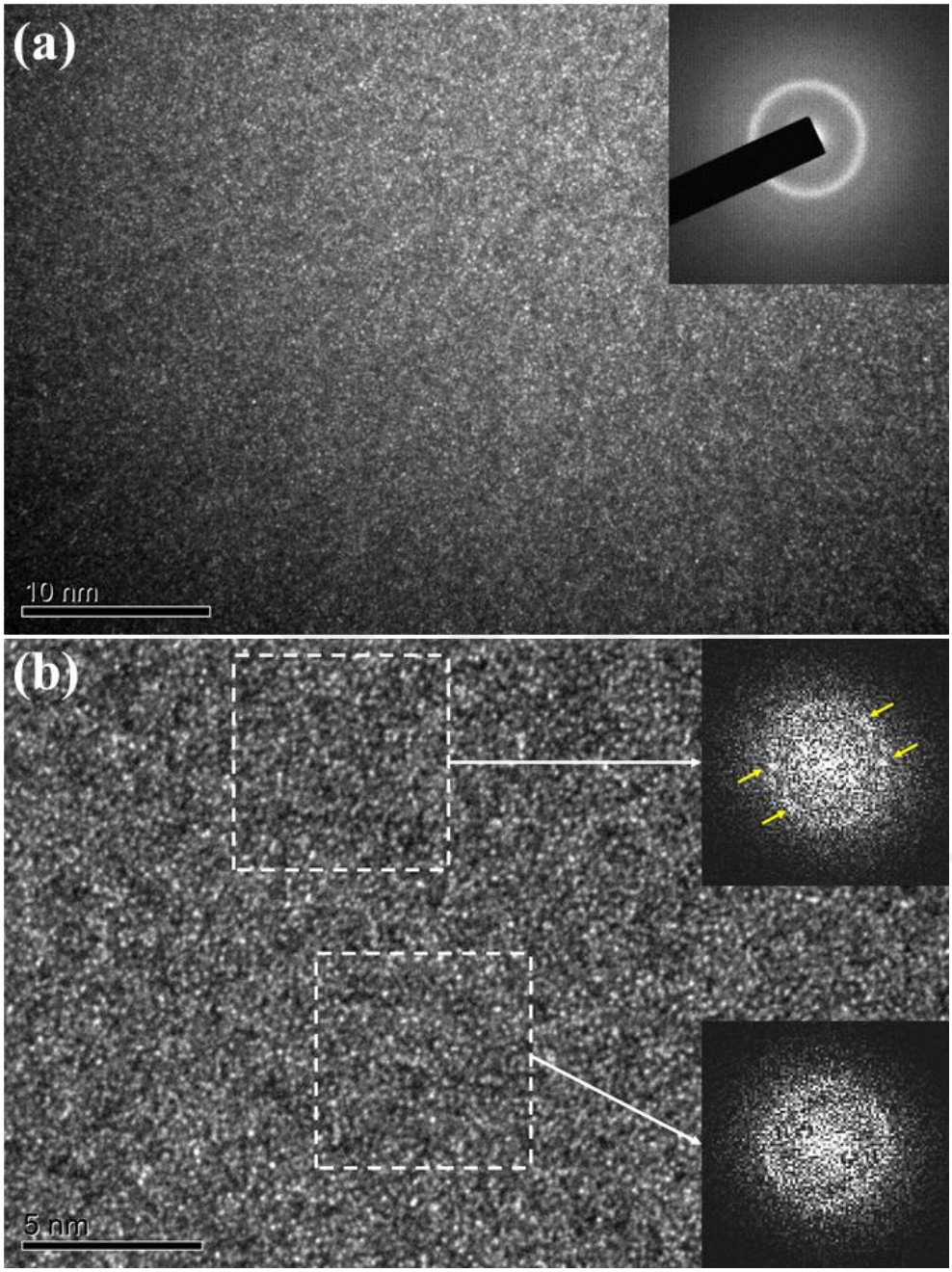

Figure 4.16 High resolution transmission electron microscope (HRTEM) image of the co-sputtered composite cathode with a composition of LSC-113:LSC-214=0.50:0.50. Note that part (b) is the magnified image of part (a) showing nanocrsytals embedded in amorphous matrix.

The featureless structure in Fig. 4.15 as well as diffraction pattern given in Fig 4.16 verifies that both phases are mixed intimately with each other yielding an amorphous structure. There were also small amount of nanocrystals embedded in the amorphous matrix as it is shown in Figure 4.16 (b). In this structure, it should be noted that there was a lack of separate phases and therefore, it is difficult to claim that the interfacial area is maximized between LSC-113 and LSC-214.

Since the initial structure of the cathode layer would not remain at the elevated temperatures, it is more crucial to investigate structural features of the material at such high temperatures. For this purpose, the cathode was annealed at a temperature of 700 °C for 10 days. Fig 4.17 shows the high resolution TEM image and the selected area diffraction pattern of the annealed cathode.

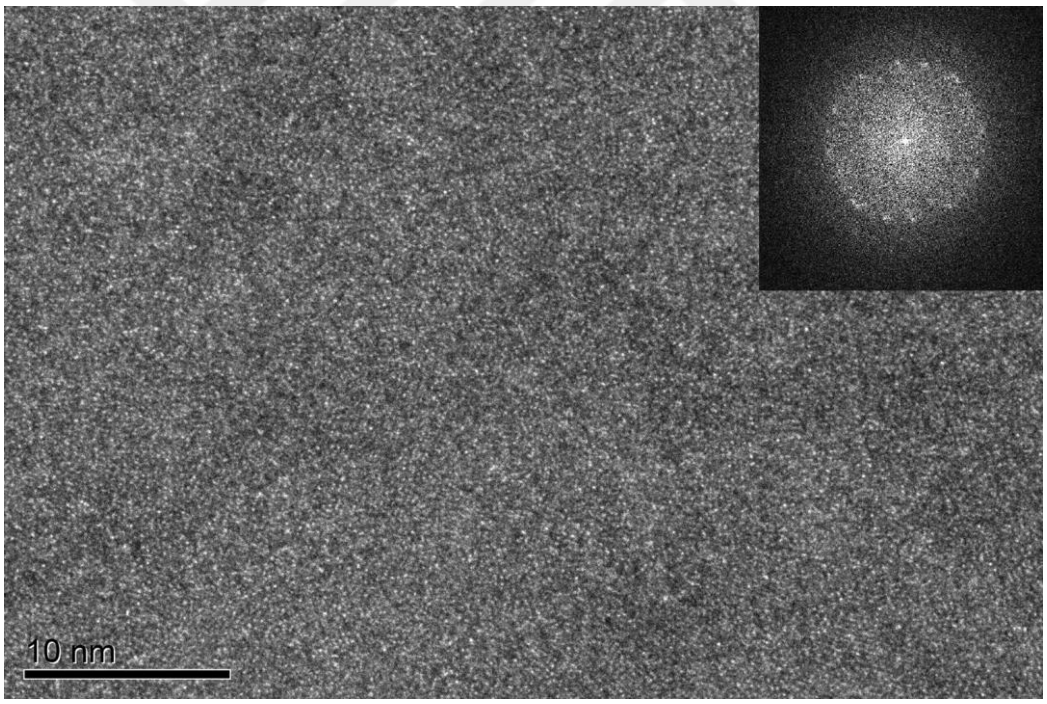

Figure 4.17 High resolution TEM image of the co-sputtered composite cathode with a composition of LSC-113:LSC-214=0.50:0.50 after annealing at 700°C for 10 days.

It should be noted that the spots became much more explicit after annealing which is the indication of crystallization of amorphous regions and crystal growth of pre-existing nanocrystals in the cathode layer. The sizes of the nanocrystals in the annealed cathode was in the range of 4-10 nm. This continuos and uniformly distributed nanocrystalline structure increases the density of interfacial regions between LSC-113 and LSC-214 phases.

In order to confirm the validity of crystallization that takes place during annealing XRD data were collected before and after annealing, Figure 4.18.

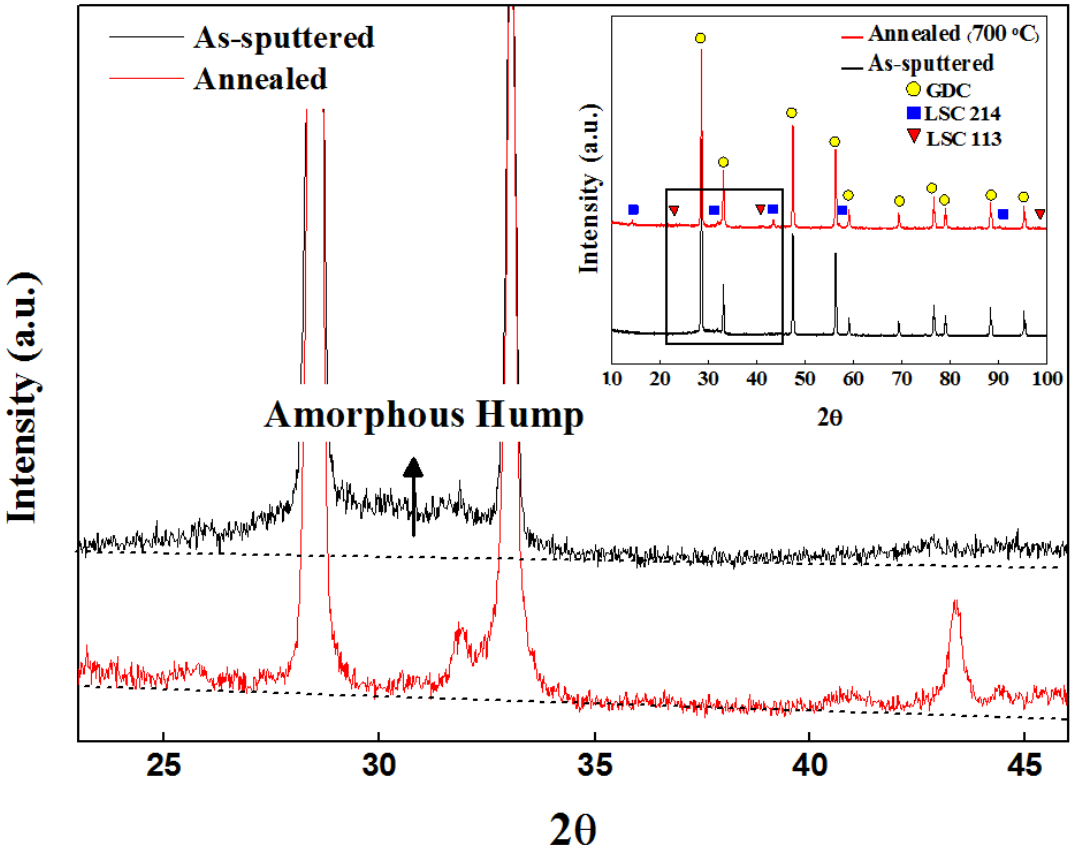

4.18 X-ray diffractograms of co-sputtered cathode in as-sputtered (black) and annealed (red) conditions. The entire XRD patterns of both samples are given in the inset. Note the presence of an amorphous hump in as-sputtered condition.

Since the cathode layers were very thin and they were deposited on relatively rough electrolyte surfaces, it was difficult to collect reliable X-ray data. The peaks corresponding to GDC electrolyte and gold current collector were observed in both of the pre-annealed and as-sputtered conditions. In addition to these peaks, at around $2\theta=30^{\circ}$ there was a hump which is an indication of an amorphous-like structure as implied by TEM analysis. The position of this hump is compatible with the ring observed in the selected area diffraction pattern given in Fig. 4.16. Thus, it is certain that the hump belongs to the cathode layer and the observation of an amouphous like structure is not a local feature but representative for the entire cathode.

Also given in Fig. 4.18 is the corresponding section of XRD pattern obtained from the annealed sample. The hump is not present in this annealed condition which implies that the cathode is probably not amouphous anymore. It should be noted that there are new peaks in the annealed cathode corresponding to LSC-113 and LSC-214 phases which verifies that the cathode is now crystalline. This feature which was already determined by TEM is a representative feature of the cathode as a whole.

XRD pattern given in Fig 4.18 was obtained in Bragg-Brentano geometry. Since the cathode layer is quite thin, it would be useful to examine this film in grazing incidence geometry. Figure 4.19 is the XRD pattern obtained in this geometry. As seen from the figure, the cathode peaks were identified clearly in this XRD pattern.

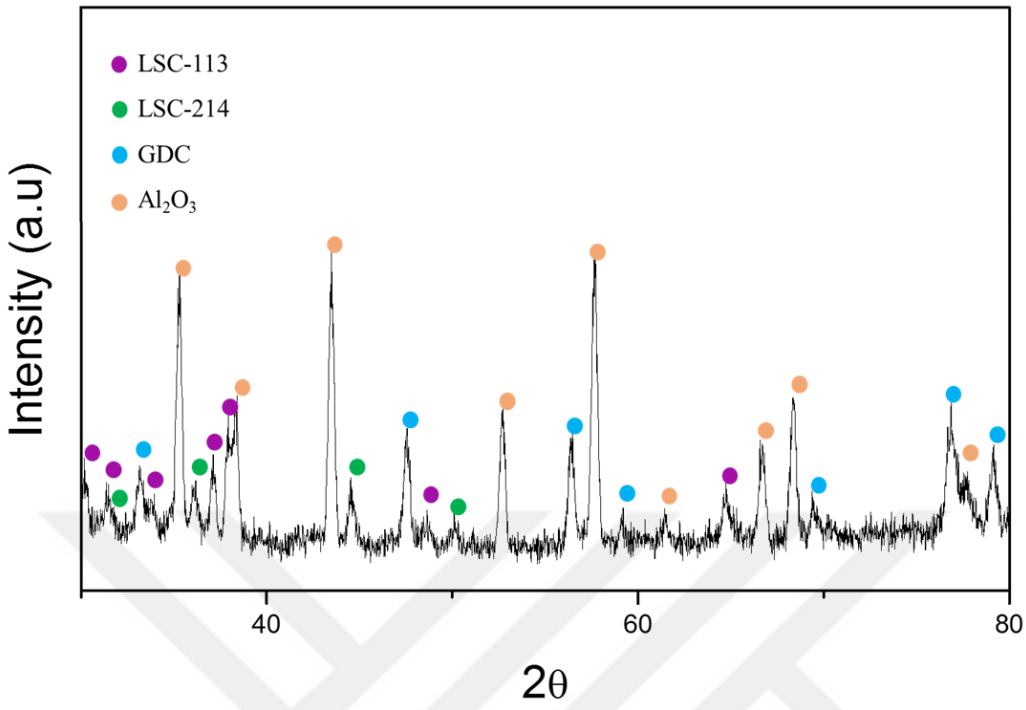

Figure 4.19 XRD pattern of the co-sputtered cathode collected with grazing incidence geometry. Note the presence of well defined LSC113 and LSC 214 peaks. Alumina peaks occur because of the contamination since the sample was removed from alumina tube.

It should be mentioned that the cathode material with LSC-113/LSC-214 = 0.50:0.50 composition could be used at temperatures as low as 575 °C. Here, although annealing temperature was deliberately selected high to promote crystallization in the cathode, the scale of the structure was still extremely fine. Considering the sizes of crystals at 700 °C after 10 days, it can be concluded that cathode would be quite stable at the operating temperature of 575 °C.

In the light of these observations, the sputter deposited LSC-113/LSC-214 gives an extremely refined structure where dissimilar interfaces would be maximized at the operating temperatures.

4.4 Conclusions

Collecting the results of EIS measurements as well as structural observations several points may be worth emphasizing;

First of all the combinatorial approach is very beneficial to detect the optimum composition in the composite cathode system. This practical approach enables to search the effect of compositional variations with a single step production satisfied by co-sputtering of the components. Another major advantage of this technique is the ability of refocusing to the desired areas. Thus, high speed compositional investigation was provided via combinatorial approach.

Secondly, EIS results of the first set of samples show a potential high performance region in terms of cathode ORR activity. Therefore, in the second set, the focus is given to this high potential region with narrower compositional range and the best composition was detected in this system. The best compositional region is appeared to be in the range of 0.45 < LSC-214 < 0.55 which was not studied in the literature so far. When a common target of ASR=0.15 ohm.cm^2 is used to determine the operating temperatures of the cathodes, the enhancement proposed by simultaneous deposition, provides that the operating temperatures of this system could be decreased down to 575 °C.

Another point worth emphasizing is the fact that co-sputtering leads to an amorphous structure. Even though the main purpose of this study was increasing the cathode performance by maximizing the amount of desired interfaces between LSC-113 and LSC-214 phases, the current work shows that amorphous cathode can also yield high ORR activity. This is more likely due to more open structure of the cathode facilitating cathodic processes especially at low temperatures. Although there are similar studies that show the positive effect of amorphous LSC-113 on the electrochemical performance of the cathode at temperatures as low as 400°C, the current study has an original perspective due to the presence of two dissimilar phases. At higher temperatures around 700°C or with longer usage the cathode may start to crystallize in the form of uniformly distributed nanocrystals ranging 4-10 nm in size. The presence

of two dissimilar phases prevents crystal growth of each other and preserves a high amount of desired interfaces between LSC-113 and LSC-214. Therefore, this crystallization gives a nanocrystalline cathode with performances as good as amorphous ones. It is also worth noting that, with further reduction in the temperature, the amorphous structure could be preserved throughout the operation life of the cathode. This is a new line of research which should be explored further.

All in all, LSC based oxides have proven themselves as highly active cathode materials as compared to conventional LSM based cathodes. Therefore, they are one of the best candidates, especially in the form of a composite structure (LSC-113/LSC-214), for IT-SOFCs. In literature there are several examples of heterostructured LSC-113/LSC-214 cathodes for the reduction of SOFCs. However, there was a lack of compositional optimization. As a result, the full potential of this system could not be known. To reveal the full potential of this sytem, the combinatorial study that was carried out in two consecutive steps for co-sputtered LSC-113/LSC-214 composite system, provided the detection of high performance compositions and lowered the operating temperature down to 575 °C which should be compared with other IT-SOFC operating temperatures, ranging from 550-700 °C in different cathode systems as given in section 2. In the light of these comparisons, the result seems quite promising especially in the case of IT-SOFCs where the operating temperature regime is selected in the range of 500-700 °C.

CHAPTER 5

SEGREGATION IN CO-SPUTTERED LSC-113/LSC-214 COMPOSITE CATHODE

5.1 Introduction

Attributed primarily to its high catalytic activity for oxygen reduction and high oxide ion conductivity, mixed ionic and electronic conducting (MIEC) perovskite-type oxides have attracted considerable interest for intermediate solid oxide fuel cells (IT-SOFCs). $La_{1-x}Sr_xCoO_3$ (LSC-113) is one such perovskite that is the most promising material to be utilized as a cathode material. It was also shown that the surface exchange kinetics of LSC-113 cathodes were increased 3-4 orders of magnitude by combining them with LSC-214. This composite system is of particular interest as it improves the kinetics of both oxygen transport and surface exchange at intermediate temperatures.

Although hetero-structured LSC-113/LSC-214 composite cathodes show very high ORR activity, they generally suffer from low chemical stability. At temperatures above 400 °C, negatively charged strontium dopants start to diffuse towards positively charged oxygen vacancies which are generally occupied at the surface of the cathode. As a result, Sr segregates to the surface forming an insulating SrO coverage which creates an additional resistance for the adsorption and incorporation of oxygen to the surface. These effects were observed in several studies (Orikasa et al., 2014) where sudden degradation occurs on the performance of the cathode.

There are number of studies [(Kubicek et al. 2011), (Tsvetkov & Yildiz, 2015)] focusing on the ways of preventing strontium segregation mainly with the help of surface modifications. The most common technique is to apply thin coating layer of LSM on top of the LSC cathode. Although promising results were reported, the cathodes were not durable enough for long term utilization. In a more recent study by Tsvetkov et al. (2016), it was reported that the introduction of additive cations to the surface with the help of metal chloride solutions can impede strontium segregation. According to their findings, it was shown that Sr segregation is prevented but this also caused a decay in ORR activity since kinetics of oxygen surface exchange depends also on the amount of oxygen vacancies at the surface.

In this study, a specially developed layered sample and co-sputtered samples were examined with respect to their structural and performance stability. The aim was to identify the composition in LSC-113/LSC-214 composite cathode that would have the highest possible stability.

5.2 Experimental Procedure

Fabrication of LSC-113/LSC-214 composite cathodes were given in section 3 and will not be repeated here. Similarly, the method used in EIS measurements can be found in section 4.

To follow the stability of the cathodes, prolonged experiments were conducted for a duration of 10 days. This involved isothermal annealing of the symmetric cells in which EIS meaurements were taken at an interval of 2 hours.

For the structural characterization of the surface Sr segregation, two groups of samples were prepared, Figure 5.1. One was bilayer sample especially fabricated to follow the segregation event. The other group was co-sputtered cathode of LSC-113/LSC-214 composite cathode with different volume fractions.

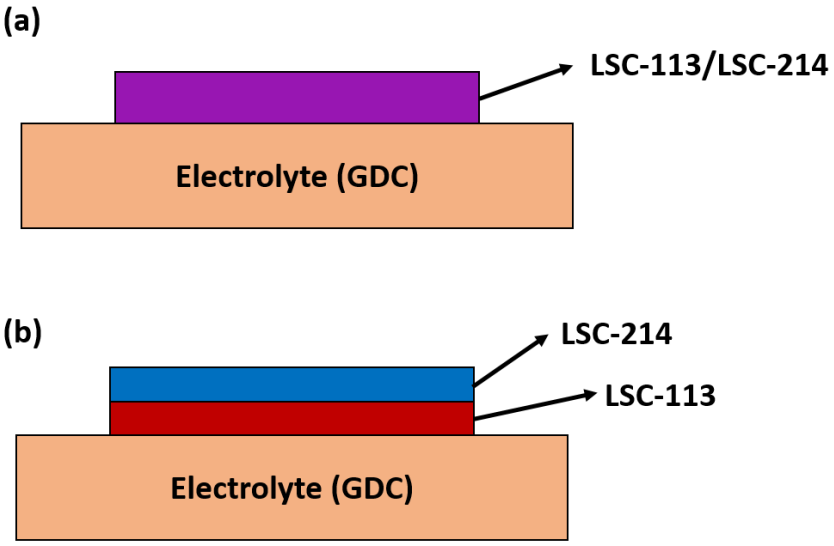

Figure 5. 1 Schematic illustration of (a) co-sputtered and (b) layerd cathodes prepared for the comparison of Sr segregation.

Structural characterization of both co-sputtered and bilayer samples were carried out by a number of techniques; XRD, SEM and TEM. XRD analyses (Cu-Kα) were carried out using D8 Advance Bruker X-ray Diffractometer with Bragg–Brentano geometry with a scan rate of 0.02°/min. SEM observations were carried out using FEI Nova NanoSEM 430 model field emission scanning electron microscope. TEM observations were performed using JEOL JEM 2100F (200kV-FEG). Since both co-sputtered and layered samples are brittle, TEM samples were prepared by focused ion beam (FIB). In order to observe the segregation behavior of samples bright-field (BF), high resolution transmission microscope (HRTEM) images were accompanied with selected area diffraction (SAED) and elemental analyses. Chemical analyses were performed using EDS with line scans in TEM-STEM mode. Spherical aberration coefficient Cs, beam convergence angle α, were, 0.5mm and 14.2 mrad, respectively.

5.3 Results and Discussion

In order to study the segregation process and the extent to which it occurs at reduced temperatures, e.g. 700 °C, two samples were prepared with a special configuration. In this configuration, LSC-113 thin film was deposited onto GDC substrate to a thickness of approximately 350 nm. Then, above this layer, LSC-214 was deposited to the same thickness yielding a bilayered cathode with a total thickness of 700 nm. In terms of volume fractions, this corresponds to LSC-113:LSC-214=0.50:0.50. One of these samples was kept in as-sputtered condition while the other was annealed at 700°C for a duration of 10 days to promote Sr segregation, Figure 5.2. This temperature was chosen on the basis of observation that LSC based cathodes become vulnerable to surface Sr segregation at temperatures above 400 °C (Tsvetkov & Yildiz, 2015). Thus, annealing procedure of 10 days at 700 °C should be well enough to observe structural changes in the cathode layers.

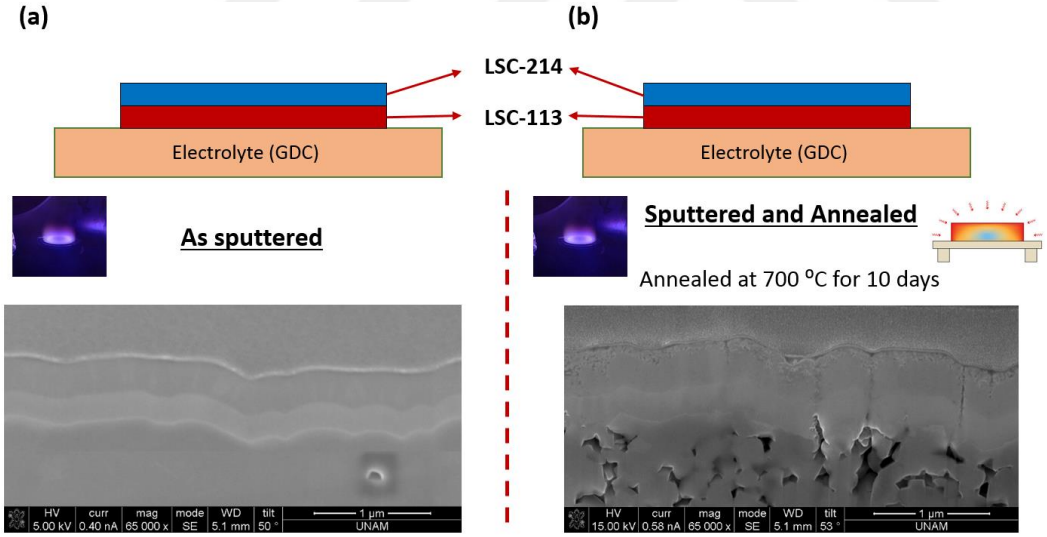

Figure 5. 2 SEM micrographs of bilayer samples in (a) as-sputtered and (b) annealed conditions.

As seen in Fig. 5.2, cathode layers were well separated from each other especially in as-sputtered condition. After annealing the border between the layers was disturbed

probably due to the structural changes in the respective phases. In order to follow these changes in detail, a TEM study was carried out on annealed cathode bilayer, samples being prepared by FIB.

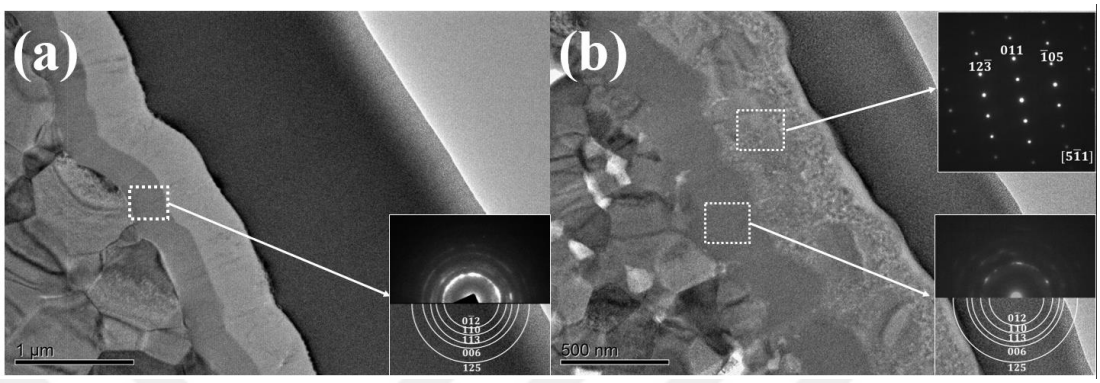

Figure 5. 3 Bright field images of bilayer samples, (a) in as-sputtered condition, (b) in annealed condition.

Bright field images and selected area diffraction patterns taken from each cathode layers are given in Figure 5.3. As seen in the Figure 5.3 (a), there are total of four layers. Except the top layer which is Pt deposited for sampling by FIB, there are two consecutive featurlesss layers which correspond to LSC-214 and LSC-113, respectively. The bottom layer which is multi-grain is that of electrolyte GDC. Fig. 5.3 (b) refers to the same cathode in the annealed condition. The structure is quite similar in that the same layers can be identifed quite easily despite some morphological alterations. It sould be noted that there is an additional layer at the external surface of the bilayer cathode, i.e. the air exposed surface of LSC-214.

Diffraction pattern taken from the layer are included in the figures reported. Unfortunately the additional surface layer which was formed as a result of annealing was too thin to take the diffraction pattern. The other layers were well defined with rings reflecting the polycrystalline nature of the deposited layer both in as co-sputtered and annealed condition. Since the nature of additional layer could not be clarified via diffraction patterns, layers were subjected to detailed EDS analysis in terms of linescans in TEM-STEM mode.

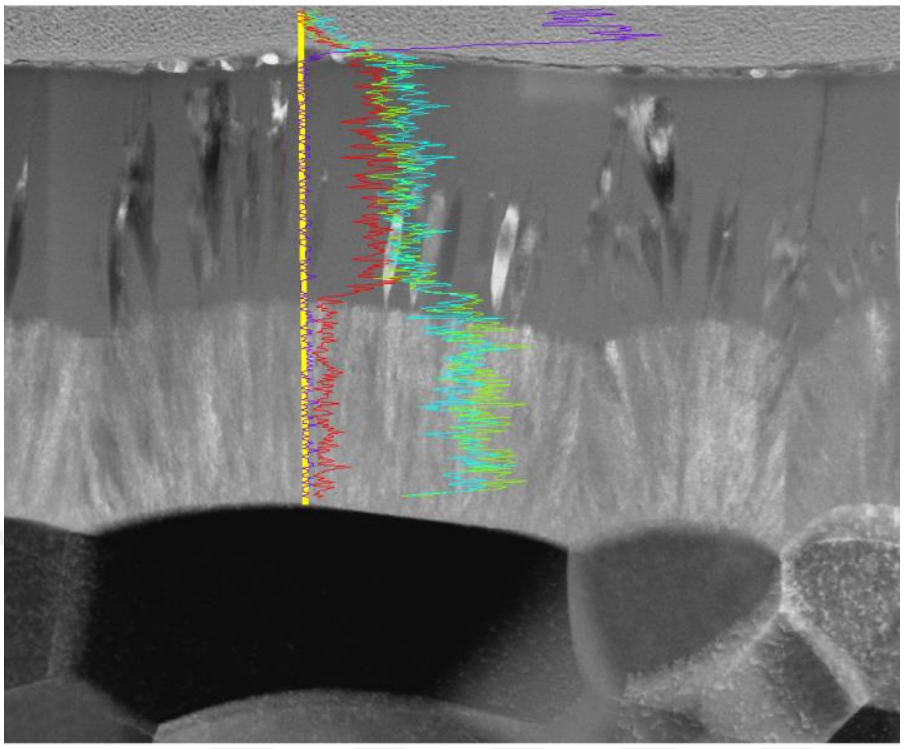

Figure 5. 4 STEM image of bilayer cathode in as-sputtered condition (Note Sr, La and Co are represented by red, green and blue lines, respectively).

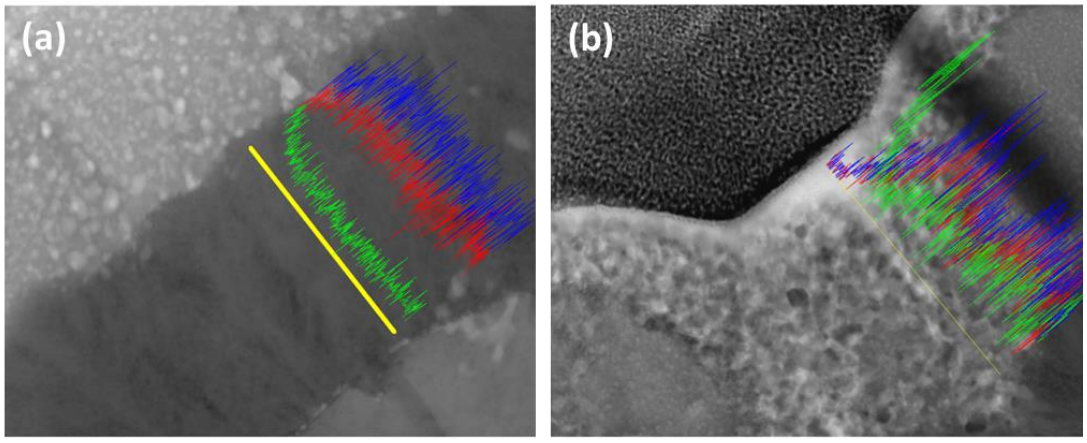

Figure 5. 5 STEM images of (a) LSC-113 and (b) LSC-214 layers of bilayer cathode after annealing at 700 $^{\circ}$C for a duration of 10 days (Note that green line corresponds to Sr while La and Co represented with red and blue, respectively).

Results of linescans with respect to Sr, La and Co in co-sputtered bilayer are shown in Fig.5.4, superimposed on the STEM image. As seen in the figure, the compositional distributions in both LSC-113 and LSC-214 are homogeneous with a transition at the interface. Linescans in annealed condition is given in two parts, one of them is placed across LSC-113 layer starting from GDC interface while the other is placed across LSC-214 layer starting from the interface between LSC-113 and LSC-214 to the outer surface. It should be noted that the profiles in the first layer, following the transition at the interface, are quite uniform. The same is true for the second LSC-214 layer except for the very end. Sr content which was relatively low and unifrom across LSC-214, show a sharp rise close to the surface. Thus it can be concluded that the new layer formed at the surface, observed with TEM, is very rich in Sr content. Looking at the profile of La and Co, it appears that the new layer is almost pure Strontium Oxide. Therefore, there is a severe Sr segregation at air exposed surface of the bilayer cathode.

It should be mentioned that Sr segregation is a well known fact in LSC-113 cathode, which results in gradual drop of cathode performance with time. This is often attibuted to the blockage of oxygen vacancies at the surface which decreases the rate of oxygen surface exchange step which is normally the rate determining step in thin cathodes. Based on the above observations, it appears that the same would probably be applicable for the current bilayer cathode since the depostion of LSC-214 on top of LSC-113 did not prevent the segragation of Sr to the surface.

In order to investigate the effect of surface Sr segregation to lifetime of LSC-113/LSC-214 co-sputtered cathodes, a stability study was carried out with different composite compositions. A total of 6 samples were produced where the volume fractions of LSC-214 varied from 0.10 to 0.90. The stability was measured in terms of EIS responses at selected temperatures at an interval of 2 hours. Values of ASR were extracted from EIS responses and are shown plotted in Figure 5.6.

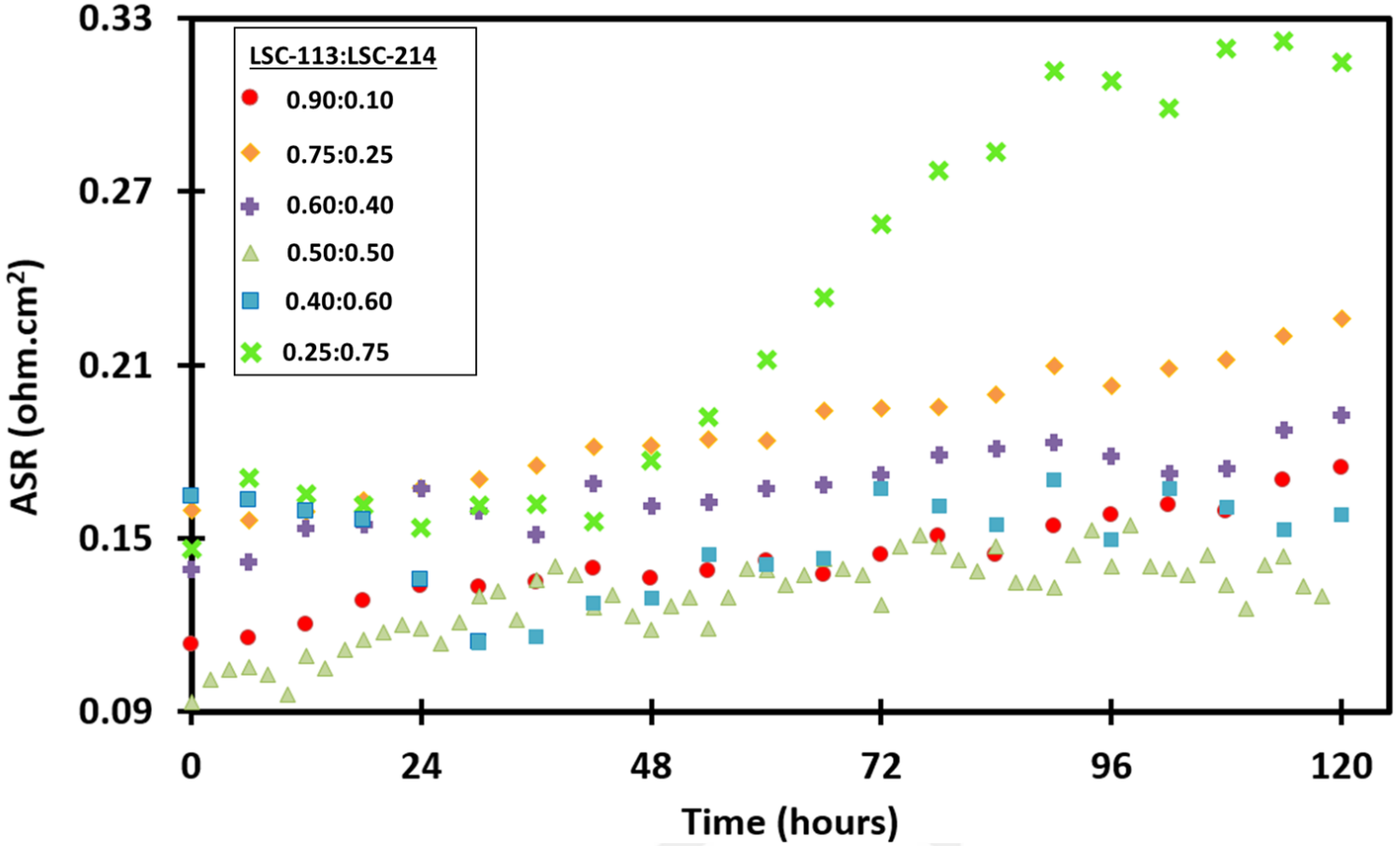

Figure 5.6 Performance stability of the samples in terms of ASR vs Time at the operating temperatures

The figure shows the variation of ASR values which refers to a constant temperature annealing for a duration of 120 hours. The temperatures were selected so that ASR has a value of ASR = ~0.15 ohm.cm^2. Thus, the anealing temperatures vary from sample to sample but all have an intial ASR value of ~ 0.15 ohm.cm^2. It is seen in Fig. 5.6, the composite cathodes are quite stable and there are only small variations in their ASR values. Only in one of the composite cathode, LSC-113:LSC-214=0.25:0.75, there is a relatively sizeable increase in ASR value, i.e. an increase from 0.15 Ω.cm^2 to 0.3 Ω.cm^2. Although this value seems high when compared with the other present cathodes, it is negligibly small compared to the LSC cathodes reported in lierature. For instance, Kubicek et al. (2011) studying LSC-113 cathode, reported an increase of ASR from 0.8 Ω.cm^2 to 75 Ω.cm^2 after an operation time of 72 hours at 650 °C. Similarly, Cai et al. (2012) reports in again LSC-113 from 0.7 Ω.cm^2 to 20 Ω.cm^2 after an operation time of 72 hours at 650 °C.

It should be noted that, though small, there is some increase in ASR with time. It should also be worth noting that the ASR in some of the composite cathodes increases almost with a constant rate. In some compositions, this linear degradation bevaiour starts from the beginning. In some others, composites in the range of 0.25:0.75<LSC-113:LSC-214 < 0.40:0.60, the ASR value decreases at first and then starts to increase with a constant rate[2].

[2] This variation is probably due to the crystallization of the phases, i.e. before the structure is stabilized at the test temperature.

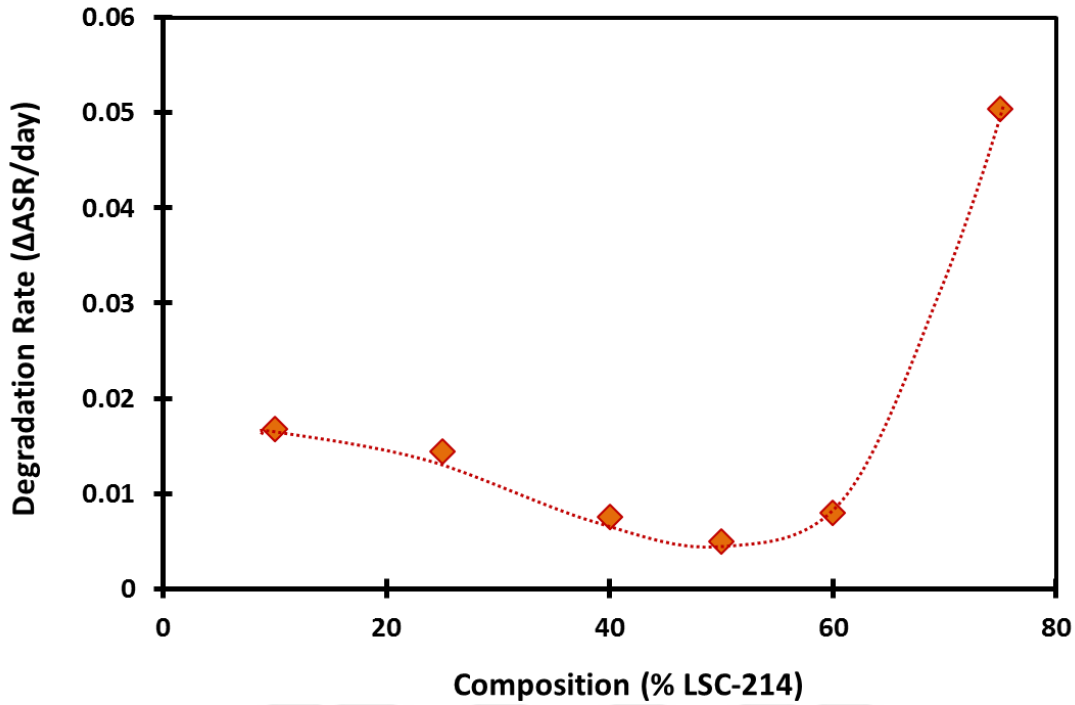

Figure 5.7 The relationship between degradation rate and cathode composition.

The degradation rates after stabilization are shown in Fig. 5.7 as a function of composite composition. As seen in the figure, the degradation rates of cathodes decreases with increasing LSC-214 content and reaches the slowest rate in 0.40< LSC-214 < 0.60. Beyond LSC-214= 0.60, the rate increases quite sharply. Degradation rate of the composite with LSC-214=0.90 (not reproted in Fig 5-7) is 20 times higher than the best composite (LSC-214=0.50).

It is important to keep in mind that the annealing temperatures of the cathodes were different in each composite. Therefore the composite at which $ASR_{cathode} = 0.15\ \Omega.cm^2$ was obtained at lower temperature has the obvious advantage in terms of stability. Therefore, it is not surprising that minimum degradation rate was obtained in composites that have the lowest cathode operating temperatures (i.e. where $ASR_{cathode} = 0.15\ \Omega.cm^2$). The lowest cathode operating temperatures were obtained at mid-

compositions. These are also the most stable compositions in terms of prolonged operation.

Since the rate of degradation was slowest in LSC-113:LSC-214=0.50:0.50, this composite cathode was taken to a detailed structural characterization with TEM. Fig. 5.8 shows the bright field image and high resolution image of the intial co-sputtered composite. The scale of the structure was extremely fine. As seen from the Fig. 5.8(b), there is a single ring in the diffraction pattern indicating an almost amorphous structure in the cathode layer.

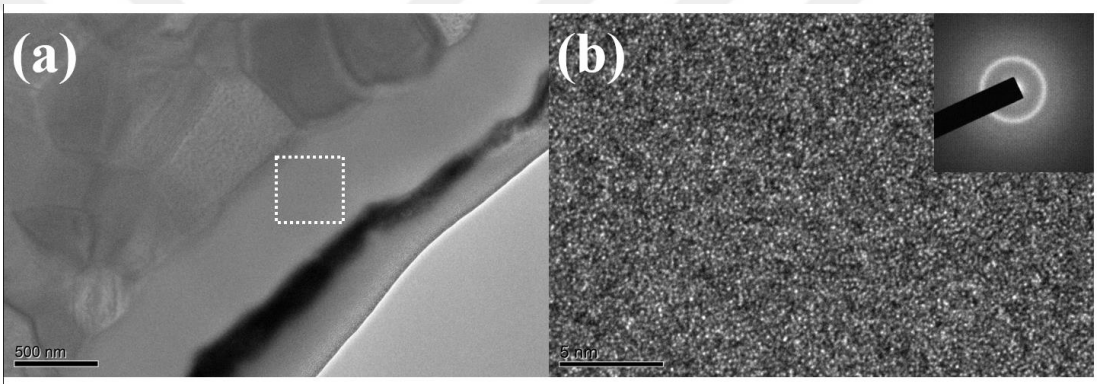

Figure 5. 8. Bright field and high resolution TEM images of co-sputtered cathode.

Fig. 5.9 reports the same structure after 10 days of annealing at 700°C. It is seen that, single ring which was observed in the as-sputtered condition is altered with the formation of additional spots which are the indications of crystallization.

The nanocrystalline structure reported in Fig 5.9, is too fine and quite homogeneous without any sign of formation of new phase. The structure was further analysed with EDS linescans in TEM-STEM mode. Figure 5.10 shows the variation of element concentration with respect to La, Sr and Co.

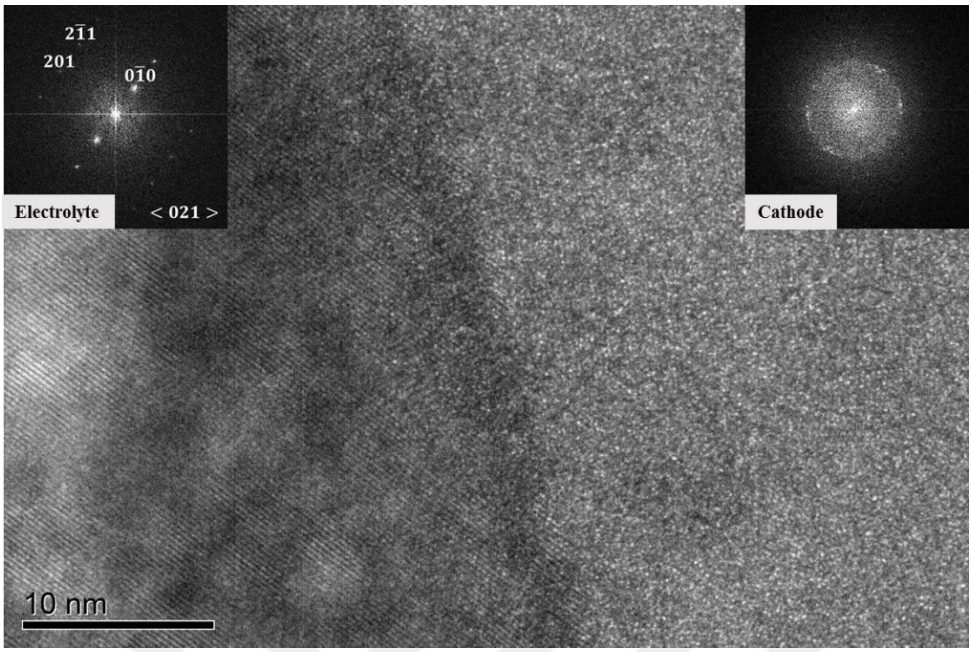

Figure 5.9 High resolution TEM images of co-sputtered cathode and the electrolyte after annealing at 700 °C for 10 days.

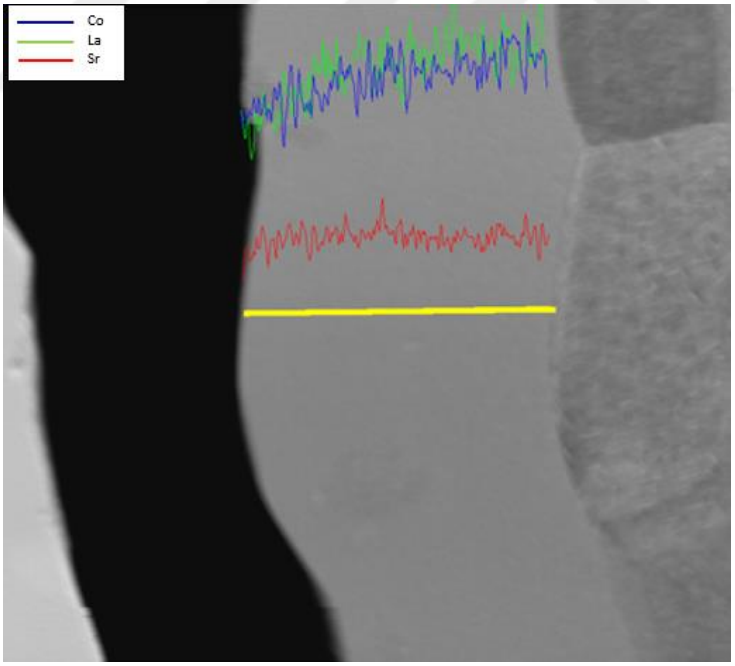

Figure 5.10. STEM image of co-sputtered cathode after operation at 575 °C for 10 days.

As seen from the measurements, the element Sr is uniformly distributed across the the thickness of the composite cathode. It should therefore be concluded that, there is no segregation of Sr to the surface which was the case in the bilayer sample.

5.4 Conclusions

Since Sr segregation occurs at temperatures above 400 °C in LSC based cathode materials, and since the composite with the best operating temperature (575 °C) is above this temperature, the current study was undertaken to investigate the stability of co-deposited cathodes. The followings can be concluded from the present work:

i.) According to the TEM analyses, simultaneous deposition resulted in a very fine structure. This was initially an amorphous-like but with prolonged use turned into nano-crystalline structure.

ii.) The bi-layered cathodes especially developed to investigate Sr segregation did develop a surface layer rich in Sr segragation at 700 °C, verifying that Sr segragation do occur even when LSC-113 was covered by LSC-214.

iii.) In co-sputtered composite cathodes, no Sr segregation was oberved with STEM analysis. The study of stability of co-sputtered cathodes at temperatures where ASR=0.15 $\Omega.cm^2$ showed that the LSC-113/LSC-214 co-sputtered composite cathodes are highly stable with extremely low degradation rate. The composite with the best operating temperature (575 °C) is expected to have an ASR of approximately 3 $\Omega.cm^2$ after 10.000 hours of operation.

CHAPTER 6

GENERAL CONCLUSIONS

In this study, a combinatorial approach was used to develop cathode materials which would reduce the operating temperatures of SOFCs to the range of 500 - 600 °C. The kinetics of cathodic processes were investigated for LSC-113/LSC-214 composite cathode films deposited with magnetron sputtering and screened with meaurement of EIS responses on symmetric cells. The study is separated into three parts. Part I is related to fabrication of sputtering targets. Part II comprises the main study which was on combinatorial screening of LSC-113/LSC-214 co-sputtered cathodes and Part III is related to the stability of composite LSC cathodes for prolonged use.

In the first part of this study, a novel approach is illustrated to fabricate sputtering targets for thin film production. In this approach, deformable dies made up of poly-tetrafluoroethylene (Teflon) were used instead of conventional rigid dies. It was shown that this method is suitable for products of low volume productions. With the use of teflon rings LSC-113 and LSC-214 sputtering targets were succefully fabricated and used for the deposition of thin film cathodes.

In the second part, a combinatorial approach was used to obtain the optimum composition in LSC-113/LSC-214 composite system. A thin film composite cathode library was obtained by co-sputtering of LSC-113 and LSC-214 onto suitably positioned substrates each with controlled compositions. The cathode library was screened with an electrochemical impedance spectroscopy and showed the followings;

i) Co-sputtered LSC-113/LSC-214 composite cathodes have low area specific resistance values (ASR) as compared to those reported in the literature. Practically useful ASR value of 0.15 $\Omega.cm^2$ was obtainable at many of the

compositions in LSC-113/LSC-214 below 700 °C. The best compositional range is 0.40<LSC-214<0.60 where the operating temperature can be as low as 615 °C.

Refocusing the combinatorial screening to 0.40<LSC214<0.60, a new set of co-sputtered cathodes were prepared and were analysed with the same technique. This has shown that;

ii) The lowest operating temperature of 575 °C was possible in LSC-113/LSC-214 composite cathodes at mid-compositions, the best being LSC-113:LSC-214 =0.45:0.55.

iii) Composite cathodes have an amouphous like structures in co-sputtered conditions, the structure crystallizes during its use. The nanocrystals formed at 700 °C are extremely small, their sizes are in the range of 4-10 nm. The composite structure is thought to restrict the grain growth, contributing to the stability of the as-deposited structure.

In the third part, the study aimed to estimate the stability of co-deposited cathodes and their resistances against Sr segregation which was commonly observed in LSC based cathode materials at temperatures above 400 °C. This part of the study has shown the followings;

iv.) According to TEM analysis, simultaneous deposition resulted in a very fine structure. This was initially an amorphous like but with prolonged use turned into nano-crystalline structure.

v.) The bi-layered cathodes especially developed to investigate Sr segregation did develop a surface layer rich in Sr segragation at 700 °C, verifying that Sr segragation do occur even when LSC-113 was covered by LSC-214.

vi.) In co-sputtered composite cathodes, no Sr segregation was observed with STEM analysis. The study of stability of co-sputtered cathodes at temperatures where ASR=0.15 $\Omega.cm^2$ showed that the LSC-113/LSC-214 co-sputtered

composite cathodes are highly stable with extremely low degradation rate. The composite with the best operating temperature (575 °C) is expected to have an ASR of approximately 3 $\Omega.cm^2$ after 10.000 hours of operation.

REFERENCES

Adler, S. B. (2000). Limitations of charge-transfer models for mixed-conducting oxygen electrodes, *135*, 603–612.

Adler, S. B. (2004). Factors governing oxygen reduction in solid oxide fuel cell cathodes. *Chemical Reviews*, *104*(10), 4791–4843. https://doi.org/10.1021/cr020724o

Aguadero, A. (2011). Electrochemical Performance of La_2NiO_4 -based Cathode for Solid Oxide Fuel Cells . Single Cell Test, (1), 91–101. https://doi.org/10.1002/fuce.201000066

Aguadero, A., Pérez-coll, D., Calle, C. De, Alonso, J. A., Escudero, M. J., & Daza, L. (2009). $SrCo_{1-x}Sb_xO_{3-l}$ perovskite oxides as cathode materials in solid oxide fuel cells, *192*, 132–137. https://doi.org/10.1016/j.jpowsour.2008.12.138

Badwal, S. (2001). Stability of solid oxide fuel cell components. *Solid State Ionics*, *143*(1), 39–46. https://doi.org/10.1016/S0167-2738(01)00831-1

Bai, Y., Liu, M., Ding, D., Blinn, K., Qin, W., Liu, J., & Liu, M. (2012). for intermediate-temperature solid oxide fuel cells. *Journal of Power Sources*, *205*, 80–85. https://doi.org/10.1016/j.jpowsour.2012.01.021

Baumann, F. S., Fleig, J., Habermeier, H. U., & Maier, J. (2006). Impedance spectroscopic study on well-defined (La,Sr)(Co,Fe)O_{3-d} model electrodes. *Solid State Ionics*, *177*(11–12), 1071–1081. https://doi.org/10.1016/j.ssi.2006.02.045

Bidrawn, F., Lee, S., Vohs, J. M., & Gorte, R. J. (2008). and Cathode Performance of LaFeO 3, 660–665. https://doi.org/10.1149/1.2907431

Boehm, E., Bassat, J., Steil, M. C., Dordor, P., Mauvy, F., & Grenier, J. (2003). mixed conducting oxides, *5*, 973–981. https://doi.org/10.1016/S1293-2558(03)00091-8

Brett, D. J. L., Atkinson, A., Brandon, P., Skinner, S. J., Atkinson, A., & Brett, D. J. L. (2008). Intermediate temperature solid oxide fuel cells, 1568–1578. https://doi.org/10.1039/b612060c

Cai, Z., Kubicek, M., Fleig, J., & Yildiz, B. (2012). Chemical Heterogeneities on $La_{0.6}Sr_{0.4}CoO_{3-\delta}$ Thin Films—Correlations to Cathode Surface Activity and Stability. *Chemistry of Materials*, *24*(6), 1116–1127. https://doi.org/10.1021/cm203501u

Cathode, A. S. L. M., Chen, A., Bourne, G., Siebein, K., Dehoff, R., Wachsman, E., & Jones, K. (2008). Characterization of Lanthanum Zirconate Formation at the A-Site-Deficient Strontium-Doped Lanthanum Manganite Cathode/ Yttrium-Stabilized Zirconia Electrolyte Interface of Solid Oxide Fuel Cells, *2675*(23759), 2670–2675. https://doi.org/10.1111/j.1551-2916.2008.02524.x

Cathodes, L. S. P. (2011). A Comparative Study of Oxygen Reduction Reaction on Bi- and La-Doped $SrFeO_{3-d}$ Perovskite Cathodes, 132–138. https://doi.org/10.1149/1.3521316

Chang, A., Skinner, S. J., & Kilner, J. A. (2011). Electrical properties of $GdBaCo_2O_{5+x}$ for IT-SOFC applications, *177*(2006), 2009–2011. https://doi.org/10.1016/j.ssi.2006.05.047

Chen, H., Yu, H., Cronin, J. S., Wilson, J. R., Barnett, S. A., & Thornton, K. (2011). Simulation of coarsening in three-phase solid oxide fuel cell anodes. *Journal of Power Sources*, *196*(3), 1333–1337. https://doi.org/10.1016/j.jpowsour.2010.08.010

Chen, Y., Orlovskaya, N., Klimov, M., Huang, X., Cullen, D., Graule, T., & Kuebler, J. (2012). Layered YSZ / SCSZ / YSZ Electrolytes for Intermediate Temperature SOFC Part I : Design and Manufacturing, (5), 722–731. https://doi.org/10.1002/fuce.201200008

Co, S., & Fe, O. (2014). Oxidation properties of the Crofer 22 APU steel coated, 825–834. https://doi.org/10.1007/s10973-013-3594-1

Crumlin, E. J., Mutoro, E., Ahn, S. J., La O, G. J., Leonard, D. N., Borisevich, A., Shao-Horn, Y. (2010). Oxygen reduction kinetics enhancement on a heterostructured oxide surface for solid oxide fuel cells. *Journal of Physical Chemistry Letters*, *1*(21), 3149–3155. https://doi.org/10.1021/jz101217d

Ding, D., Li, X., Lai, Y., & Liu, M. (2014). Energy & Environmental Science Enhancing SOFC cathode performance by surface modification through infiltration, 552–575. https://doi.org/10.1039/c3ee42926a

Ding, J., & Liu, J. (2009). Short communication A novel design and performance of cone-shaped tubular anode-supported segmented-in-series solid oxide fuel cell stack, *193*, 769–773. https://doi.org/10.1016/j.jpowsour.2009.04.049

Ding, X., Ding, L., Wang, L., Zhu, W., Hua, G., Liu, H., Yuan, G. (2017). Electrochimica Acta cathodes achieved by an in - situ reaction. *Electrochimica Acta*, *236*, 378–383. https://doi.org/10.1016/j.electacta.2017.03.184

Enoki, M., Yan, J., Matsumoto, H., & Ishihara, T. (2006). High oxide ion conductivity in Fe and Mg doped LaGaO 3 as the electrolyte of solid oxide fuel cells, *177*, 2053–2057. https://doi.org/10.1016/j.ssi.2006.01.015

Feng, Z., Crumlin, E. J., Hong, W. T., Lee, D., Mutoro, E., Biegalski, M. D., Shao-horn, Y. (2013). Perovskite Thin Films, (1).

Fergus, J. W. (2005). Metallic interconnects for solid oxide fuel cells, *397* (June 2004), 271–283. https://doi.org/10.1016/j.msea.2005.02.047

Fu, Q. X., Zha, S. W., Zhang, W., Peng, D. K., Meng, G. Y., & Zhu, B. (2002). Intermediate temperature fuel cells based on doped ceria ± LiCl ± $SrCl_2$ composite electrolyte, *104*, 73–78.

Fu, Y., & Bazant, M. Z. (2014). Theoretical and Experimental Study of Solid Oxide Fuel Cell (SOFC) Using Impedance Spectra, (2006), 107.

Gong, W., Gopalan, S., & Pal, U. B. (2006). Performance of intermediate temperature (600 – 800 °C) solid oxide fuel cell based on Sr and Mg doped

lanthanum-gallate electrolyte, *160*, 305–315. https://doi.org/10.1016/j.jpowsour.2006.01.039

Goodenough, J. B., & Huang, Y. (2007). Alternative anode materials for solid oxide fuel cells, *173*, 1–10. https://doi.org/10.1016/j.jpowsour.2007.08.011

Gorte, B. R. J., Park, S., Vohs, J. M., & Wang, C. (2000). Anodes for Direct Oxidation of Dry Hydrocarbons in a Solid-Oxide Fuel Cell, (19), 1465–1469.

Gupta, R. K., Choi, I., Cho, Y., Lee, H., & Hyun, S. (2009). Journal of Power Sources, *187*, 371–377. https://doi.org/10.1016/j.jpowsour.2008.10.136

Han, J. W., & Yildiz, B. (2012). Mechanism for enhanced oxygen reduction kinetics at the $(La,Sr)CoO_{3-\delta}/(La,Sr)_2CoO_{4+\delta}$ hetero-interface. *Energy & Environmental Science*, *5*(9), 8598. https://doi.org/10.1039/c2ee03592h

Horn, A., Gamarra, D., Munuera, G., Conesa, J. C., & Mart, A. (2007). Catalytic properties of monometallic copper and bimetallic copper-nickel systems combined with ceria and Ce-X (X = Gd, Tb) mixed oxides applicable as SOFC anodes for direct oxidation of methane, *169*, 9–16. https://doi.org/10.1016/j.jpowsour.2007.01.074

Imanishi, N., Matsumura, T., Sumiya, Y., Yoshimura, K., Hirano, A., Takeda, Y., Kanno, R. (2004). Impedance spectroscopy of perovskite air electrodes for SOFC prepared by laser ablation method. *Solid State Ionics*, *174*(1–4), 245–252. https://doi.org/10.1016/j.ssi.2004.06.019

Ishihara, T., Tabuchi, J., Ishikawa, S., Yan, J., & Enoki, M. (2006). Recent progress in $LaGaO_3$ based solid electrolyte for intermediate temperature SOFCs, *177*, 1949–1953. https://doi.org/10.1016/j.ssi.2006.01.044

Iwanschitz, B., Sfeir, J., Mai, A., & Schütze, M. (2010). Degradation of SOFC Anodes upon Redox Cycling : A Comparison Between Ni / YSZ and Ni / CGO. https://doi.org/10.1149/1.3271101

Janek, J. (2009). Influence of interface structure on mass transport in phase

boundaries between different ionic materials Experimental studies and formal considerations, 1069–1080. https://doi.org/10.1007/s00706-009-0125-7

Januschewsky, J., Ahrens, M., Opitz, A., Kubel, F., & Fleig, J. (2009). Optimized $La_{0.6}Sr_{0.4}CoO_{3-d}$ thin-film electrodes with extremely fast oxygen-reduction kinetics. *Advanced Functional Materials*, *19*(19), 3151–3156. https://doi.org/10.1002/adfm.200900362

Ji, Y., Wei, T., Zhang, Y., Meng, X., & Shiquan, L. (2008). Intermediate-temperature solid oxide fuel cells, *183*, 581–585. https://doi.org/10.1016/j.jpowsour.2008.05.052

Jun, A., Kim, J., Shin, J., & Kim, G. (2012). Optimization of Sr content in layered $SmBa_{1-x}Sr_xCo_2O_{5+d}$ perovskite cathodes for intermediate-temperature solid oxide fuel cells, *7*, 4–11. https://doi.org/10.1016/j.ijhydene.2012.09.048

Kim, G., Wang, S., Jacobson, A. J., Reimus, L., Brodersen, P., & Mims, C. A. (2007). Rapid oxygen ion diffusion and surface exchange kinetics in $PrBaCo_2O_{5+x}$ with a perovskite related structure and ordered A cations, 2500–2505. https://doi.org/10.1039/b618345j

Kim, H., Lu, C., Worrell, W. L., Vohs, J. M., Gorte, R. J., Soc, J. E., Gorte, R. J. (2002). Cu-Ni Cermet Anodes for Direct Oxidation of Methane in Solid-Oxide Fuel Cells service Cu-Ni Cermet Anodes for Direct Oxidation of Methane in Solid-Oxide Fuel Cells, *149*(3), 8–12. https://doi.org/10.1149/1.1445170

Kim, Y., Kim-lohsoontorn, P., & Bae, J. (2010). Effect of unsintered gadolinium-doped ceria buffer layer on performance of metal-supported solid oxide fuel cells using unsintered barium strontium cobalt ferrite cathode. *Journal of Power Sources*, *195*(19), 6420–6427. https://doi.org/10.1016/j.jpowsour.2010.03.095

Kim, Y., Kim-lohsoontorn, P., Baek, S., & Bae, J. (2010). Electrochemical performance of unsintered fuel cells, *6*(82), 0–8. https://doi.org/10.1016/j.ijhydene.2010.10.065

Kubicek, M., Limbeck, A., Fro, T., & Hutter, H. (2011). Relationship between Cation Segregation and the Thin Film Electrodes, *158*(6), 727–734. https://doi.org/10.1149/1.3581114

Kubicek, M., Limbeck, A., Frömling, T., Hutter, H., & Fleig, J. (2011). Relationship between Cation Segregation and the Electrochemical Oxygen Reduction Kinetics of La0.6Sr0.4CoO3−δ Thin Film Electrodes. *Journal of The Electrochemical Society*, *158*(6), B727. https://doi.org/10.1149/1.3581114

Kuklja, M. M., Kotomin, E., Merkle, R., Mastrikov, Y., & Maier, J. (2013). Combined theoretical and experimental analysis of processes determining cathode performance in solid oxide fuel cells. *Physical Chemistry Chemical Physics : PCCP*, *15*(15), 5443–5471. https://doi.org/10.1039/c3cp44363a

Lalanne, C., Prosperi, G., Bassat, J., Mauvy, F., Fourcade, S., Stevens, P., Grenier, J. (2008). Neodymium-deficient nickelate oxide $Nd_{1.95}NiO_{4+1}$ as cathode material for anode-supported intermediate temperature solid oxide fuel cells, *185*, 1218–1224. https://doi.org/10.1016/j.jpowsour.2008.06.072

Lee, C., Lee, C., Lee, H., & Oh, S. M. (1997). Microstructure and anodic properties of Ni / YSZ cermets in solid oxide fuel cells, *98*, 39–48.

Lee, D., Han, J., Kim, E., Song, R., & Shin, D. (2008). Performance of strontium- and magnesium-doped lanthanum gallate electrolyte with lanthanum-doped ceria as a buffer layer for IT-SOFCs, *185*(3), 207–211. https://doi.org/10.1016/j.jpowsour.2008.06.028

Lee, D., Myung, J., Tan, J., Hyun, S., Irvine, J. T. S., Kim, J., & Moon, J. (2017). Direct methane solid oxide fuel cells based on catalytic partial oxidation enabling complete coking tolerance of Ni-based anodes. *Journal of Power Sources*, *345*, 30–40. https://doi.org/10.1016/j.jpowsour.2017.02.003

Leng, Y., Chan, S. H., & Liu, Q. (2008). Development of LSCF-GDC composite cathodes for low-temperature solid oxide fuel cells with thin film GDC electrolyte. *International Journal of Hydrogen Energy*, *33*(14), 3808–3817.

https://doi.org/10.1016/j.ijhydene.2008.04.034

Leng, Y. J., Chan, S. H., Khor, K. A., & Jiang, S. P. (2004). Performance evaluation of anode-supported solid oxide fuel cells with thin film YSZ electrolyte. *International Journal of Hydrogen Energy*, *29*(10), 1025–1033. https://doi.org/10.1016/j.ijhydene.2004.01.009

Leonard, D. N., Kumar, A., Jesse, S., Biegalski, M. D., Christen, H. M., Mutoro, E., Borisevich, A. Y. (2013). Nanoscale Probing of Voltage Activated Oxygen Reduction / Evolution Reactions in Nanopatterned (La_xSr_{1-x}) $CoO_{3-\delta}$ Cathodes, 788–797. https://doi.org/10.1002/aenm.201200681

Li, W., Xiong, C. Y., Jia, L. C., Pu, J., Chi, B., Chen, X., Li, J. (2015). Strontium-doped samarium manganite as cathode materials for oxygen reduction reaction in solid oxide fuel cells, *284*, 272–278. https://doi.org/10.1016/j.jpowsour.2015.03.027

Li, Y., Rui, Z., Xia, C., Anderson, M., & Lin, Y. S. (2009). Performance of ionic-conducting ceramic / carbonate composite material as solid oxide fuel cell electrolyte and CO 2 permeation membrane, *148*, 303–309. https://doi.org/10.1016/j.cattod.2009.08.009

Lik, J., Chau, H., Chou, Y., & Wang, S. (2013). Preparation of Ag-AZO Nanocomposite Powder Compact for RF Magnetron Sputtering Target Application, *886*, 879–886. https://doi.org/10.1111/ijac.12017

Liu, B., Jiang, Z., Ding, B., Chen, F., & Xia, C. (2011). fuel cells. *Journal of Power Sources*, *196*(3), 999–1005. https://doi.org/10.1016/j.jpowsour.2010.08.057

Lo, C., & Hsieh, T. (2012). Preparation of IGZO sputtering target and its applications to thin-film transistor devices. *Ceramics International*, *38*(5), 3977–3983. https://doi.org/10.1016/j.ceramint.2012.01.052

Lou, X., Wang, S., Liu, Z., Yang, L., & Liu, M. (2009). Solid State Ionics, *180*, 1285–1289. https://doi.org/10.1016/j.ssi.2009.06.014

Lu, X. C., & Zhu, J. H. (2008). Effect of Sr and Mg Doping on the Property and Performance of the $La_{1-x}Sr_xGa_{1-y}Mg_yO_{3-d}$ Electrolyte, 494–503. https://doi.org/10.1149/1.2895064

Ma, W., Kim, J. J., Tsvetkov, N., Daio, T., Kuru, Y., Cai, Z., Yildiz, B. (2015). Vertically aligned nanocomposite $La_{0.8}Sr_{0.2}CoO_3$ /$(La_{0.5}Sr_{0.5})_2CoO_4$ cathodes – electronic structure, surface chemistry and oxygen reduction kinetics. *J. Mater. Chem. A*, *3*(1), 207–219. https://doi.org/10.1039/C4TA04993D

Malavasi, L., Fisher, A. J., & Islam, M. S. (2010). Oxide-ion and proton conducting electrolyte materials for clean energy applications : structural and mechanistic features. https://doi.org/10.1039/b915141a

Matsui, T., Kishida, R., Muroyama, H., & Eguchi, K. (2012). Comparative Study on Performance Stability of Ni – Oxide Cermet Anodes under Humidified Atmospheres in Solid Oxide Fuel Cells, *159*(8), 456–460. https://doi.org/10.1149/2.053208jes

Medvedovski, E., Alvarez, N., Yankov, O., & Olsson, M. K. (2008). Advanced indium-tin oxide ceramics for sputtering targets, *34*, 1173–1182. https://doi.org/10.1016/j.ceramint.2007.02.015

Meng, G. Y., Fu, Q. X., Zha, S. W., Xia, C. R., Liu, X. Q., & Peng, D. K. (2002). Novel intermediate temperature ceramic fuel cells with doped ceria-based composite electrolytes, *148*, 533–537.

Munnings, C. N., Skinner, S. J., Amow, G., Whitfield, P. S., & Davidson, I. J. (2005). Oxygen transport in the $La_2Ni_{1-x}Co_xO_{4+d}$ system, *176*, 1895–1901. https://doi.org/10.1016/j.ssi.2005.06.002

Mutoro, E., Crumlin, E. J., Biegalski, M. D., Christen, H. M., & Shao-Horn, Y. (2011). Enhanced oxygen reduction activity on surface-decorated perovskite thin films for solid oxide fuel cells. *Energy & Environmental Science*, *4*(9), 3689. https://doi.org/10.1039/c1ee01245b

Navarrete, L., Solís, C., & Serra, J. M. (2015). Boosting the oxygen reduction reaction mechanisms in IT-SOFC cathodes by catalytic functionalization. *J. Mater. Chem. A*, *3*(32), 16440–16444. https://doi.org/10.1039/C5TA05187H

Niedrig, C., Wagner, S. F., Menesklou, W., Baumann, S., & Ivers-Tiffee, E. (2015). Oxygen equilibration kinetics of mixed-conducting perovskites BSCF, LSCF, and PSCF at 900 °C determined by electrical conductivity relaxation. *Solid State Ionics*, *283*, 30–37. https://doi.org/10.1016/j.ssi.2015.11.004

Ning, Z., Da-ming, Z., & Gong, Z. (2010). An investigation on preparation of CIGS targets by sintering process, *166*, 34–40. https://doi.org/10.1016/j.mseb.2009.09.026

Omar, S., Wachsman, E. D., & Nino, J. C. (2008). Higher conductivity Sm_{3+d} and Nd_{3+d} co-doped ceria-based electrolyte materials, *178*, 1890–1897. https://doi.org/10.1016/j.ssi.2007.12.069

Orikasa, Y., Crumlin, E. J., Sako, S., Amezawa, K., Uruga, T., Biegalski, M. D., Shao-Horn, Y. (2014). Surface Strontium Segregation of Solid Oxide Fuel Cell Cathodes Proved by In Situ Depth-Resolved X-ray Absorption Spectroscopy. *ECS Electrochemistry Letters* , *3*(4), F23–F26. https://doi.org/10.1149/2.006404eel

Pi, F., & Öztürk, T. (2017). Combinatorial screening of Pd-Ag-Ni membranes for hydrogen separation, *524*(August 2016), 631–636. https://doi.org/10.1016/j.memsci.2016.11.066

Politova, T. I., & Irvine, J. T. S. (2004). Investigation of scandia – yttria – zirconia system as an electrolyte material for intermediate temperature fuel cells - influence of yttria content in system $(Y_2O_3)_x$ $(Sc_2O_3)_{(1-x)}(ZrO_2)$ 89, *168*, 153–165. https://doi.org/10.1016/j.ssi.2004.02.007

Qu, B., Long, W., Jin, F., Wang, S., & He, T. (2014). ScienceDirect material for intermediate-temperature solid oxide fuel cells. *International Journal of Hydrogen Energy*, *39*(23), 12074–12082.

https://doi.org/10.1016/j.ijhydene.2014.05.150

Raza, R., Wang, X., Ma, Y., Liu, X., & Zhu, B. (2010). Improved ceria – carbonate composite electrolytes. *International Journal of Hydrogen Energy*, *35*(7), 2684–2688. https://doi.org/10.1016/j.ijhydene.2009.04.038

Rezaei, F., Kakroudi, M. G., Shahedifar, V., Vafa, N. P., & Golrokhsari, M. (2016). Densification , microstructure and mechanical properties of hot pressed Tantalum Carbide Author ' s Accepted Manuscript. *Ceramics International*, (October). https://doi.org/10.1016/j.ceramint.2016.10.067

Sari, D., Torunoglu, Z. C., Kalay, Y. E., & Ozturk, T. (2017). compaction die. *Ceramics International*, (April). https://doi.org/10.1016/j.ceramint.2017.08.050

Sase, M., Hermes, F., Yashiro, K., Sato, K., Mizusaki, J., & Kawada, T. (2008). Enhancement of Oxygen Surface Exchange at the Hetero-interface of LSC-113 and LSC-214 with PLD-Layered Films, 793–797. https://doi.org/10.1149/1.2928612

Sase, M., Hermes, F., Yashiro, K., Sato, K., Mizusaki, J., Kawada, T., Yokokawa, H. (2008). Enhancement of oxygen surface exchange at the hetero-interface of $(La,Sr)CoO_3$ / $(La,Sr)_2CoO_4$ with PLD-layered films. *J Electrochem Soc*, *155*(8), B793--B797. https://doi.org/10.1149/1.2928612

Sase, M., Yashiro, K., Sato, K., Mizusaki, J., Kawada, T., Sakai, N., Yokokawa, H. (2008). Enhancement of oxygen exchange at the hetero interface of $(La,Sr)CoO_3$/$(La,Sr)_2CoO_4$ in composite ceramics. *Solid State Ionics*, *178*, 1843–1852. https://doi.org/10.1016/j.ssi.2007.11.039

Scribe, P., Breliere, C., Kusukawa, T., Biradha, K., Fujita, M., Yoshizawa, M., Fujita, M. (2006). Double Perovskites as Anode, *2*(April).

Shaigan, N., Qu, W., Ivey, D. G., & Chen, W. (2010). A review of recent progress in coatings , surface modifications and alloy developments for solid oxide fuel cell ferritic stainless steel interconnects, *195*, 1529–1542.

https://doi.org/10.1016/j.jpowsour.2009.09.069

Shaikh, S. P. S., Muchtar, A., & Somalu, M. R. (2015). A review on the selection of anode materials for solid-oxide fuel cells. *Renewable and Sustainable Energy Reviews*, *51*, 1–8. https://doi.org/10.1016/j.rser.2015.05.069

Shen, Y., Wang, F., Ma, X., & He, T. (2011). $SrCo_{1-y}Ti_yO_{3-d}$ as potential cathode materials for intermediate-temperature solid oxide fuel cells. *Journal of Power Sources*, *196*(18), 7420–7425. https://doi.org/10.1016/j.jpowsour.2011.04.025

Shi, H., Ran, R., & Shao, Z. (2011). Wet powder spraying fabrication and performance optimization of IT-SOFCs with thin-film ScSZ electrolyte. *International Journal of Hydrogen Energy*, *37*(1), 1125–1132. https://doi.org/10.1016/j.ijhydene.2011.02.077

Sin, A., Kopnin, E., Dubitsky, Y., Zaopo, A., Aric, A. S., Rosa, D. La, Antonucci, V. (2007). Performance and life-time behaviour of NiCu – CGO anodes for the direct electro-oxidation of methane in IT-SOFCs, *164*, 300–305. https://doi.org/10.1016/j.jpowsour.2006.10.078

Singhal, S. . (2000). Advances in solid oxide fuel cell technology. *Solid State Ionics*, *135*(1), 305–313. https://doi.org/10.1016/S0167-2738(00)00452-5

Skinner, S. J., & Kilner, J. A. (2000). Oxygen diffusion and surface exchange in $La_{2-x}Sr_xNiO_{4+d}$, *135*, 709–712.

Soo, J., Pergolesi, D., Camaratta, M. A., Yoon, H., Wook, B., Taek, K., Wachsman, E. D. (2009). Electrochemistry Communications High-performance bilayered electrolyte intermediate temperature solid oxide fuel cells. *Electrochemistry Communications*, *11*(7), 1504–1507. https://doi.org/10.1016/j.elecom.2009.05.041

Souza, R. a De, & Kilner, J. a. (1999). Oxygen transport in LSC-113, *126*, 153–161.

Stambouli, A. B., & Traversa, E. (2002). Solid oxide fuel cells (SOFCs): A review of an environmentally clean and efficient source of energy. *Renewable and*

Sustainable Energy Reviews, *6*(5), 433–455. https://doi.org/10.1016/S1364-0321(02)00014-X

Sun, C., Hui, R., & Roller, J. (2010). Cathode materials for solid oxide fuel cells : a review, 1125–1144. https://doi.org/10.1007/s10008-009-0932-0

Suzuki, T., Awano, M., Jasinski, P., Petrovsky, V., & Anderson, H. U. (2006). Composite (La, Sr) MnO_{3-d} YSZ cathode for SOFC, *177*, 2071–2074. https://doi.org/10.1016/j.ssi.2005.12.016

Tarancón, A., Burriel, M., Santiso, J., Skinner, S. J., & Kilner, J. A. (2010). Advances in layered oxide cathodes for intermediate temperature solid oxide fuel cells. *Journal of Materials Chemistry*, *20*(19), 3799–3813. https://doi.org/10.1039/B922430K

Tarancón, A., Skinner, S. J., Chater, R. J., Hernández-Ramírez, F., Kilner, J. A., Brandon, N. P., García-Muñoz, J. L. (2007). Layered perovskites as promising cathodes for intermediate temperature solid oxide fuel cells. *Journal of Materials Chemistry*, *17*(30), 3175. https://doi.org/10.1039/b704320a

Taskin, A. A., Lavrov, A. N., Ando, Y., Taskin, A. A., Lavrov, A. N., & Ando, Y. (2007). Achieving fast oxygen diffusion in perovskites by cation ordering Achieving fast oxygen diffusion in perovskites by cation ordering, *91910*(2005), 1–4. https://doi.org/10.1063/1.1864244

Thokchom, J. S., Xiao, H., Rottmayer, M., Reitz, T. L., Kumar, B., Patterson, W., & Force, A. (2008). Heterogeneous electrolyte (YSZ – Al_2O_3) based direct oxidation solid oxide fuel cell, *178*, 26–33. https://doi.org/10.1016/j.jpowsour.2007.12.009

Torres-garibay, C., Kovar, D., & Manthiram, A. (2009). yttria-stabilized zirconia electrolytes for intermediate temperature solid oxide fuel cells, *187*, 480–486. https://doi.org/10.1016/j.jpowsour.2008.11.025

Tsvetkov, N., Chen, Y., & Yildiz, B. (2014). Reducibility of Co at the

$La_{0.8}Sr_{0.2}CoO_3/(La_{0.5}Sr_{0.5})_2CoO_4$ hetero-interface at elevated temperatures. *J. Mater. Chem. A*, *2*(35), 14690–14695. https://doi.org/10.1039/C4TA01889C

Tsvetkov, N., Lu, Q., Sun, L., Crumlin, E. J., & Yildiz, B. (2016). Improved chemical and electrochemical stability of perovskite oxides with less reducible cations at the surface. *Nature Materials*, *15*(9), 1010–1016. https://doi.org/10.1038/NMAT4659

Tsvetkov, N., & Yildiz, B. (2015). Improved electrochemical stability at the surface chemical modification. *Faraday Discussions*, *182*, 257–269. https://doi.org/10.1039/C5FD00023H

Van herle, J., Ihringer, R., Vasquez Cavieres, R., Constantin, L., & Bucheli, O. (2001). Anode supported solid oxide fuel cells with screen-printed cathodes. *Journal of the European Ceramic Society*, *21*(10–11), 1855–1859. https://doi.org/10.1016/S0955-2219(01)00130-3

Wang, F., Zhou, Q., He, T., Li, G., & Ding, H. (2010). Novel $SrCo_{1-y}Nb_yO_{3-d}$ cathodes for intermediate-temperature solid oxide fuel cells, *195*, 3772–3778. https://doi.org/10.1016/j.jpowsour.2009.12.081

Wang, L., Merkle, R., Kotomin, E. A., & Maier, J. (2012). Oxygen exchange kinetics on solid oxide fuel cell cathode materials — general trends and their mechanistic interpretation. https://doi.org/10.1557/jmr.2012.186

Wu, M. (2012). Two-step sintering of aluminum-doped zinc oxide sputtering target by using a submicrometer zinc oxide powder. *Ceramics International*, *38*(8), 6229–6234. https://doi.org/10.1016/j.ceramint.2012.04.076

Yang, Z., Xia, G., Maupin, G. D., & Stevenson, J. W. (2006). Conductive protection layers on oxidation resistant alloys for SOFC interconnect applications, *201*, 4476–4483. https://doi.org/10.1016/j.surfcoat.2006.08.082

Yashiro, K., Nakamura, T., Sase, M., Hermes, F., Sato, K., Kawada, T., & Mizusaki, J. (2009). Composite Cathode of Perovskite-Related Oxides, $(La,Sr)CoO_{3-d}$

/$(La,Sr)_2CoO_{4-d}$, for Solid Oxide Fuel Cells. *Electrochemical and Solid-State Letters*, *12*(9), B135. https://doi.org/10.1149/1.3170903

Yoo, S., Chen, D., Xu, H., & Lu, Q. (2017). Environmental Science oxygen reduction in solid oxide fuel cells. *Energy & Environmental Science*, *10*, 964–971. https://doi.org/10.1039/c6ee03656b

Yoo, S., Choi, S., Kim, J., Shin, J., & Kim, G. (2013). Electrochimica Acta oxide fuel cells. *Electrochimica Acta*, *100*, 44–50. https://doi.org/10.1016/j.electacta.2013.03.041

Young, G., Ho, Y., Wook, S., & Bae, J. (2015). ScienceDirect High-performance thin film solid oxide fuel cells with scandia-stabilized zirconia (ScSZ) thin film electrolyte. *International Journal of Hydrogen Energy*, *40*(45), 15704–15708. https://doi.org/10.1016/j.ijhydene.2015.09.124

Yu, X., Long, W., Jin, F., & He, T. (2014). Electrochimica Acta Cobalt-free perovskite cathode materials $SrFe_{1-x}Ti_xO_{3-d}$ and performance optimization for intermediate-temperature solid oxide fuel cells. *Electrochimica Acta*, *123*, 426–434. https://doi.org/10.1016/j.electacta.2014.01.020

Zha, S., Zhang, Y., & Liu, M. (2005). Functionally graded cathodes fabricated by sol-gel / slurry coating for honeycomb SOFCs, *176*, 25–31. https://doi.org/10.1016/j.ssi.2004.07.010

Zhan, Z., & Ik, S. (2010). Thin film solid oxide fuel cells with copper cermet anodes. *Journal of Power Sources*, *195*(11), 3494–3497. https://doi.org/10.1016/j.jpowsour.2009.12.017

Zhang, L., Lan, R., Petit, C. T. G., & Tao, S. (2010). Durability study of an intermediate temperature fuel cell based on an oxide e carbonate composite electrolyte. *International Journal of Hydrogen Energy*, *35*(13), 6934–6940. https://doi.org/10.1016/j.ijhydene.2010.04.026

Zhang, L., Ping, S., Quan, H., Chen, X., Ma, J., & Chao, X. (2010). A comparative

study of H_2S poisoning on electrode behavior of Ni / YSZ and Ni / GDC anodes of solid oxide fuel cells. *International Journal of Hydrogen Energy*, *35*(22), 12359–12368. https://doi.org/10.1016/j.ijhydene.2010.08.067

Zhang, L., Zhou, Q., He, Q., & He, T. (2010). Double-perovskites A_2FeMoO_{6-d} (A = Ca , Sr , Ba) as anodes for solid oxide fuel cells. *Journal of Power Sources*, *195*(19), 6356–6366. https://doi.org/10.1016/j.jpowsour.2010.04.021

Zhao, L., Nian, Q., He, B., Lin, B., Ding, H., Wang, S., Liu, X. (2010). Novel layered perovskite oxide $PrBaCuCoO_{5+d}$ as a potential cathode for intermediate-temperature solid oxide fuel cells, *195*, 453–456. https://doi.org/10.1016/j.jpowsour.2009.08.009

Zhou, W., Liang, F., Shao, Z., Chen, J., & Zhu, Z. (2011). Heterostructured electrode with concentration gradient shell for highly efficient oxygen reduction at low temperature. *Scientific Reports*, *1*, 155. https://doi.org/10.1038/srep00155

Zhou, Y., Meng, X., Ye, X., Li, J., Wang, S., & Zhan, Z. (2014). Metal-supported solid oxide fuel cells with impregnated. *Journal of Power Sources*, *247*, 556–561. https://doi.org/10.1016/j.jpowsour.2013.08.134

Zhu, C., Liu, X., Yi, C., Yan, D., & Su, W. (2008). Electrochemical performance of $PrBaCo_2O_{5+d}$ layered perovskite as an intermediate-temperature solid oxide fuel cell cathode, *185*(3), 193–196. https://doi.org/10.1016/j.jpowsour.2008.06.075

Zhu, W. Z., & Deevi, S. C. (2003). A review on the status of anode materials for solid oxide fuel cells, *362*(July), 228–239. https://doi.org/10.1016/S0921-5093(03)00620-8